

# Dissertation

## **Application of Secondary Ion Mass Spectrometry (SIMS) in the Development of New Materials**

ausgeführt zum Zwecke der Erlangung des akademischen Grades eines Doktors  
der technischen Wissenschaften unter der Leitung von

ao. Univ.-Prof. DI Dr. Herbert Hutter

E164

Institut für Chemische Technologien und Analytik

eingereicht an der Technischen Universität Wien

Fakultät für Technische Naturwissenschaften und Informatik

von

DI Martin Rosner

Matrikelnummer: 9126511

Neustiftgasse 56/24

1070 Wien

Wien, im Oktober 2003



## Danksagung

Viele haben zum Erfolg dieser Arbeit beigetragen, bei denen ich mich an dieser Stelle bedanken möchte. Als erster sei **Prof. Herbert Hutter** erwähnt, der mir in seiner Arbeitsgruppe *Physikalische Analytik* die Möglichkeit gab, mich weiter in der Sekundärionenmassenspektrometrie zu vertiefen. Er stand mir immer sowohl mit wissenschaftlichem als auch mit privatem Rat und Tat zur Seite, hat durch die Finanzierung meiner Arbeit über den Fonds zur Förderung der wissenschaftlichen Forschung (FWF) dafür gesorgt, dass ich die Jahre meiner Dissertation nicht brotlos durchbringen musste.

Besonders bedanken möchte ich mich bei **Kurt Piplits**, der immer wieder viel Geduld bewies und sich Zeit nahm, wenn ich mit der Komplexität der SIMS überfordert war. Ich würde noch immer am Gerät stehen und mit dem Einstellen verschiedenster Parameter beschäftigt sein.

Eine wesentliche Voraussetzung für das Gelingen der Arbeit eines analytischen Chemikers sind Kooperationspartner, die dafür sorgen, dass ausreichend zu analysierende Proben vorhanden sind. Von denen möchte ich besonders **Dr. Peter Wilhartitz, Dr. Gottfried Pöckl, Dr. Christoph Kleber, Prof. Christoph Eisenmenger-Sittner, Dr. Erich Neubauer, DI Karine Lisak, DI Torsten Bachmann** und **DI Vassilka Vassileva** erwähnen.

Meinen (ehemaligen) Kollegen der Arbeitsgruppen Physikalische Analytik, **DI (Dr.) Hans Foisner, Dr. Katharina Gammer, DI Dragan Krecar** und **DI Karl Mayerhofer** danke ich für ihre Freundschaft und Unterstützung oft auch in nichtwissenschaftlichen Angelegenheiten.

**Prof. Mariano Anderle** und **Dr. Massimo Bersani** haben es mir ermöglicht, bei ihrer Arbeitsgruppe *Fisica Chimica delle Superfici e Interfacce* am *Istituto Trentino di Cultura*, in Trento, Italien ein Forschungssemester zu verbringen. Vielen Dank auch an meine Kollegen am ITC, **Damiano Giubertoni, Paolo Lazzeri, Mario Barozzi, Erica Jacob** und **Lia Vanzetti**, für die ich nicht nur der „Austriaco“ war, sondern dass sie mich von Anfang an freundlich aufgenommen haben und mir immer bei Problemen und Schwierigkeiten, die das Leben in einem fremden Land bereitet, weitergeholfen haben.

Der größte Dank gilt aber meinen Eltern, **Franziska** und **Josef**, meiner Freundin **Doris** und ihren Eltern, für die moralische Unterstützung während der Höhen und Tiefen meines Studiums. Danke.

## Abstract

Secondary Ion Mass Spectrometry (SIMS) is a common surface analytical method for the characterization of thin layers in material science and in semiconductor development both in the industrial routine and in research. SIMS allows the detection of all elements and their isotopes (even hydrogen) both in the depth profiling mode with a depth resolution down to 1 nm, and in the imaging mode with a lateral resolution in the range of 0.5  $\mu\text{m}$ . SIMS is able to measure concentrations from percentage down to the ppm range.

The present work gives an overview into the principles of dynamic-SIMS, time-of-flight-SIMS, and the newest developments in instrumentation. The successful application of the method in selected fields of material sciences is described. The main feature of SIMS, its depth profiling capabilities, is demonstrated in the fields of semiconductor development, the analysis of PVD-coatings, and in studies on the corrosion of brass. Due to effects induced by the primary beam, SIMS depth profiles are always distorted, which results in reduced depth resolution. To countervail this distortion a practical approach with a convolution method was applied for the precise characterization of sharp interfaces on semiconductors. As SIMS is not only limited to inorganic samples, one work presents the analysis of surface modified organic polymers with time-of-flight SIMS. The possibilities of acquiring 3-dimensional images from the distribution of main components and impurities is shown in three representative works dealing with the characterization of steel and newly developed electrochemical sensors.

## Kurzfassung

Sekundärionenmassenspektrometrie (SIMS) ist eine gebräuchliche oberflächenanalytische Technik in der Werkstoffanalytik und in der Halbleiterentwicklung zur Analyse dünner Schichten von Proben sowohl aus der industriellen Routine als auch in der Forschung. SIMS ermöglicht die Detektion aller chemischen Elemente und deren Isotope (auch Wasserstoff) sowohl durch Erstellung von Tiefenprofilen mit einer Tiefenauflösung von bis zu 1nm, als auch im abbildenden Modus mit einer lateralen Auflösung im Bereich von 0.5µm. Der messbare Konzentrationsbereich reicht von Hauptelementen bis in den Spurenbereich.

Die vorliegende Arbeit liefert einen Einblick in die möglichen Einsatzgebiete von dynamischer - SIMS, von Flugzeit - SIMS (TOF-SIMS) und in die neuesten instrumentellen Entwicklungen. Weiters wird die erfolgreiche Anwendung in ausgewählten Bereichen der Materialwissenschaften demonstriert. Die Hauptanwendungsmöglichkeit von SIMS, die Erstellung von Tiefenprofilen, wird durch die Analyse von Proben aus der Halbleiterentwicklung, von PVD - Beschichtungen und Korrosionsstudien an Messing gezeigt. SIMS - Tiefenprofile sind durch Einflüsse vom Primärionenstrahl stets verzerrt. Um diesen Effekt auszugleichen wurde für die exakte Charakterisierung von scharfen Interfaces in Halbleitern eine Faltungsmethode angewandt. SIMS ist nicht nur auf die Analyse von anorganischen Proben beschränkt. Eine Arbeit präsentiert daher den Einsatz von TOF-SIMS zur Analyse oberflächenmodifizierter organischer Polymere. Die Möglichkeit auch 3-dimensionale Verteilungen sowohl von Haupt- als auch von Spurenelementen darzustellen wird in drei repräsentativen Arbeiten, die über die Analyse von Stahlproben und neu entwickelten elektrochemischen Sensoren handeln, beschrieben.

<b>1</b>	<b>INTRODUCTION</b>	<b>2</b>
<b>2</b>	<b>SECONDARY ION MASS SPECTROMETRY</b>	<b>4</b>
<b>2.1</b>	<b>Dynamic SIMS</b>	<b>4</b>
2.1.1	Principles	4
2.1.2	Considerations to perform good SIMS analysis	8
2.1.3	Instrumental Set-Up	11
2.1.4	Mass Spectra	17
2.1.5	Depth Profiling	18
2.1.6	2D- and 3D Imaging	20
2.1.7	Scanning SIMS	22
2.1.8	Quantification	22
2.1.9	New Developments in dyn-SIMS	23
<b>2.2</b>	<b>Static SIMS (TOF-SIMS)</b>	<b>26</b>
2.2.1	Principles	26
2.2.2	Instrumental details	26
2.2.3	Advantages and differences to dyn-SIMS	30
<b>3</b>	<b>OTHER SURFACE ANALYTICAL TECHNIQUES</b>	<b>36</b>
<b>3.1</b>	<b>Atomic Force Microscopy (AFM)</b>	<b>36</b>
<b>3.2</b>	<b>Scanning Electron Microscopy (SEM)</b>	<b>38</b>
<b>3.3</b>	<b>Auger Electron Spectroscopy (AES)</b>	<b>39</b>
<b>4</b>	<b>APPLICATIONS FOR SIMS</b>	<b>41</b>
<b>4.1</b>	<b>Improvement of Depth Resolution by Convolution</b>	<b>41</b>
<b>4.2</b>	<b>TOF-SIMS studies of modified polymer surfaces</b>	<b>44</b>
<b>4.3</b>	<b>New developments in PVD Sputter Coating</b>	<b>46</b>
<b>4.4</b>	<b>Conservation of Cultural Heritage</b>	<b>58</b>
<b>4.5</b>	<b>Semiconductor Development</b>	<b>79</b>
<b>4.6</b>	<b>Development of Electrochemical Sensors</b>	<b>95</b>
<b>4.7</b>	<b>Powder Metallurgy and Steel</b>	<b>105</b>
<b>5</b>	<b>REFERENCES</b>	<b>120</b>

## 1 INTRODUCTION

Secondary Ion Mass Spectrometry (SIMS) is a common surface analytical method for the characterization of thin layers in material science and in semiconductor development both in the industrial routine and in research. SIMS allows the detection of all elements and their isotopes (even hydrogen) both in the depth profiling mode with a depth resolution down to 1nm, and in the imaging mode with a lateral resolution in the range of 0.5 $\mu$ m. SIMS is able to measure concentrations from percentage down to the ppm range.

Most of the works presented in this thesis have been performed on a CAMECA IMS 3f, an instrument from the first commercial generation that is 20 years old by now. Up to now it was consequently upgraded with a new primary ion column for the use of two different ion species ( $O_2^+$ ,  $Cs^+$ ), a new scanning generator for precise scanning SIMS, and a completely new interface for the exchange of data between the controlling computer and the instrument. All the software for controlling the instrument and for evaluating the data is in-house developed.

To answer special questions in material science SIMS is not always sufficient due to its limits in acquiring chemical information or in lateral resolution. To meet these requirements different analytical methods as Auger Electron Spectroscopy (AES), or Scanning Electron Microscopy (SEM) in different set-ups, or AFM have to be combined with SIMS.

Although SIMS is in commercial use for more than 30 years SIMS manufacturers are still spending high efforts to increase the analytical performance of the method. The requirement of semiconductor industry to characterize ultra shallow structures led to the development of low energy primary ion columns to gain highest depth resolution in the analysis of ultra thin coatings or of ultra shallow implantations. The other trend leads to unattended, automated analysis to apply SIMS at in-line or near-line analysis for the manufactures quality control. For these applications shortest down-times with the minimum of user interaction are necessary.

The present work gives an overview of the principles of dynamic-SIMS, time-of-flight-SIMS, and the newest developments in instrumentation. The successful application of the method in selected fields of materials science is described in chapters 4.1 to 4.7.

The studies in chapters 4.1 and 4.5 give an insight into the depth profiling capabilities of dynamic SIMS in semiconductor development. Both works have in common, that the demands to characterize sharp interfaces can not be fulfilled sufficiently with high energetic

primary ion beams. Due to influences of the primary beam atomic mixing occurring in the analyzed sample, the depth resolution suffers and acquired depth profiles are distorted. To counteract this distortion a practical approach with a convolution method was applied for a precise characterization of sharp interfaces on semiconductors. One of these works (chapter 4.5) was performed with a new developed dynamic SIMS instrument (CAMECA IMS Wf) during a research stage at the Istituto Trentino di Cultura (ITC) in Trento, Italy.

As SIMS is not only limited to inorganic samples, one work (chapter 4.2) presents the analysis of surface modified organic polymers with TOF-SIMS also performed at the ITC with an ION-TOV IV instrument.

Furthermore the depth profiling capabilities of dynamic-SIMS are demonstrated by the analysis of PVD-coatings (chapter 4.3), where the influence of nitrogen plasma treatment in coatings of copper on glassy carbon was investigated either for as-deposited and for heat treated samples. The plasma treatment time influences the adhesion of the coating on the substrate.

To get an insight into corrosion processes on objects of cultural value, different brasses have been weathered in ambient atmosphere (humid air with SO<sub>2</sub> addition), and characterized with SIMS and with Atomic Force Microscopy (AFM). It was found, that the zinc content influences the corrosion behavior of the brasses. The results are described in chapter 4.4.

The possibilities of acquiring 3-dimensional images from the distribution of main components and impurities is shown in three representative works dealing with the characterization of newly developed electrochemical sensors (chapter 4.6) based on vanadium/titanium casts and steel (chapter 4.7). In these electrochemical sensors, the ratio of vanadium and titanium influences the formation of an oxidized layer gained by anodic oxidation in H<sub>2</sub>SO<sub>4</sub>. The structure of this layer changes the photoelectric and electrochemical properties. One of the steel studies deals with the influence of the temperature on the sintering of hot-pressed steel powders, the other one describes non-metallic inclusions formed during the desoxidation process in the production of low-carbon steel.

## 2 SECONDARY ION MASS SPECTROMETRY

For surface analysis in material science a various number of techniques is available. They all have in common the excitation of the sample with different probe types as ions, photons (x-ray) or electrons and the detection of emitted particles or radiation caused by specific processes at the surface or surface-near regions. The detected species can be photons, electrons, ions or ionized neutrals. The SIMS technique uses ions both as probe and detected species. An overview of common surface analytical methods is given in [1].

SIMS is an excellent tool for the sample characterization in microelectronics and material science as it allows the detection of all elements (even isotopes) with a detection limit of less than 1ppm. It provides the capability of measuring depth profiles, direct imaging and 3-dimensional species distribution.

### 2.1 *Dynamic SIMS*

#### 2.1.1 Principles

Primary ions at an energy range of 250 eV – 20 keV are used to bombard a sample surface [2]. As primary ions most commonly  $O_2^+$ ,  $Cs^+$ ,  $Ga^+$ ,  $Ar^+$  are used. Depending on the energy, the impact angle, the ion species, and the nature of the sample these ions induce several phenomena [3] in the material.

#### Implantation of Primary Ions and Atomic Mixing

The primary ion strikes the sample surface, it will not be stopped by the first atomic layer and continues its trajectory into the surface until it stops as a result of energy loss due to collisions with matrix atoms. Atoms from the solid will be displaced which will displace additional atoms and so on. This collision cascade (Figure 1) causes atomic mixing in the solid and depends on the species of the primary ions, the sample, the impact energy, and the impact angle. Atomic mixing determines the achievable depth resolution of a SIMS measurement. The penetration depth for primary ions and the atomic mixing can be calculated with programs such as SRIM – Stopping and Ranging of Ions in Matter [4]. The theoretical background is described in Ref. [5].

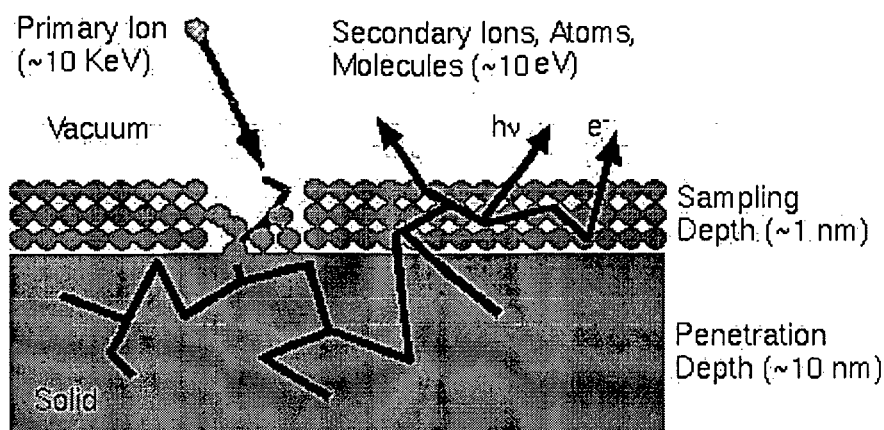


**Figure 1.** Schematic of a collision cascade induced by sample bombarding with primary ions. The image is taken from [6].

### Surface Sputtering and Secondary Ion Formation

Beside the moving of target atoms into the material there is a probability that particles leave the surface. These sputtered particles are mainly uncharged (atoms, neutral clusters or molecules), only less than 1% are ionized. More than 95% of these secondary particles originate from the top two monolayers. The equilibrium between implanted primary ions and sputtered particles is described with equation 1 [7].

$$I_{S(A)} = I_p \cdot S \cdot \alpha_A^\pm \cdot c_A \cdot f_{S(A)} \cdot \eta_A \quad \text{equation 1}$$

In this basic SIMS equation  $I_{S(A)}$  means the secondary ion intensity for element A,  $I_p$  is the primary ion intensity,  $S$  is the sputter yield in atoms per primary ion,  $\alpha_A^\pm$  means the ionization probability for element A,  $c_A$  is the atomic concentration of A within the sample,  $f_{S(A)}$  is the isotopic abundance of the measured species, and  $\eta$  is the efficiency (transmission) of the spectrometer.

The secondary ion yield is mainly influenced by the ionization potential detecting positive ions and the electron affinity detecting negative ions [6]. Three main theories try to explain the formation of secondary ions:

### **Electron Tunneling Model**

Under cesium bombardment the work function is reduced by implantation of the primary ions. One electron of the conducting band tunnels to the leaving atom and vice versa. The tunneling probability depends on the ionization potential of the sputtered element, the velocity of the atom, and the work function. Increased availability of electrons leads to increased negative ion formation.

### **Broken-bond model**

Especially under oxygen bombardment compounds form an oxide layer (metal-oxygen bond) on the surface. During the emission process the bonds are broken and the binding electron remains at the oxygen, which gets negatively charged. The metal is left positively charged and therefore positive ions are emitted. Oxygen sputtering increases the concentration of oxygen in the surface layer, but it does not lead to full oxidation of the surface.

### **Local Thermal Equilibrium**

Under ion bombardment a near surface plasma is generated in which the sputter atoms are ionized. This model has only historic importance.

Also changes in the matrix composition (e.g. multilayer systems, native oxide layer, inclusions) can affect the secondary ion yields, either by increasing or lowering the signal. This so-called matrix effect can be reduced by the use of an oxygen leak in the range of  $10^{-3}$  Pa to oxidize the sample surface fully and to minimize the effects of variation in sample oxygen concentration. Also the detection of  $CsM^+$  secondary ions can reduce the matrix effect, because the secondary ion formation is supposed to be matrix independent.

Emitted atomic and molecular secondary ions have distinctly different energy distributions. For atomic ions the kinetic energy ranges from 0 to several hundred eV, with the major fraction within the first 100 eV. Molecular ions have relatively narrow energy distributions, because their energy is consumed by internal vibrations and rotations. Figure 2 shows a typical energy distribution for atomic ( $M^+$ ) and molecular ions ( $M_2^+$ ,  $M_3^+$ ). Applying an additional voltage at the sample (so-called energy off-set) repels ions with lower kinetic energy at the exit slit of the electrostatic analyzer.

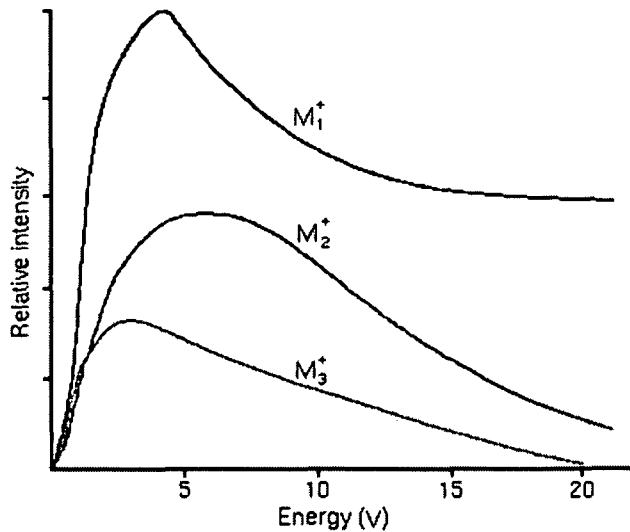


**Figure 2.** Energy distribution and relative intensity for atomic ( $M^+$ ) and molecular ( $M_2^+$ ,  $M_3^+$ ) ions. The image is taken from [6].

### Sample Charging

The bombardment of samples with (usually) positive charged primary ions and the emission of secondary ions and electrons changes its electrostatic potential, which results in sample charging and a corresponding drift of the secondary ion energy. The charging effect does not occur during analyzing conducting samples, because the charges can drain into the metallic sample holder. On the other hand analyzing insulators that charging can reach values which repels the secondary ions to the surface and extraction into the analyzer is impossible. Several techniques are available to compensate these charging effects [8]. With a normal incidence electron gun (NEG) the sample can be aligned to optimal extraction potential with an “electron shower”. Another method is the adapting of the extraction voltage by software control continuously according to the potential drift.

### Surface Roughening

The ion bombardment changes the surface topography for polycrystalline as well as for monocrystalline samples [9] and leads to a reduced depth resolution. For the polycrystalline case this surface roughening can be explained with the different sputtering yield for different crystal orientations. For monocrystalline surfaces until now there is no satisfactory explanation. By variation of the incidence angle of the primary ions or by using a rotating sample stage this effect can be reduced. Also measurements under conditions of an oxygen leak are reported [10].

## 2.1.2 Considerations to perform good SIMS analysis

### Detected Area

In a depth profiling analysis the total scanned area cannot be used for detection of secondary ions [11]. Contributions of the crater walls cause distortion of the depth profile. To avoid these sidewall effects the detected area has to be reduced by apertures and by electronic gating to assure that the extracted secondary ions only stem from the flat region of the crater bottom. A typical ratio is  $350 \times 350 \mu\text{m}^2$  of illuminated area to a detected area of  $150 \mu\text{m}$  in diameter.

### Memory Effects

When a sample is sputtered, some of the sputtered atoms are deposited on the extraction lens, which is positioned close to the sample surface. Resputtering of such deposited atoms at subsequent SIMS measurements of the same species of secondary ions increase the background signal for just this mass independent from the raster size of the primary beam. This effect limit the dynamic range of an analysis and causes a weak detection limit. The most common method to reduce memory effects, is to cover the impurity on the extraction lens by sputtering the sample matrix for a period of hours [12].

### Mass Interferences

Mass interference can occur when the matrix consists of more than one element, the matrix elements have more than one isotope, several naturally occurring isotopes are of significant intensity, and some molecular species have low mass.

For example  $^{56}\text{Fe}$  and  $^{28}\text{Si}_2$  have the same nominal mass. In mass spectrometry mass resolution for two species is defined as the ratio  $m/\Delta m$  ( $m$ : nominal mass of the ion,  $\Delta m$ : the mass difference). To separate both masses ( $^{56}\text{Fe}$ : 55.9349  $^{40}\text{Ca}^{16}\text{O}$ : 55.9575) a mass resolution of 2500 is necessary. By adjusting the entrance slit of the mass spectrometer the mass resolution can be changed. Unfortunately the transmission of the instrument suffers at high mass resolution. Several methods can be applied to control such interferences. The most simple one is to choose a minor isotope of the analyzed element. For the case mentioned above this works very well for iron with the use of  $^{57}\text{Fe}$  instead of  $^{56}\text{Fe}$ . The interference of atomic and

molecular species can be suppressed by the application of an energy off-set at the secondary ion extraction. As molecular secondary ions have a less wide energy distribution the lowering of the extraction voltage disables them to pass the energy analyzer in the mass spectrometer with the unfavorable effect of reduced signal intensity of the other species.

### Primary Beam Energy, Angle of Incidence, and Depth Resolution

A measured SIMS depth profile is usually distorted due to the sputter induced atomic mixing [2]. The mixing depth is related to the penetration depth (projected range) of the primary ions, what is the limiting factor for the depth resolution. It increases with the primary ion energy and decreases with the impact angle with respect to the sample surface normal. The impact angle ( $\theta$ ) is calculated for common instrument with primary column angle of  $30^\circ$  ( $\alpha$ ) to surface normal and given sample ( $V_s$ ) and primary ( $V_p$ ) voltages according to equation 2.

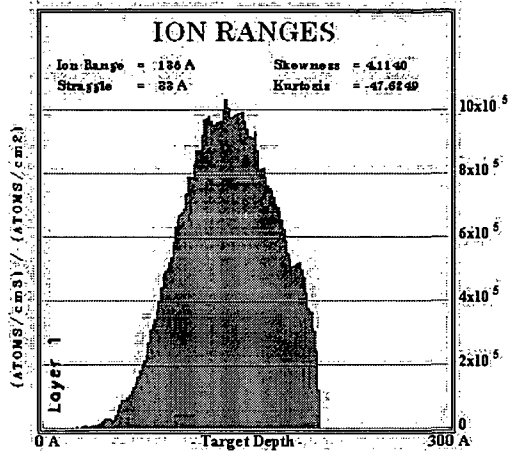
$$\sin \theta = \frac{\sin(\alpha = 30)}{\sqrt{1 - \frac{V_s}{V_p}}} \quad \text{equation 2}$$

A coarse estimation for the penetration depth (R) depending on the used primary ion species is determined from experimental data [13]:

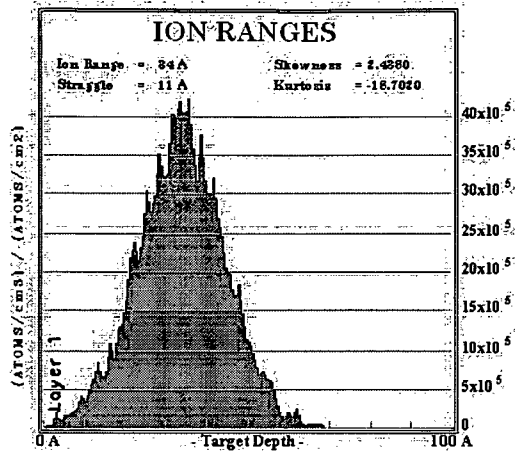
$$\text{O}_2^+: \quad R = 2.15 * V_p * \cos\theta$$

$$\text{Cs}^+: \quad R = 1.838 * V_p^{0.68} * \cos\theta$$

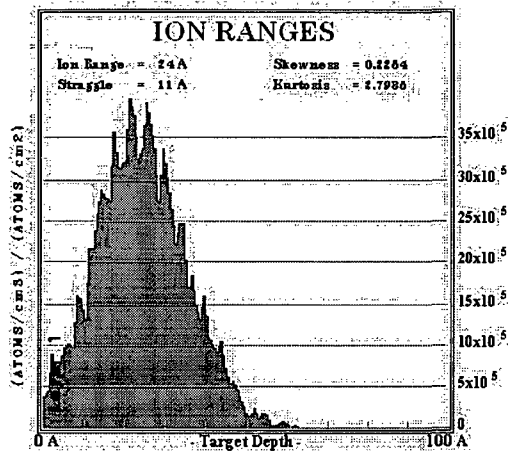
A more exact penetration depth can be calculated with the Monte-Carlo simulation. SRIM [4] is a good program for this approach. Compared to a normal incidence beam, the beam at an angular incidence has a shallower penetration, and more of the recoiled sample atoms intersect the surface, which results in a higher sputter yield. To demonstrate the effects of different impact parameters for  $\text{Cs}^+$  primary ions some representative SRIM calculations have been performed (Figure 3).



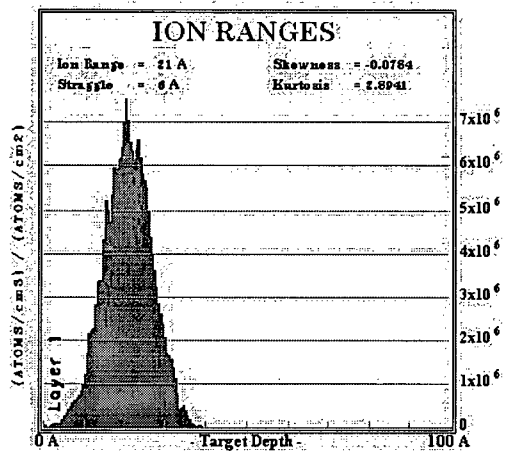
a)  $\text{Cs}^+$ @14.5keV,  $24^\circ$



b)  $\text{Cs}^+$ @1keV,  $45^\circ$



c)  $\text{Cs}^+$ @1keV,  $60^\circ$



d)  $\text{Cs}^+$ @250eV,  $45^\circ$

Figure 3. SRIM result of the penetration depth for different primary ion beam conditions.

For common primary ion conditions the resulting  $\text{Cs}^+$  ion ranges are listed in Table 1. In case (a) typical parameters for a CAMECA IMS 3f instrument are chosen. Cases (b) – (d) are possible with modern instruments such as the IMS 6f or the IMS Wf, which allow a wider variety of angles and energies. The comparison between (c) and (d) demonstrates, that it is not always necessary to reduce the impact energy to the limits of the instrument (250 eV). Even a variation of the incidence angle leads to comparable results in the ion range. With lowering the impact energy the sputter rate decreases enormous, so it is more practicable to perform measurements at higher energies, but with lower impact angles.

	Energy [keV]	Angle [°]	Ion range [Å]
a	14.5	24	135
b	1	45	34
c	1	60	24
d	0.25	45	21

**Table 1.** Projected implantation ranges calculated with SRIM

The decay length  $\lambda$  [14] is used to compare the depth resolution and defines the depth it takes a signal to drop from 1 to  $1/e$  (0.366). Knowing the signal intensities ( $I_x$ ) for two data points within a decay slope ( $x_1, x_2$ )  $\lambda$  can easily be calculated using equation 3.

$$\lambda = \frac{-(x_2 - x_1)}{\ln\left(\frac{I_{x_2}}{I_{x_1}}\right)} \quad \text{equation 3}$$

An accurate value of  $\lambda$  can be obtained by taking the exponentially decaying part of the profile. Another way to describe the depth resolution is the so-called Raleigh Criterion, which is the minimum distance that 2 features can be distinguished.

### 2.1.3 Instrumental Set-Up

Figure 4 shows a typical set-up of a dynamic SIMS instrument as it is used in the CAMECA IMS 3f and in the IMS Wf. The main parts are the primary ions guns, the primary ion column to adjust the intensity and the focus of the beam, the sample stage, secondary column with extraction system, mass spectrometer and detection unit. The system must be operated under ultra high vacuum (UHV). In the following section the single parts are explained in detail. All the schematic images are taken from [6].

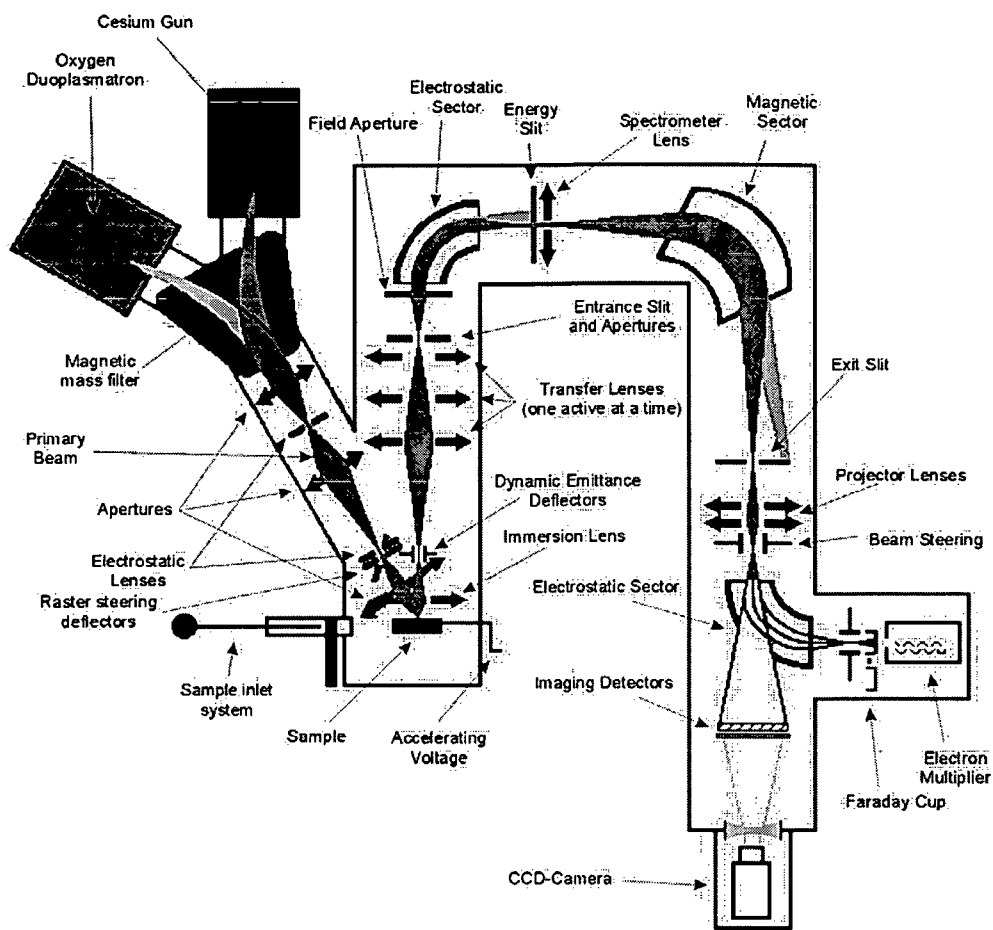


Figure 4. SIMS instrumentation The image is taken from [15]

### 2.1.3.1 Ion Sources

Depending on the application a variety of ions guns has been developed for SIMS. In practice the following criteria are desired from a good ion gun:

- High brightness (intensity per area)
- High stability
- Low beam diameter
- Ion beam purity
- Long service times

The following types of ions guns give a choice of common used sources. A complete explanation, considerations for the design and demands for ions guns are given in [16].

### Duoplasmatron Source

This plasma discharge ion source was developed by von Ardenne [17] already in the 1930's and is used for surface bombardment with primary ions generated by different types of gases e. g.  $O_2$  or Ar. Between a cathode and an anode a low voltage arc is burning and a strong magnetic field forms a high density plasma. An external electrostatic field extracts the ions into the primary column. The set-up is shown in

Figure 5. Currents up to several  $\mu A$  and a minimum beam diameter  $0.5 \mu m$  can be generated, where a decrease of the beam diameter is associated with a reduction of the current. For dynamic SIMS the use of  $O_2^+$  is common because of a chemical enhancement effect. The source usually emits a variety of ion species (atomic and cluster ions), therefore a magnet sector after the source is required for purification [18].

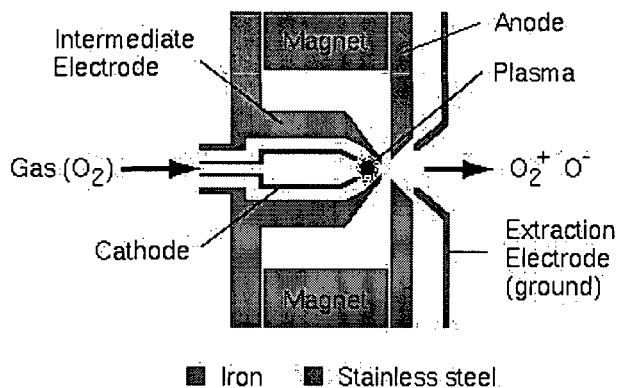


Figure 5. Duoplasmatron ion source.

### Surface Ionization Source

This type is mainly used for generation of  $Cs^+$  primary ions. The principle is the thermal ionization of atoms with low ionization energy on a hot solid surface [19]. A reservoir containing cesium or a cesium containing compound is heated, the vapor passes along a capillary with an end of a heated porous tungsten frit. The vapor is nearly fully ionized and the  $Cs^+$  ions are extracted to the primary column by applying a high voltage (Figure 6).

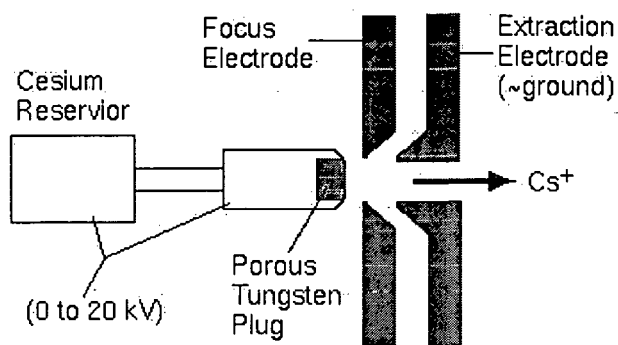


Figure 6. Cesium ionization source.

### Liquid Metal Ion Source (LMIS)

LMIS is mainly used for TOF-SIMS instruments and is described in section 2.2.2.1.

#### 2.1.3.2 Mass Analyzer

The secondary ions leave the sample with a kinetic energy distributed in a range of several hundreds eV. In a double focusing sector field analyzer (Figure 7) the accelerated and focused secondary ions pass through an electrostatic energy analyzer (ESA) consisting of a cylindrical electrostatic field. Particle with equal charge and kinetic energy will have the same flight radius regardless of its mass. The energy analyzer bends lower energy ions more than higher energy ions. So an energy focusing is achieved. By modifying the energy slit a defined energetic fraction can be chosen.

The following magnetic field analyzer separates the secondary ions beam due to its mass to charge ratio ( $m/z$ ) defined in equation 4.

$$\frac{m}{z} = \frac{B^2 r^2}{2U} \quad \text{equation 4}$$

- m particle mass
- z particle charge
- B magnetic field
- r radius of trajectory
- U acceleration potential

Only particles having the same  $m/z$  ratio will be deflected into a circle with the radius  $r$ . By scanning the magnetic field, masses can be detected sequentially. Most ions are single charged ( $M^+$ ), but also higher charged particles can occur ( $M^{2+}$ ,  $M^{3+}$ , ...). These multiple charged ions appear at half or third of their mass and their formation probability is considerably lower than for single charged species. By variation of the broadness of the entrance and the exit slits the mass resolution can be adjusted in a typical range from  $m/\Delta m = 300$  to  $m/\Delta m = 10000$ . With higher mass resolution the transmission of the spectrometer suffers. Comparable to a light microscope a magnet sector field mass analyzer is capable of direct imaging due to the stigmatic arrangement of lenses, ESA and magnetic sector field.

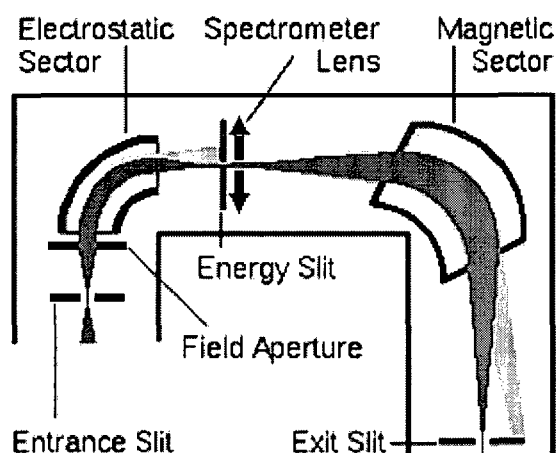


Figure 7. Double focusing sector field mass analyzer.

Other configurations for mass analyzers are the quadrupole analyzer, where masses are separated by applying radio frequencies according to the stable path of the secondary ions through the mass filter [20] and the time-of-flight (TOF) analyzer as described in 2.2.2.2.

### 2.1.3.3 Detection system

After the ions leave the mass spectrometer through the exit slit they can be detected either with an electron multiplier, a Faraday cup or a channel plate in combination with a CCD camera (Figure 8).

### Electron Multiplier

An incoming particle (ion) strikes an electrode (dynode, coated with a material having an high secondary electron yield) and causes electrons from the outer layers of the dynode to be released. These electrons are accelerated towards the next dynode where each secondary electron starts a new cascade. A typical EM has between 12 and 24 such sequential dynodes. After detecting an ion pulse the EM requires a recovery time (dead time) until the next pulse can be detected. A signal amplification of up to  $10^8$  and a dynamic range from less than 1 counts per second up to 5 million counts (corresponding to a current of  $10^{-12}$  A) is possible with this arrangement. The upper limit is given by the dead time of the EM.

### Faraday Cup

If currents are higher than the upper limit of the EM, the secondary ions are measured with a Faraday cup. It has a simple set-up consisting of a metal cage with an applied electrical potential, which traps the incoming ions and measures the current with an ampere-meter. Compared to an EM the FC is limited in its sensitivity by the sensitivity of the connected ampere meter. For measurements requiring an extremely high dynamic range the upper limit of the EM can be aligned with a threshold where the detection systems should switch to the FC.

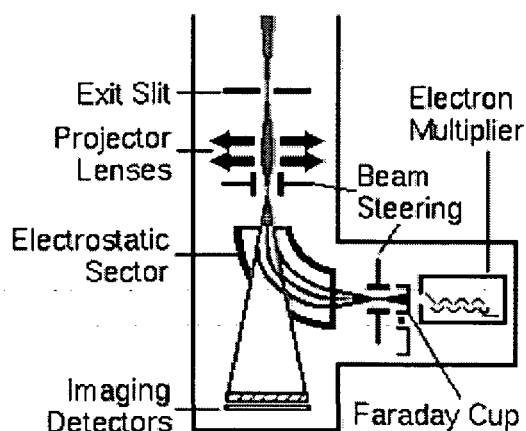


Figure 8. Detection unit, consisting of electron multiplier, Faraday cup, and channel plate.

### Channel Plate

To display the lateral distribution of ions in the direct imaging mode a double microchannel plate is used. It consists of an 2D - array of microchannels, each working similar to an electron multiplier. The signal amplification is in the range of  $10^6$  which allows even single ion

detection. By variation of the channel plate high voltage a high dynamic range can be achieved. The resulting electron cascades are visualized by a following phosphor screen in combination with a CCD camera.

#### 2.1.3.4 Vacuum requirements

To get reasonable detection limits and a good reproducibility the vacuum in the columns and in the sample chamber has to be in the UHV range.

The mean free path ( $\lambda$ ) of the traveling particles is calculated according to equation 5.

$$\lambda = \frac{1}{\sigma * \sqrt{2}} * \frac{kT}{p} \quad \text{equation 5}$$

- k Boltzmann constant
- T temperature
- p pressure
- $\sigma$  cross section of the particles

$\lambda$  must be high enough to avoid collisions of the ions with the molecules of the residual gas ( $N_2$ ,  $O_2$ ,  $CO_2$ ,  $H_2$ ,  $H_2O$ ). To guarantee a flight path within the instrument in the range of a few meters the pressure has to be lower than  $10^{-3}$  Pa. Further the time to adsorb 1 monolayer of residual gas on the sample surface has to be considered. At a pressure of  $10^{-7}$  Pa it takes 1000 s to adsorb 1 monolayer, so this vacuum is sufficient for most SIMS analysis. For high precision measurements (high depth and mass resolution, low detection limit) a vacuum of  $10^{-8}$  Pa will be necessary.

#### 2.1.4 Mass Spectra

The first step of analyzing an unknown sample is to perform a mass spectrum to get an overview of the matrix and the impurity elements [21]. Therefore the mass analyzer is scanned over the selected mass range (usually  $m/z = 6$  to  $m/z = 250$ ) in small steps. Atomic and molecule ions are detected in this mode and give a coarse overview what elements are present in the sample. If the sample is bulk material the analysis is straightforward. If the sam-

ple has a layer structure or inclusions, then the sample thickness, the sputtering rate, and the selection of the analyzed spot must be considered and traded off. Also possible mass interferences of atomic and molecular species have to be taken into account. Due to the different distribution of the kinetic energy of secondary atomic and molecular ions the application of an energy off-set at the sample high voltage solves this problem.

A typical mass spectrum is shown in Figure 9. The surface of a silicon/germanium sample is sputtered with  $O_2^+$  primary ions and the masses from  $m/z = 6$  to  $m/z = 150$  have been recorded. The diagram also shows the peak identification. For silicon ( $m/z = 28, 29, 30$ ) and germanium ( $m/z = 70, 72, 73, 74, 76$ ) the characteristic isotopes with their isotope ratios and their oxides can be recognized. The spectrum was recorded with 100V energy off-set, so high-molecular species are successfully suppressed.

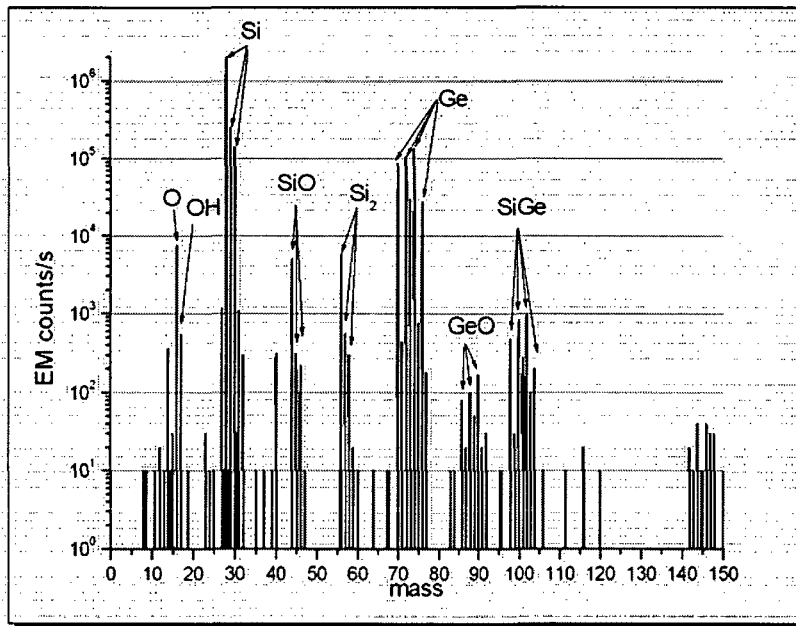


**Figure 9.** Mass Spectrum of a Si/Ge sample.  $O_2^+$  primary ions with 5.5 keV. An off-set voltage was applied to suppress high-molecular ion species

### 2.1.5 Depth Profiling

During the sputtering process secondary ion intensities are recorded as a function of time. The mass analyzer is switched to discrete masses, which have to be selected by the analyst

before the measurement according to the information gained from the mass spectrum. In a raw depth profile the electron multiplier counts are plotted against the analysis time.

The depth calibration of the raw profile is done ex-situ with a depth profilometer using a mechanical stylus to determine the ultimate depth of the sputtered crater. Crater depth divided by the total sputter time gives the average sputter rate (usually nm/s). This value is used to transform the x-axis to a depth scale. For the depth quantification of multilayer system the stylus method becomes unreliable, because the changing sputter rates during the analysis cannot be reconstructed in this way. Modern SIMS instruments (section 2.1.9) offer the possibility of in-line depth measurement by laser interferometry to monitor the actual depth, even when the sputter rate changes.

Figure 10 shows a depth calibrated profile of PVD deposited copper (500nm) on a carbon substrate. The y-axis remains unquantified and shows only EM counts. The quantification can be performed with well-defined standards (e.g. implantation standards for semiconductor quantification) via calculation with relative sensitivity factors (RSF). This method is explained in section 2.1.8.

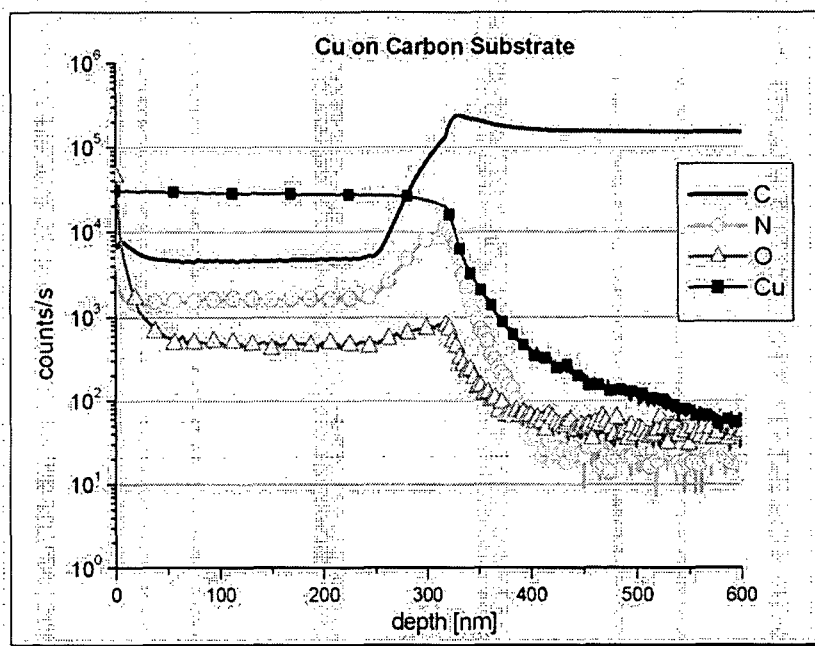
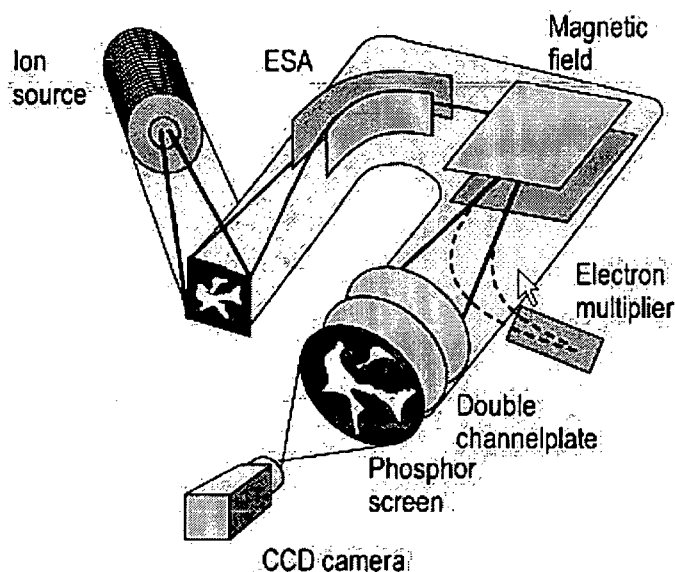


Figure 10. Depth profile of a PVD coated carbon substrate; coating material: 500nm copper; measuring conditions:  $\text{Cs}^+$  primary ions with 100nA@5.5 keV.

### 2.1.6 2D- and 3D Imaging

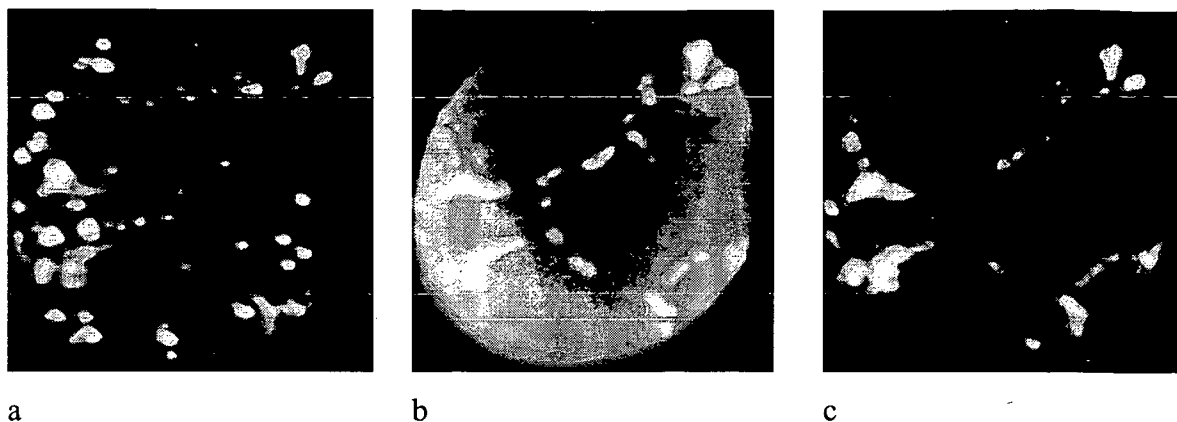
Due to the stigmatic optics of double focusing magnetic sector SIMS instruments (Figure 11) a point to point representation of the sample surface on the channel plate detector [22] is possible.



**Figure 11.** Schematic of the stigmatic ion optics of a double focusing magnetic sector SIMS. Each illuminated point of the sample surface corresponds to a point on the double channel plate.

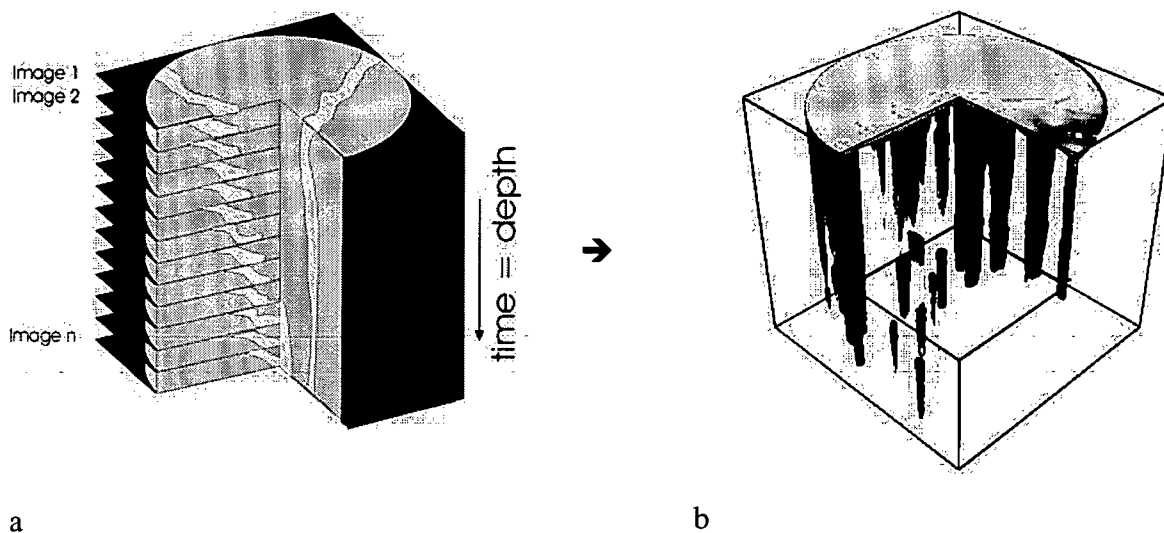
The primary beam is scanned very fast over the sample surface and the detector (channel plate with phosphor screen and CCD camera) records the ion image according to the  $m/z$  – ratio adjusted with the mass separator. The image size is usually  $150\ \mu\text{m}$  in diameter and round, because of the detector geometry. Primary ion beam intensities are chosen rather high for direct imaging, which results in excellent and noise-free images for main components and even for trace elements. For low secondary ion intensities the images become noisy. By adding several images (256 or more) the signal-to-noise ratio can be improved.

Figure 12 shows the ion images of  $^{11}\text{B}$  (a),  $^{52}\text{Cr}$  (b) and  $^{98}\text{Mo}$  (c) from a sintered powder metallurgical steel sample, image diameter is  $150\ \mu\text{m}$ . Boron (sinter activator) is enriched at the grain boundaries.



**Figure 12.** Ion images of  $^{11}\text{B}$  (a)  $^{52}\text{Cr}$  (b) and  $^{98}\text{Mo}$  (c) from a P/M steel sample. Boron is enriched at the grain boundaries.

By recording images as a function of sputtering time [23] and piling them up with 3D imaging software 3-dimensional distributions of selected species can be achieved. In practice a routine to acquire 2D images is implemented into the depth profiling program and the processing can be done with an especially developed software [24]. Representative volumes of  $150 \times 150 \mu\text{m}$  in lateral and about  $10 \mu\text{m}$  in depth can be measured.



**Figure 13.** Single images acquired as a function of time during the sputtering process (a) can be piled up with 3D imaging software and displayed as a cube with  $150 \times 150 \times 10 \mu\text{m}^3$ . (b) shows the 3D distribution of  $^{16}\text{O}$  in an electrochemically oxidized vanadium-titanium alloy. Oxygen forms a continuous surface layer during the oxidation.

### 2.1.7 Scanning SIMS

In the scanning mode a finely focused beam is scanned step by step with a defined holding time per pixel over the sample surface. The secondary ion intensities are recorded by the electron multiplier as a function of the beam position and then recalculated to a 2D image. Depending on the used ion gun a depth resolution down to 20 nm (for liquid metal ion guns) can be achieved. The long acquisition time (up to 1 hour) of such images exhibits one major problem: the recoverage of the sample surface with adsorbed residual gas atoms. Software controlled quick intermediate sputtering of the analyzed area to remove this coverage can avoid this problem.

### 2.1.8 Quantification

The ionization probability of secondary ions is strongly dependent on the surrounding matrix. Therefore quantitative SIMS analysis requires standard materials from which the relative sensitivity factors (RSF) have to be determined. RSF take into account all system specific parameters as primary beam conditions, vacuum conditions and matrix influences. A good method to calculate RSF values is to analyze an implantation standard with a comparable matrix to the sample, e.g. implantation in Si for the quantification of semiconductor samples) and with the same analysis conditions as used for the sample. RSF values are defined according to equation 6, where *ref* specifies the matrix element and *el* indicates the analyzed element (*I* are the respective signal intensities and *c* are the element concentrations).

$$\frac{I_{el}}{I_{Ref}} = RSF * \frac{c_{el}}{c_{Ref}} \quad \text{equation 6}$$

Knowing the implantation dose ( $Q_T$ ), the crater depth (*d*), the isotopic abundances of the analyzed element and the reference ( $f_{el}$ ,  $f_{ref}$ ), the matrix density ( $\rho$ ), the molecular mass of the matrix (*M*), the signal intensities ( $I_{el}$ ,  $I_{ref}$ ), the number of measured cycles (*Cyc*) and the concentration of the reference ( $c_{ref}$ ) the RSF of the mean intensity ratio is calculated with equation 7. The relative precision is up to 1%, if the concentration range of the analyte in the sample and the matrix is in the 1% (at/at) range.

$$RSF = \frac{c_{ref} \cdot f_{ref} \cdot \rho \cdot N_L \cdot D}{f_{el} \cdot Q_t \cdot M \cdot Cyc} \cdot \sum_{i=1}^{Cyc} \frac{I_{el}(i)}{I_{ref}(i)} \quad \text{equation 7}$$

The analysis of one species in a multilayer system exhibits the major problem, that for each layer a RSF has to be determined, because the matrix dependent ionization rate can change enormous from layer to layer. By using  $\text{Cs}^+$  primary ions and detecting  $\text{CsM}^+$  secondary ions the matrix effect can be reduced significantly [25].

### 2.1.9 New Developments in dyn-SIMS

In recent years the demand to use dynamic SIMS toward an in-line analysis in semiconductor industries led to the development of a new type of SIMS instrument. Following requirements are desired for such an instrument:

Ultra shallow depth profiling at well-controlled ultra low energy conditions is required.

Due to the change from the wafer size from 200 mm to 300mm diameter the need for full wafer analysis is growing. In some cases every wafer must be measured.

To reduce the cost of personnel, and to achieve measurements with high reproducibility and high precision the trend leads to unattended and automated analysis.

To meet these requirements the IMS Wf (SC Ultra) has been developed by Cameca [26]. The IMS Wf has two primary ion columns ( $58^\circ$  and  $36^\circ$  to surface) which allow sputtering at impact energies down to 250 eV with maximum current density at optimized impact angles. For this reason the concept of a "floating column" was developed [27]. All the electrostatic lenses and deflectors in the column are biased with respect to an electrostatic chamber, while this chamber is biased with respect to the grounded vacuum chamber. The primary ions can reach the sample surface with an impact energy adjustable from 250 eV to 10 keV while they keep their acceleration energy (1 keV to 10 keV) in the column. The last focusing lens is not included in the floating column and is biased directly with respect to ground. This set-up allows the ions to be extracted at optimum conditions at the source and to get high current densities even at low impact energies. To focus the beam onto the sample a cross-over image of the beam is used for illuminating a square aperture (stencil), which is imaged onto the sample surface. With this stencil geometry the beam is restricted to its central part, where the brightness is maximum and any cross-over tails are suppressed. A following shiftable identical stencil is used to modify the rectangular beam size.

The secondary ion extraction system is shown in Figure 14. It provides a field free space from the last primary lens to the secondary extraction field to uncouple the extraction and the focusing functions of the immersion lens by including two independently biased electrodes in the immersion lens. It is possible to produce an extraction field as low as required to accommodate low impact energy operation mode, while keeping a high secondary acceleration voltage.

With geometries of the "floating column" and the extraction system as described above an impact energy of 250 eV combined with an high extraction voltage can be reached, including high depth resolution, high sensitivity, and high mass resolution. In contrast to older instruments the floating set-up provides variation of the incidence angle independent from the secondary ion polarity and from the impact energy.

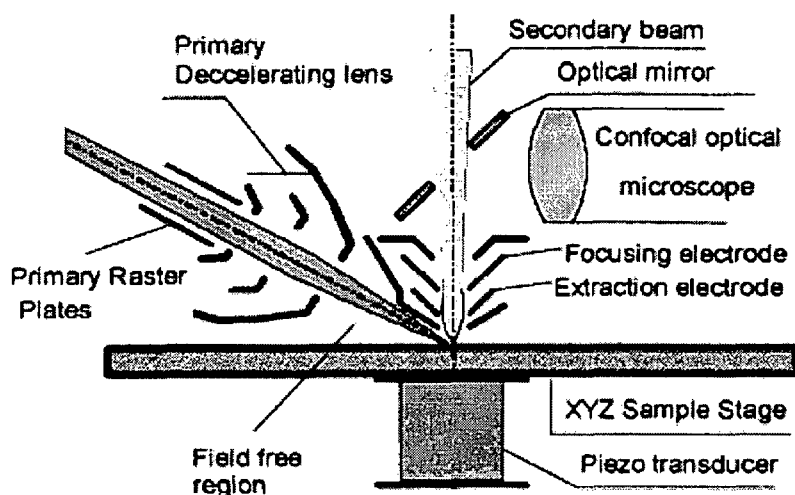
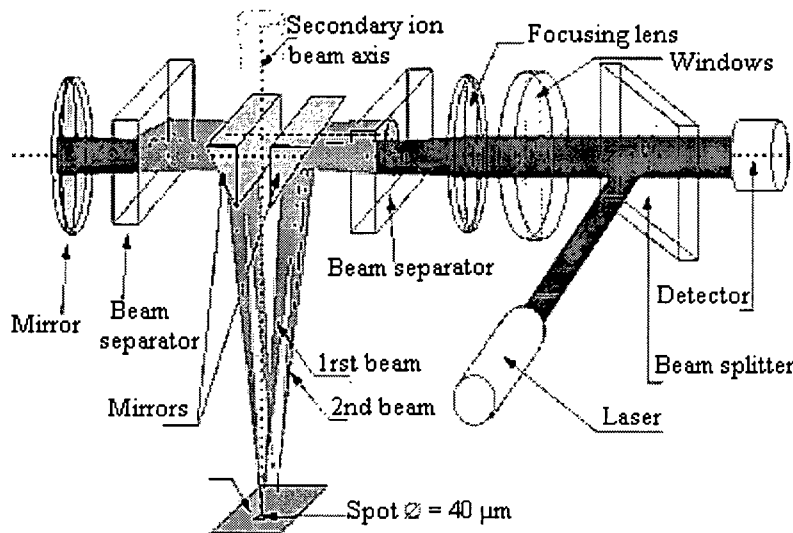


Figure 14. Secondary extraction system of the CAMECA IMS Wf. Image taken from [27]

In conventional SIMS analysis the crater depth measurement for depth calibration can only be done ex-situ with a surface profilometer after removing the sample from the measuring chamber. The IMS Wf is equipped with an on-line crater depth measuring system based on laser interferometry [28]. It consists of two laser beams reflected from the sputtered area and the sample surface. The incident laser beam is directed into the specimen chamber through a window, focused by a lens and split in two beams, which are focused on the sample surface: one in the crater bottom and the other on the unsputtered surface. After their first reflection by the surface the beams are retroreflected with a mirror on the same points at the surface. After this second reflection the two return beams are recombined before reaching the interfer-

ometer detector (Figure 15). The ultimate depth resolution of this system is 0.6 nm, defined by the laser wavelength of 633 nm and the phase resolution of the interferometer.

During the measurement the actual depth and the sputter rate can be observed in real time. This set-up is also advantageous for the on-line depth calibration of multilayer systems, when the sputter rate changes within the layers. Light transmitting coatings (e.g. SiO<sub>2</sub>) falsify the results of the laser measurement and make an ex-situ depth measurement necessary.



**Figure 15.** Dual laser beam set-up for on-line crater depth measurement for the CAMECE IMS Wf. Image taken from [29]

The whole Wf system is computer controlled with motor controlled apertures and a sample stage for unattended automatic measurements as they are needed in industrial routine. For this reason it can also be equipped with a sampling robot for in-line analysis directly at the production line in semiconductor industry. An additional equipment is an eucentric rotating sample stage to reduce sputter induced crater bottom roughening especially for polycrystalline materials [30].

## 2.2 *Static SIMS (TOF-SIMS)*

The first commercially applicable TOF-SIMS instrument was built by Prof. A. Benninghoven at the University of Münster [31]. TOF mass spectrometry is based on the fact that ions with the same energy but different masses travel with different velocities. It is considered to be “static” because the dose of the primary ions is below the threshold for surface damage due to sputtering. Spectra and images can be obtained by removing less than 1% of the top monolayer of the sample. Nevertheless with two independent ion beams (“sputter gun” and “analyzer gun”) depth profiles in quasi-dynamic (interlaced) mode can be performed.

### 2.2.1 Principles

A pulsed primary ion beam is used to desorb and ionize species from a sample surface. The resulting secondary ions are accelerated into a mass spectrometer, where they are analyzed by measuring their time-of-flight from the sample surface to the detector. A finely focused beam is scanned across the sample surface. Due to the parallel detection nature of TOF-SIMS, the entire mass spectrum is acquired from every pixel. The energy of the primary beam (pA range) is not sufficient to erode the sample surface. Because of this fact static SIMS is extremely sensitive to the uppermost layer of a sample. The considerations on the collision cascade and atomic mixing equals dynamic SIMS. An unified theory of secondary ion formation in static SIMS does not exist yet. Over 95% of the secondary particles originate from the top two monolayers of the sample and therefore TOF-SIMS is a highly surface sensitive method.

### 2.2.2 Instrumental details

A TOF-SIMS consists of two main parts:

- The primary ion source(s), where the primary ions are generated and accelerated to the sample surface.
- The mass analyzer, where the extracted ions are detected due to their flight time.
- Additional components as an optical microscope, a sample handling unit and a SEM detector complete the set-up of the instrument.

### 2.2.2.1 Ion Sources

The first type of possible ions guns for TOF-SIMS instruments are electron impact (EI) or plasma sources, using noble gases (argon, krypton, xenon) or reactive gas (oxygen). The produced ions are extracted, accelerated to the sample surface and focused in an electrostatic ion optical column. EI ion guns operate in an energy range of 0.2 – 10 keV with a maximum current of 1  $\mu\text{A}$  dc, while discharge guns can be operated at energies up to 15 keV with a dc current up to 20  $\mu\text{A}$ .

The other type of ions guns [32] is called liquid metal ion source (LMIS) and produce ions from a liquid metal, mostly gallium (Figure 16). A liquid metal is drawn up from a reservoir along a fine needle of refractory metal by capillary action. A voltage of 10-30 keV between the needle and the extractor electrode draws the liquid into a cusp. In the region just above this cusp ions are generated and accelerated through an aperture and focused through the ion optical column onto the sample surface. Because of its low melting point of 30°C Gallium is mainly used as the liquid metal. Ga liquid metal ion sources are very bright and the beam can be focused to a fine spot between 0.2  $\mu\text{m}$  (10keV) and 20 nm (30 keV). Deflection plates in the ion optics allow to scan the beam over surface areas from a few square micrometers to many square millimeters. Additional deflection plates (buncher) can pulse the ion beam in a wideness of 1 ns.

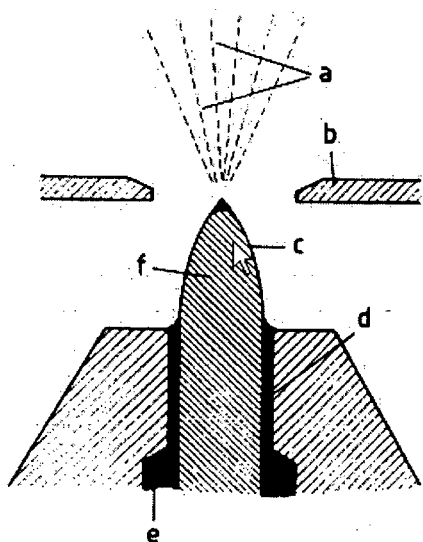


**Figure 16.** Schematic diagram of a liquid-metal ions source (LMIS); (a) extracted ions; (b) extractor; (c) liquid metal film; (d) capillary tube; (e) liquid metal; (f) needle. Image taken from [32]

### 2.2.2.2 Mass Analyzer

All sputtered secondary ions are accelerated to a potential of 2 – 8 keV in a TOF analyzer (Figure 17), so the kinetic energy of all secondary ions equals. The ions can drift field free through a given path length L before they strike the detector. The time of traveling through the mass analyzer is defined in equation 8

$$t = \sqrt{\frac{mL^2}{2qU}} \quad \text{equation 8}$$

- t drift time
- m ion mass
- L path length
- q ion charge
- U accelerating voltage before entering the flight path

According to this equation light ions travel more rapid through the tube than identically charged heavy ions. A very well defined start time is required for flight time measurements. This can be guaranteed when the ion gun is operated in a pulsed mode to generate discrete ion packages. The flight path must be sufficient long (1 – 1.5 m) and a very sophisticated high frequency pulsing and counting system must be employed to record the flight time within a tenth of nanoseconds. The capability of simultaneous detection of all masses enables the reconstruction of TOF spectra for any ion species as a function of depth and lateral resolution.

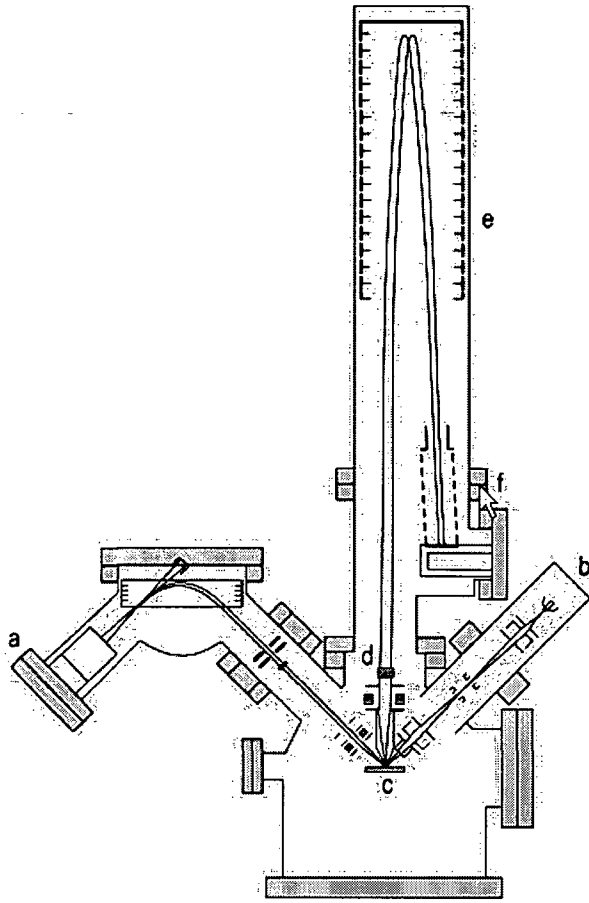


**Figure 17.** Diagram of the TOF-SIMS IV (ION-TOF, Münster). a: EI ion source, b: LMIS, c: target holder, d: secondary ion optics, e: reflectron, f: deflector and counting system. Image is taken from [32].

### 2.2.2.3 Additional components

A typical arrangement for sample handling includes a sample stage being able to get shifted in x-, y- and z-plane, to be rotated, and to be tilted. Rotation is very useful if samples have different orientations due to their topography and the adjustment of a tilt angle can be changed to become normal to the analyzer gun and grazing to the sputter gun. It has to be ultra low sensitive for vibrations. For specific samples it may be useful acquiring SIMS data as a function of surface temperature. Therefore special temperature controlled sample holders can be used. To adjust the sample in the analysis chamber all the manipulations can be observed with an optical microscope at different magnifications. A secondary electron (SE) detector can be equipped to gain topographical images produced by ion induced secondary electrons and to align the ion beams in the dual beam mode.

### 2.2.3 Advantages and differences to dyn-SIMS

Due to its low current densities, realized by pulsed ion guns, static SIMS is an extremely surface sensitive technique. Less than 1% of the top monolayer is sampled during acquiring a spectrum. The instrument offers extremely high mass resolution in the region of  $m/\Delta m = 5000 - 20000$ . The mass resolution is defined by the settings and the capabilities of the electronics in the instrument as the pulsing time in the primary optics and the rapidness of the detection unit (electron multiplier). With such high mass resolutions interferences between peaks from different species but with the same nominal mass can be avoided.

A TOF-SIMS instrument provides a high transmission, this means that almost all secondary ions are extracted to the analyzer. With a single pulse a complete mass spectrum can be obtained and by adding more spectra a better signal-to-noise ratio can be achieved. Because all elements are detected and stored at the same time, the analyst can decide after the analysis which masses should be evaluated. This is in contrast to dynamic SIMS with magnetic sector analyzer, where the analyzed masses have to be considered before the analysis by generating a mass table, which is executed cycle by cycle. A total mass spectrum of each scanned pixel can be obtained and by selecting a desired mass images of one ion species (ion maps) can be generated.

The possible mass ranges is up to atomic weights of 10.000 amu, which allows the analysis of organic substances, polymers, and even biological samples. Charge compensation at the analysis of insulating samples can be performed with an additional electron gun (electron shower). TOF-SIMS instruments of the newest generation also offer the possibility of depth profiling with an independent sputter gun and reach almost the capabilities of dynamic SIMS instruments.

#### 2.2.3.1 Sample Handling for TOF-SIMS

As static SIMS is an extremely surface sensitive method, important considerations concerning to sample handling and sample manipulation have to be done. Unfortunately in laboratories routinely low-cost plastic bags are first choice for the storage of samples. But such bags are unsuitable as sample carriers for subsequent TOF-SIMS analysis. As the liquid polymer polydimethylsiloxane (PDMS) is an ubiquitous compound used as mould-release agent in common plastic products it can creep over sample surfaces obscuring the original surface and falsify TOF-SIMS measurements. Other common used substances for industrial poly-

mers are phthalates, mostly di-iso octyl phthalate (DOP). The positive mass spectra of PDMS and DOP are displayed in Figure 18 and Figure 19 [33]. The presence of the characteristic peaks  $m/z = 28, 43, 73, 133, 127, 221,$  and  $281$  indicates PDMS on a sample. At the appearance of mass 149 higher related peaks as  $261, 279$  and  $391$  should be checked to confirm the presence of phthalate. For inorganic samples it may be acceptable to sputter clean the surface with the primary beam to remove unwanted contaminants before the analysis. Such sputter cleaning cannot be applied in the case of organic samples, since the sample surface is organic and the sample surface will be destroyed what it is not acceptable for accurate analysis.

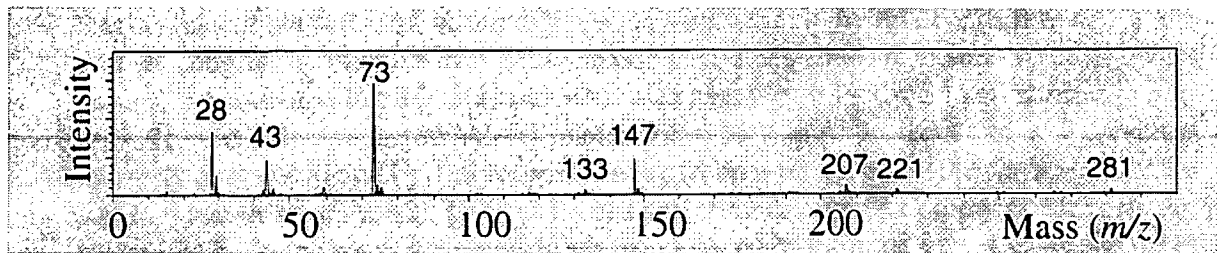


**Figure 18.** TOF-SIMS mass spectrum of polydimethyl siloxane (PDMS). The typical peaks indicate surface contamination of the sample due to wrong sample handling. Mass spectrum taken from [33].

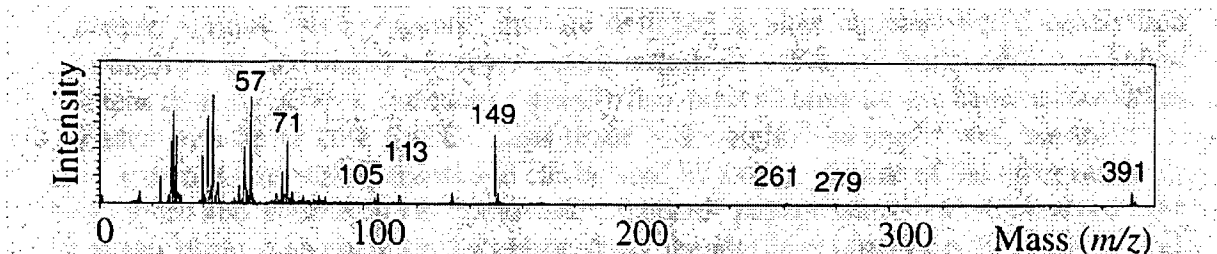


**Figure 19.** TOF-SIMS mass spectrum of di-iso octyl phthalate (DOP). DOP is a common contaminant in industrial plastic. Mass spectrum taken from [33].

Several methods can be chosen to avoid surface contamination: if the sample is inert to solvents it can be cleaned with certain solvents as hexane, methylene chloride or acetone. Another method to avoid surface contaminations is the usage of sample carriers as they are used in semiconductor industry. These containers are manufactured with a much higher cleanliness than typical molded polymer products. Such containers also have a concave inner base, and if a flat sample is placed face down, only the sample corners are in contact with the polypropylene. Samples for TOF-SIMS analysis may also be packed in aluminum kitchen foil without contamination. In the production process it is rolled with surface lubricants, but

they are removed during an annealing process before they are reeled. Surface mass spectra of such foils show only the peak  $m/z = 27$  (Al) and peaks from hydrocarbons adsorbed from the atmosphere.

In order to prevent cross-contamination of subsequently mounted samples on the same sample holder it is recommended to clean it from fatty acids, DOP and PDMS with sequential ultrasonic rinsing in methylene chloride, hexane acetone and methanol. Further the use of clean tweezers and keeping the workbench scrupulously clean is obligatory.

### 2.2.3.2 Dual Beam Depth Profiling

In dynamic SIMS one primary beam generates the secondary ions for analysis in the spectrometer (magnetic sector, quadrupole) and erodes the sample with a sufficiently high current to get in-depth information. Originally TOF-SIMS was designed for the analysis of the uppermost monolayer of a solid sample. The primary ion gun is operated in a pulsed mode with nanosecond ion pulses. Current densities are reduced a few orders of magnitude and therefore they are too low to obtain a sample erosion. Typical primary ion currents are in the range of pA and it takes up to 20 min to remove one monolayer. With this conditions depth profiles can not be performed with TOF-SIMS. To overcome this limitation a second ion beam with higher ion currents can be used for sputtering the sample [34]. The high energy pulsed analysis gun (mostly  $\text{Ga}^+$ ) is combined with a low energy sputter gun ( $\text{Cs}^+$ ,  $\text{O}_2^+$ , ...) to erode the surface. This dual beam approach allows the optimization of parameters independently for the analysis and the sputter process.

The two independent ion guns are operated in the following (interlaced) mode: a short pulse of the analysis gun with a duration of 1 – 50 ns generates secondary ions which are extracted to the TOF analyzer. After this extraction process with a typical duration of 5 – 10  $\mu\text{s}$  the extraction voltage is switched off and the ions have time to travel through the analyzer. In the meantime the sputter gun erodes the surface. The repetition rate in the kHz range influences the possible mass range. The highest useful repetition rate is 50 kHz resulting in a mass range of 50u. The time diagram of this process is shown in Figure 20. The sputter gun can be operated even at very low energies (< 1keV) to reduce the atomic mixing that an appropriate depth resolution can be achieved. Crater edge effects can be minimized by reducing the scanned area of the analysis gun (typically  $50 \times 50 \mu\text{m}^2$ ) compared to the sputter area (typically  $200 \times 200 \mu\text{m}^2$ ).

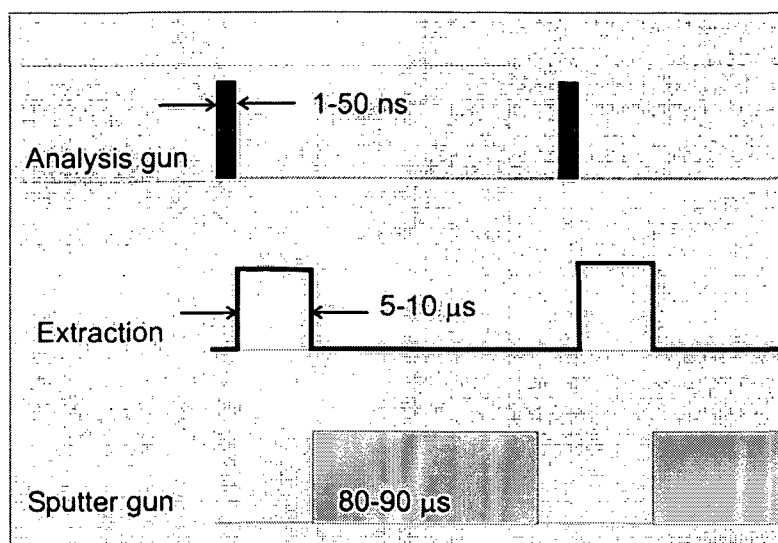


Figure 20. Time diagram for TOF-SIMS dual beam depth profiling.

### 2.2.3.3 Use of polyatomic primary ions

For the characterization of ultrashallow and abrupt dopant profiles as low energy implants or  $\delta$ -layers the use of polyatomic or cluster ions can be considered. For organic materials the use of a cluster ion beam can give large improvement in yield for characteristic secondary ions and can minimize beam-induced sample degradation. [35, 36, 37]

The polyatomic ion dissociates upon collision with the sample surface and each fragment retains a fraction of the initial beam energy. Often used ion species are  $SF_5^+$ ,  $C_xH_x^+$ ,  $CO_2^+$  or  $C_xF_x^+$  clusters. For ionization modified duoplasmatron sources can be used. The greatest disadvantage of the usage of polyatomic ions (especially  $SF_5^+$ ) is the contamination of the primary column and the sample chamber with reactive cluster fragments.

### 2.2.3.4 Interpretation of Mass Spectra

Due to the high mass resolution of TOF-SIMS instruments ( $m/z$  up to 20000) it is quite simple to identify peaks of complex organic molecules. Once an acquired organic spectrum is standardized to  $^{12}C$  (nominal mass: 12.0000) peaks can be identified and assigned to certain fragments with a spectra library, even if there are possible mass interferences. For example with a mass resolution of  $m/\Delta m$  of 1500 the peaks of  $^{55}Mn$  ( $m/z = 54,9380$ ) and  $C_4H_7^+$  ( $m/z = 55,0548$ ), which have both the same nominal mass of  $m/z = 55$ , are completely resolved.

The relationship between spectra of static SIMS and the chemical state of the surface is not straightforward as in XPS or AES. But because of the large number of molecular ions in TOF-SIMS spectra from multicomponent surfaces, chemical information is available in such spectra. The problem in using the information from a molecular ion is in the uncertainty of knowing whether or not the molecule represents the surface composition. A spectrum of an organic sample is shown in Figure 21.

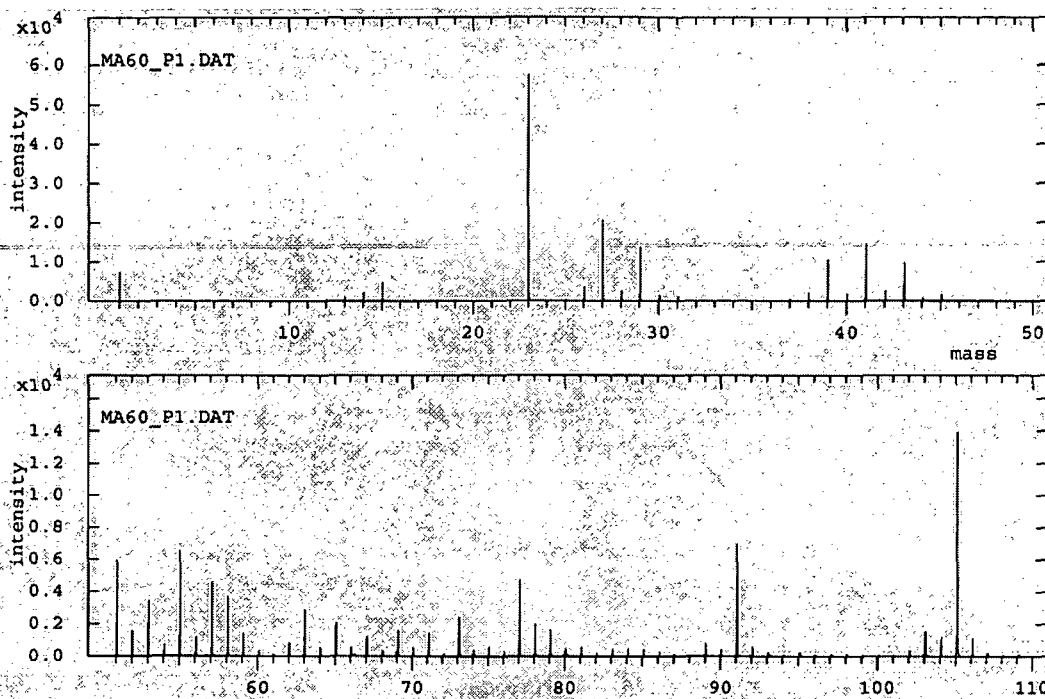


**Figure 21.** TOF-SIMS spectrum from the surface of an intraocular lens for eye surgery acquired with  $\text{Ga}^+$  primary ions at 25 keV impact energy.

All single peaks of the spectrum in figure 5 are identified with a library. A selection of these peaks is listed in Figure 22. The peaks are identified undisputable due to the mass resolution of  $m/\Delta m = 6000$  at this measurement.

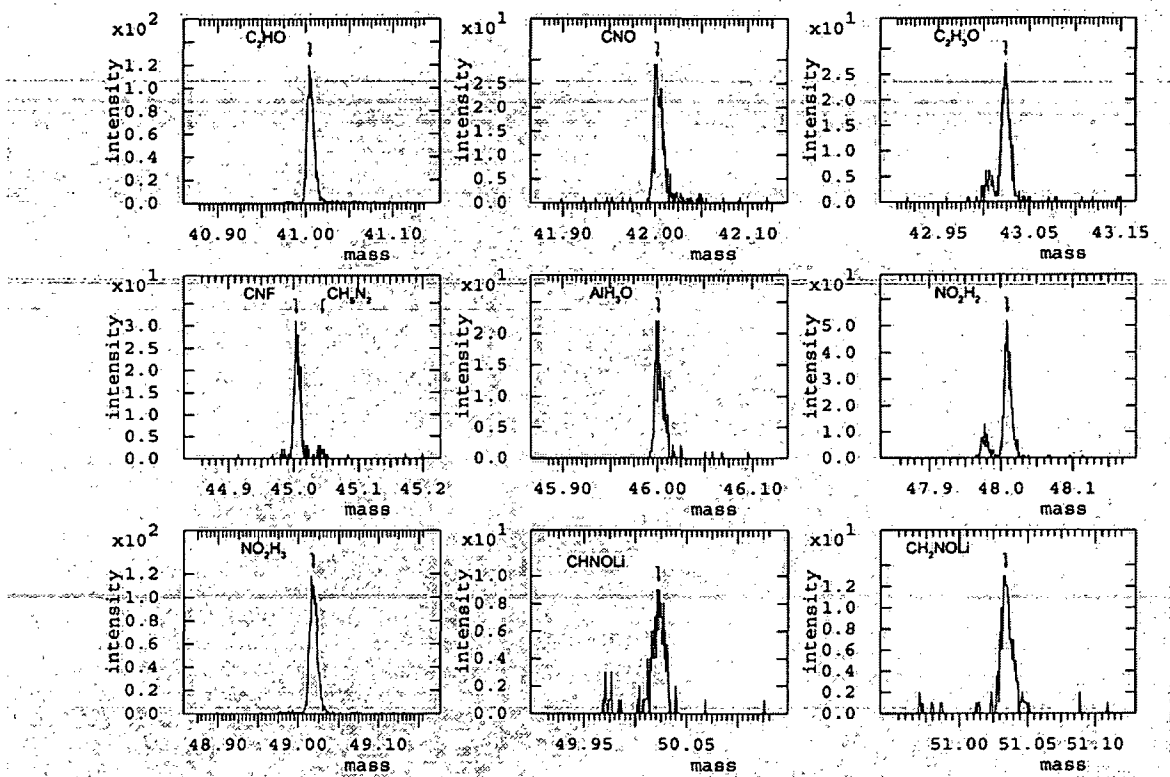


Figure 22. Peak identification performed with the "Static SIMS Library" [38]

For some materials such as polymers the observed clusters are characteristic for the material. Some examples are listed here:

- The peak of  $C_7H_7^+$  ( $m/z = 91$ ) hints to the presence of aromatic hydrogen fractures
- An intense peak of  $CF_3^+$  ( $m/z = 69$ ) can be observed at highly fluorinated polymers
- Peaks of  $CN^-$  and  $CNO^-$  are characteristic for N-containing polymers
- Series of  $m/z = 28, 73, 127, 207, 221$  and  $281$  indicates silicone rubber or silicone oil based on polydimethylsiloxane

### 3 OTHER SURFACE ANALYTICAL TECHNIQUES

For some scientific questions the capabilities of SIMS might not be sufficient. The following sections give a choice of surface analytical methods, which are necessary to gain additional information to SIMS data, when measurements with higher lateral resolution or reaction studies of samples under ambient conditions (liquid, reactive gases) are desired.

#### 3.1 *Atomic Force Microscopy (AFM)*

AFM, a variety of scanning force microscopy techniques, was invented by Binnig, Quate and Gerber in 1985. All scanning force techniques have the same principle: a sharp probe (e.g. a tip in AFM) is scanned across the sample surface by means of piezoelectric translators and the signal is recorded for every single probed point. AFM is a so-called near-field technique, since the apex of the tip and the distance between the tip and the surface is smaller than the wavelength of the analytical signal. Signal generation in AFM is based on interatomic repulsion forces, which are of extremely short range. In the ideal case it is assumed that the tip is terminated by one single atom. This direct contact with the sample surface is limited to an extremely small area (Figure 23). Although also long range attractive or repulsive forces (Coulomb, dipole-dipole interactions, van der Waals,...) contribute to the total force acting on the tip, high resolution imaging down to the atomic dimensions is only enabled by the repulsive interatomic forces. The interactions of the tip with the surface can be described with force-distance curves.

Another option to use an AFM is the tapping mode (TM-AFM), where the tip is driven near its oscillation frequency and the surface is measured under softer conditions. The resolutions of AFM are in the ideal case in the atomic range laterally and in the subatomic range in height.

The AFM can be operated in two modes, the constant force and the constant height mode. In constant force mode the deflection of the cantilever (with the tip) is held constant. Thereby the sample is readjusted in vertical direction according to the topographic features. In the constant height mode the vertical position is kept constant and the deflection of the cantilever is recorded. Higher scan rates can be reached in this mode, but large scan sizes can lead

to tip crashes with surface features. AFM does not require vacuum and can be operated also under liquid or reactive gases to study samples under ambient conditions.

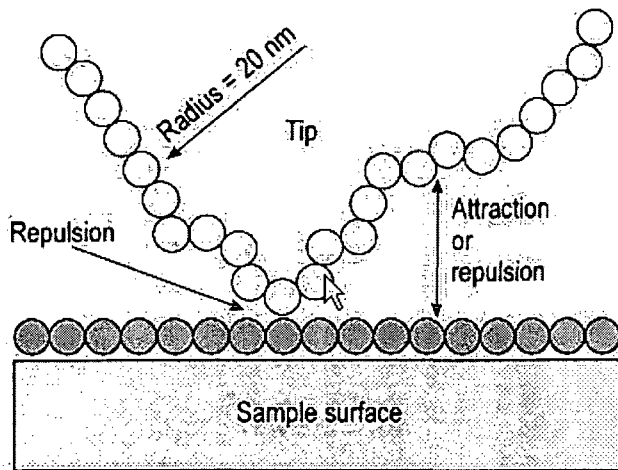


**Figure 23.** Ideal representation of an AFM tip. The tip is assumed to be limited by one single atom. Image is taken from [39].

An AFM consists of the following components (Figure 24): a sharp tip with a small radius of curvature mounted on a cantilever, which must be softer than the bonds between the sample atoms; a detection system to measure the cantilever deflection; a piezoelectric translator to move the sample; a feedback system to correct the deflection constant by height adjustment and an imaging system to convert the single measured data points into an image.

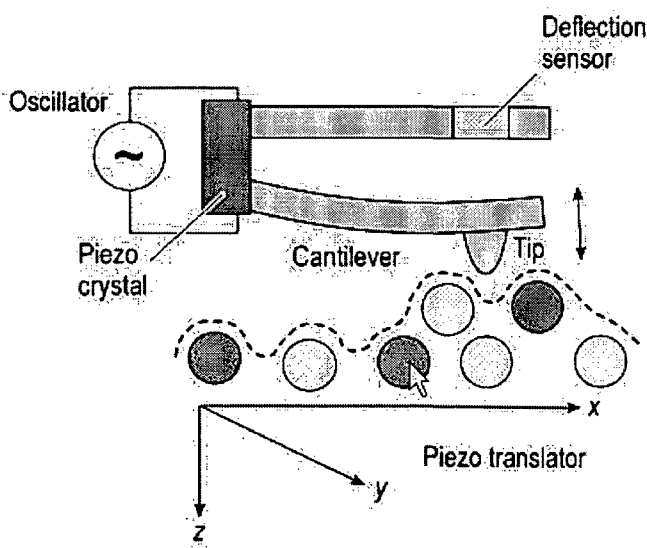


**Figure 24.** Set-up of an AFM instrument. Image is taken from [39]

### 3.2 Scanning Electron Microscopy (SEM)

SEM is one of the most commonly used surface analytical techniques. Its main advantages are a high lateral resolution and the possibility to quantify samples with moderate effort [40]. As the primary electron beam is scanned across the surface, electrons of a wide range of energies will be emitted from the surface in the region where the beam is incident. These electrons will include backscattered primary electrons and Auger electrons, but the vast majority will be secondary electrons formed in multiple inelastic scattering processes (these are the electrons that contribute to the background and are completely ignored in Auger spectroscopy).

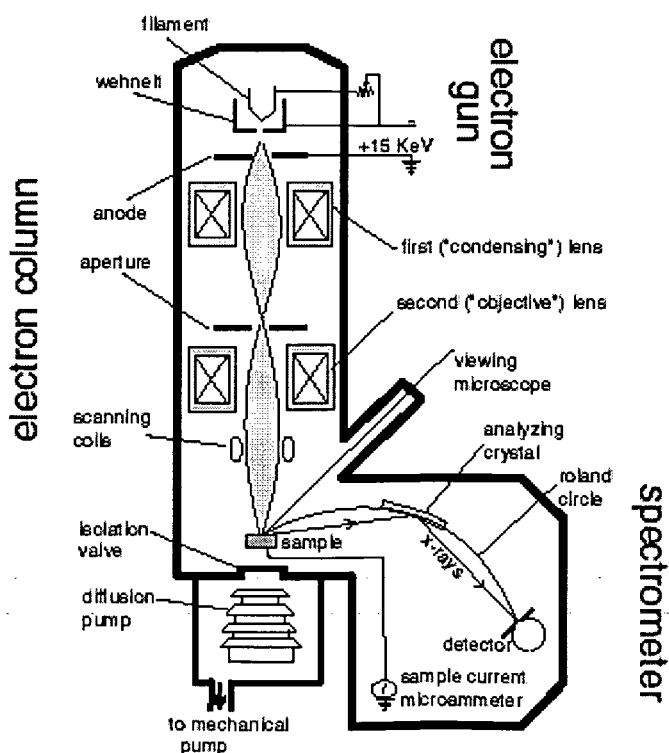


Figure 25. Set-up for an EPMA. Image is taken from [40]

The secondary electron current reaching the detector is recorded and the microscope image consists of a "plot" of this current according to the probe position on the surface. The contrast in the micrograph arises from several mechanisms, but first and foremost from variations in the surface topography. Consequently, the secondary electron micrograph is a virtual

direct image of the real surface structure. The attainable resolution of the technique is limited by the obtained minimum spot size of the incident electron beam, and ultimately by scattering of this beam as it interacts with the substrate. With modern instruments, a resolution of better than 5 nm is achievable.

To provide more information the characteristic X-rays, produced by excitation of the atoms with the electron beam, can be analyzed in an auxiliary energy dispersive detector (EDX). This method is called Electron Probe Microanalysis (EPMA) and is used for elemental identification analysis from boron to uranium. A typical instrumental setup for EPMA is shown in Figure 25. For quantification the dynamic range of this method is limited to 0.1%. By use of the scanning feature of SEM a spatial distribution in the micrometer range can be obtained, which fits well with the lateral resolution limits of SIMS.

### ***3.3 Auger Electron Spectroscopy (AES)***

Auger Electron Spectroscopy (AES) uses a primary electron beam with a range of typically 2 – 10 keV to probe the surface of a solid material. After ionization the surface atoms can relax either by ejection of a characteristic X-ray photon or by ejection of an Auger electron. The Auger process is explained in Figure 26 [41]. These Auger electrons are analyzed by determination of their kinetic energy. The identity and quantity of the elements are determined from the kinetic energy and intensity of the Auger peaks. Due to the low kinetic energy of Auger electrons they can only escape from the outer 5 - 50 Å of a solid surface. This effect makes AES an extremely surface sensitive technique. A finely focused electron beam can be scanned over the surface to create secondary electron and Auger images, or the beam can be positioned to perform microanalysis of a specific sample feature [42].

AES distinguishes itself by a high lateral resolution of 15 nm (Scanning Auger Microscopy, SAM) and by the possibility to analyze chemical species as the shape and the position of Auger peaks depend on the chemical state of the analyte. The electron beam energies used in SAM are higher (25 – 30 keV) than to conventional AES, because in this version the electron beam has to be as small as possible and can only be focused at such energies.

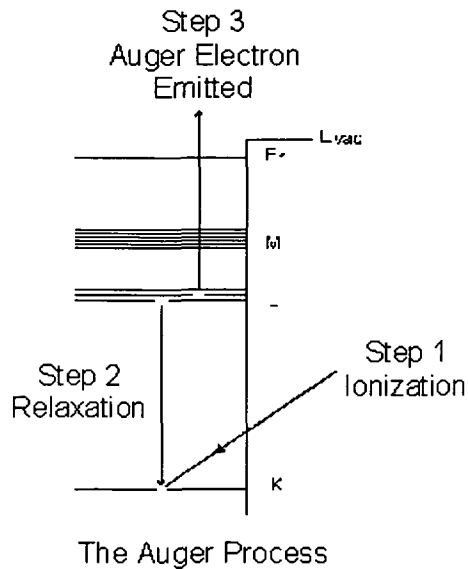


**Figure 26.** Emission of an Auger electron is induced by the drop of an electron to the vacancy after the excitation induced emission of a core electron. Image is taken from [41].

Quantification of AES measurements can be done with relative sensitivity factors (RSF) comparable to SIMS and XPS. RSFs include all the influences of the matrix and the measurement and can be derived empirically or non empirically. The typical detection limit of AES is in the percent range. This high limit is due to secondary and backscattering electrons which are superimposed to the Auger electrons.

AES and SAM are excellent techniques to complete the capabilities of SIMS, when SIMS is not sufficient regarding to lateral resolution and information on the chemical state. AES also provides the possibility to perform depth profiles by using an independent ion beam of  $\text{Ar}^+$  ions to sputter the sample surface. Preferential sputtering of light elements causes surface enrichment effects and distorts the quantification of such depth profiles.

## 4 APPLICATIONS FOR SIMS

### 4.1 Improvement of Depth Resolution by Convolution

3 samples with alternating layers of varying compositions of Si and Ge layer have been characterized with SIMS. The nominal composition was (top-down):

- 10 nm Si capping
- 50 nm 75%Si/25%Ge
- a channel of 12 nm with lowered Ge content (0%, 5%, 10%)
- 5000 nm 75% Si/25% Ge

The measurement of such samples is a challenge for SIMS, because the thickness of the channels with lowered Ge concentration is within the depth resolution limit of the method. Figure 27 shows the SIMS depth profiles of these 3 multilayer samples.  $O_2^+$  primary ions at 5.5 keV with a primary current of 30 nA have been used to sputter the surface. The diameter of the analyzed area was reduced to 60  $\mu\text{m}$  (instead of 150  $\mu\text{m}$ ) to avoid crater edge effects, which will deteriorate the depth resolution.

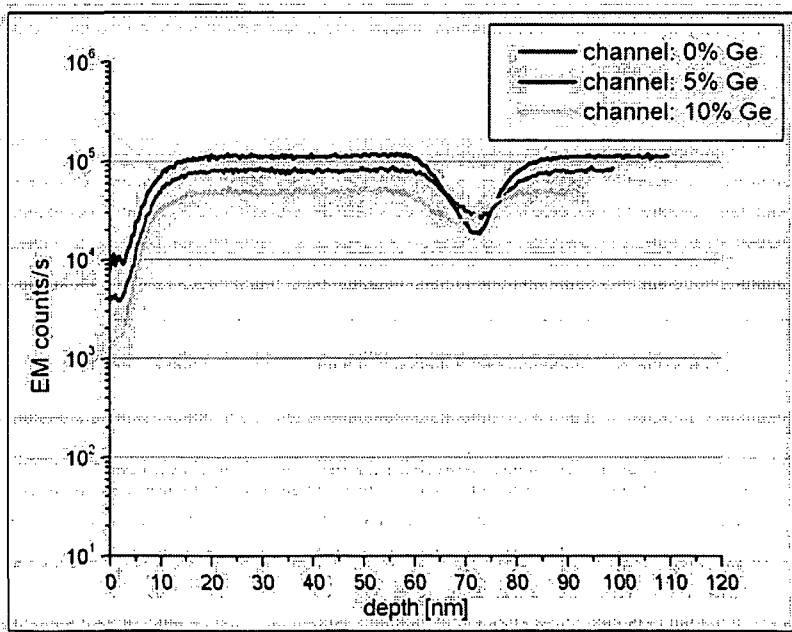


Figure 27. SIMS depth profiles of SiGe samples (primary ions:  $O_2^+$ @5.5keV). The channels in the samples should give sharp interfaces, but they are distorted due to atomic mixing induced by the high energy primary beam.

SIMS measurements of ultra-thin layers exhibit the major problem of profile distortion due to the atomic mixing induced by primary ion bombardment. Mathematically this distortion can be explained as a convolution of the real nature of the sample with a SIMS response function.

To determine the SIMS response function  $\delta$ -layer samples are used. The Ge monolayer is buried under a capping layer of Si (nominal depth: 50nm). This capping layer is essential to gain a sputter equilibrium until the  $\delta$ -layer is reached during the depth profiling. The obtained SIMS depth profile of these  $\delta$ -layers is used as response function of the SIMS-instrument [43] and has to be measured under the same conditions as the sample (Figure 28).

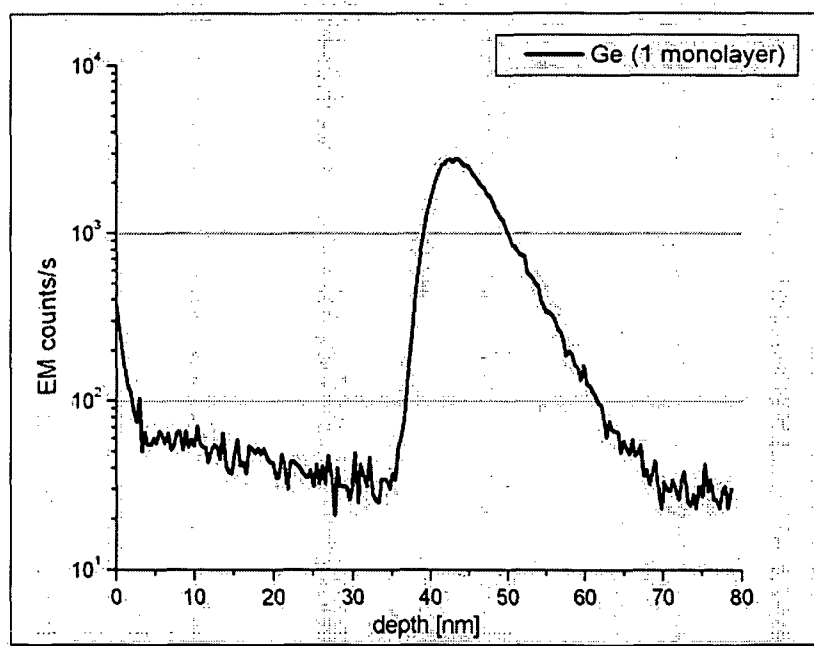
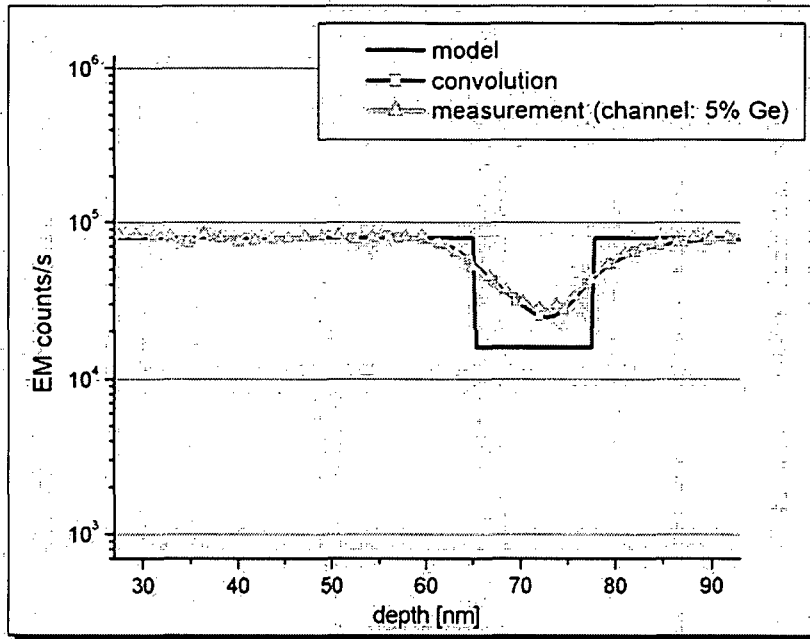


Figure 28. Depth profile of Ge- $\delta$ -layer sample. primary ions:  $O_2^+$ @5.5keV

An inverse modeling of the distorted SIMS profiles was made by convolving an assumed undistorted diffusion profile (=model profile) with the SIMS response function. For this procedure the profile of the Ge- $\delta$ -layer was normalized and then convolved with the model profile point by point. The resulting convolution was fitted to the measured Ge slope trying to vary parameters until the best match of both graphs was reached. Additionally the background level of each measurement (Ge:  $\sim 100$ cps) was added to each data point of the convo-

lution. The result for one sample (Ge concentration in the channel: 5%) is displayed in Figure 29. The depth of the Ge channel is at 65 nm and its width is 12 nm. These results show a good agreement with RBS measurements (depth: 63 nm, width: 12.4 nm). So this convolution procedure is an acceptable method to increase the depth resolution of SIMS at high primary voltages without changing the instrument parameters.



**Figure 29.** Demonstration of the convolution procedure. A model is convolved point-to-point with the SIMS response function ( $\delta$ -layer) and modified until the best agreement with the measured profile is achieved. The channel width is determined with 12 nm (RBS: 12.4 nm)

## 4.2 TOF-SIMS studies of modified polymer surfaces

Polyolefines are limited in their application in technology due to their low surface energy, lack of chemical functionalities, sensitivity to photo- or thermal oxidation, and inadequate compatibility with other synthetic polymers [44]. Grafting of aromatic azides is a possible workaround to improve the properties of such polymers. Figure 30 shows the scheme of the grafting process of these aryl-azides on polypropylene surfaces with  $R = (\text{CH}_2)_5\text{-CH}_3$  in the functional group. The aim of these TOF-SIMS studies was to clear, if only single monomers of the aryl-azide or polymerized aryl-azides are grafted onto the surface.

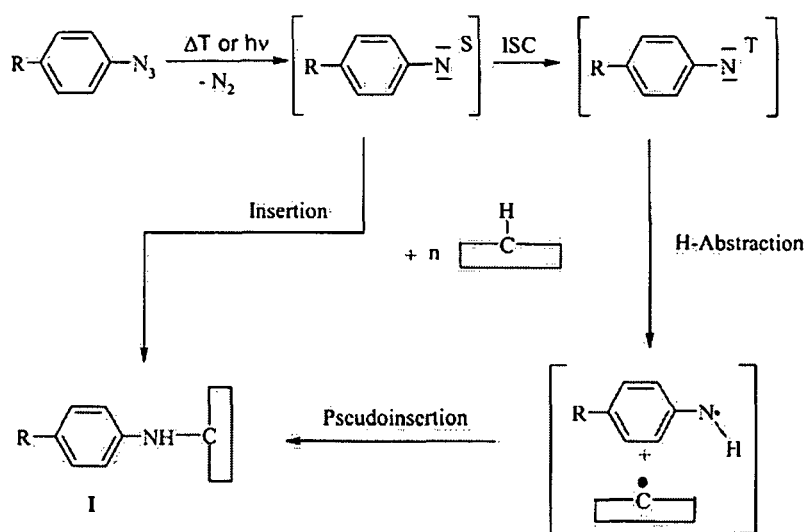
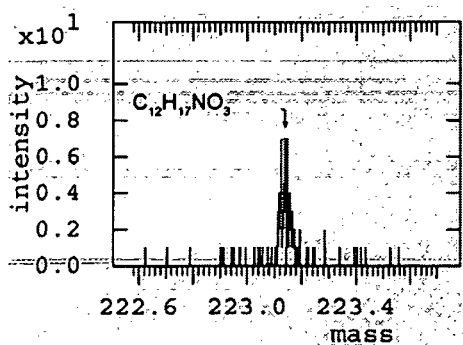


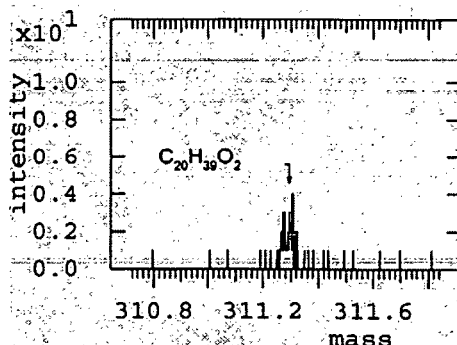
Figure 30. Schema of the grafting reaction.

As a result of this grafting process the surface modified polypropylene exhibits improved properties due to their stability against irradiation with light and to its wettability.

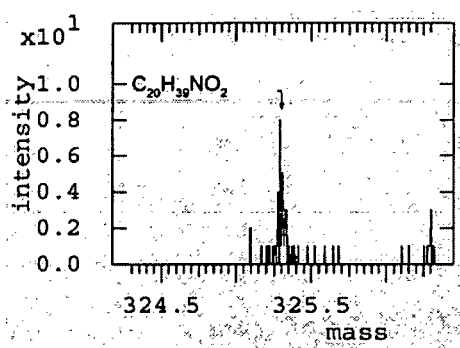
The TOF-SIMS measurements have been performed with an ION-TOF IV (ION-TOF, Münster, D) by bombarding the surface with  $\text{Ga}^+$  primary ions at 25 keV impact energy.  $\text{Ga}^+$  ions have the advantage of producing high molecular fragments of the surface coating, which allow an easy recalculation of the original substances. Figure 31 shows selected peaks from the negative TOF-SIMS spectrum, which hint to the composition of the uppermost surface layer.



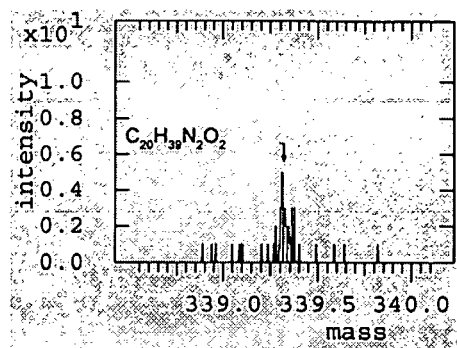
(a)



(b)



(c)



(d)

Figure 31. Peak identification spectra library [38]

The peak  $m/z = 223$  (a) can be associated with the monomer of the grafted aryl-azide as described above.  $m/z = 311$  (b) has a difference of 80 amu to peak  $m/z = 223$ , what hints to possible side branches on the original azide issuing from additions during the grafting process. Each of the peaks  $m/z = 325$  (c) and  $m/z = 339$  (d) has a difference of 14 amu according to the respective lower one. The mass difference corresponds to the fragment  $CH_2$ .

### ***4.3 New developments in PVD Sputter Coating***

PUBLICATION I

**Characterization of the Interface of sputter deposited Copper Coatings on Nitrogen Plasma treated Carbon Substrates.**

submitted to: Analytical and Bioanalytical Chemistry

# CHARACTERIZATION OF THE INTERFACE OF SPUTTER DEPOSITED COPPER COATINGS ON NITROGEN PLASMA TREATED CARBON SUBSTRATES

M. Rosner<sup>1</sup>, E. Neubauer<sup>2,3</sup>, Ch. Eisenmenger-Sittner<sup>2</sup>, H. Bangert<sup>2</sup> and H. Hutter<sup>1\*</sup>

<sup>1</sup> Vienna University of Technology, Institute for Chemical Technologies & Analytics, Div. Analytical Chemistry, A-1060 Wien, Getreidemarkt 9/E164

<sup>2</sup> Vienna University of Technology, Institute of Solid State Physics, A-1040 Wien

<sup>3</sup> ARC Seibersdorf Research, Dept. Materials & Production Engineering, A-2444 Seibersdorf

\* corresponding author: h.hutter@tuwien.ac.at

## ABSTRACT

The adhesion of copper coatings on carbon substrates is very poor. This is a result of the lack of diffusion or reaction between both constituents. Since there is a technological interest to enhance the adhesion and to improve the interface between copper and carbon, a plasma treatment of the carbon substrate was employed in this study. For the modification of the carbon surface a nitrogen plasma was used. It was confirmed by pull-off tests, that by the introduction of the plasma pre-treatment the adhesion strength of the copper coating can be improved by a factor of more than 10. This was already achieved after a very short time of treatment (1 minute).

In order to get more information about the mechanisms which take place at the interface SIMS investigations were performed on samples which were treated for different times (between 1 and 60 minutes). These measurements confirmed that nitrogen is localised at the interface. With increasing pre-treatment time the amount of nitrogen, which is detected at the interface, is increased.

Beside the characterisation of as deposited samples, another focus was to study the diffusion mechanisms of nitrogen if the samples are heat treated at 500°C.

Keywords: PVD, SIMS, adhesion, nitrogen-plasma

## INTRODUCTION

The optimisation of copper coatings on carbon substrates is of interest for various fields in material research. Especially composite materials, such as copper reinforced with carbon fibres, are of interest for applications as heat sink components in electronic or future fusion reactors or tribological applications [1-5]. Production routes for such composite materials are

based on coating of fibres followed by a consolidation process. Currently the weak interface between the electrochemical deposited copper coating and the carbon fibres limits the use of the material. The approach of using a PVD process instead of the electrochemical deposition process requires basic studies of the interfacial area between the coating and the substrate. One of these concepts follows the plasma pre-treatment of the substrate prior to the deposition of the copper coating in order to enhance the adhesion strength of the copper coating and to reduce the thermal interfacial contact resistance.

For the analysis of the interface SIMS was used in order to follow the behaviour of nitrogen as a function of pre-treatment time before and after the heat treatment of the coating-substrate composite. As an additional tool AFM was employed to characterise the surface topography of the coating after the heat treatment.

## **EXPERIMENTAL**

### **Sample Preparation**

For the characterisation of the interface and the influence of a nitrogen plasma, samples were prepared by sputter deposition of a copper layer on a glassy carbon substrate [6]. An Alcatel sputter deposition equipment was used [7]. The set-up for the pre-treatment of carbon substrates by a plasma consists of a hollow cathode which allows to get a localised plasma with a high density in a certain region inside the deposition chamber. The plasma system is made of two concentric cylinders of stainless steel. The outer cylinder is grounded and insulated from the inner cylinder by  $\text{Al}_2\text{O}_3$  ceramic insulators. A grounded outer cylinder helps to avoid the ignition of a plasma outside of the barrel and to get higher densities inside the cathode. The hollow cathode can be driven by a DC or RF power supply. The RF mode is realized by a Hüttinger RF generator with a maximum RF power of 600 W and a corresponding matching network.

Immediately after the plasma pre-treatment of the carbon substrate the deposition takes place in the same chamber just by moving the sample to the deposition place. The deposition parameters for the copper layer and the plasma pre-treatment parameters can be found in table 1 for the investigated samples.

One sample series was investigated by SIMS method immediately after the deposition of the sample in order to get knowledge about the element distribution – especially nitrogen, oxygen, copper and carbon - at the interfacial area. A second sample series was subjected to a heat treatment at 500°C. The reason why selecting this temperature is given by two reasons: the first reason is related to the fact that a hot pressing process is currently used for the con-

solidation of the copper coated carbon fibres. So to get the information what will happen if nitrogen pre-treated copper coated carbon fibres will be compacted, a heat treatment was applied to the coated plane model substrates. The second reason why a temperature of only 500°C was chosen together with a short holding time for the heat treatment is related to a dewetting of the copper coating which starts at higher temperatures (~600°C) [8] and which would influence the results of SIMS measurements. The conditions of the heat treatment were heating rates of 10°C per minute to 500°C, a holding time of 5 minutes and cooling down of the samples at 10°C per minute.

### **Setup for SIMS investigation**

The SIMS investigation were carried out with an upgraded Cameca IMS 3f (Cameca, Courbevoie, F). Cs<sup>+</sup> ions at 5.5 keV with a current of 50nA have been used as primary ions. The primary beam was rastered over an area of 256 x 256 μm<sup>2</sup>, while the sputtered secondary ions were collected from an area with a diameter of 150μm. The instrument parameters are listed in table 2. The intensity of the SIMS signal shows a high dependency of the sputtered matrix and it is essential for the analysis of these samples (two totally different matrices) to avoid this matrix effect. It can be considerably suppressed by the analysis of cesides as secondary ions. Ceside ions are formed by the recombination of ions from the analyzed material with emitted Cs<sup>+</sup> ions implanted by the primary beam [9]. The analyzed species were CsC<sup>+</sup>, CsN<sup>+</sup>, CsO<sup>+</sup>, and CsCu<sup>+</sup>.

The calibration of the depth scale was done by measuring the depth of the sputtered crater with a Dektak II surface profilometer. To take into account the different sputter rates in both matrices the sputtering process was stopped at one sample before the Cu/C interface was reached. With the measured depth of this Cu-crater the sputter rate for the Cu coating could be calculated. The sputter rate of the carbon substrate was determined by evaluating the depth differences of two craters sputtered at the same sample. With these so determined values the x-axis was transformed from time values to depth values.

## **RESULTS & DISCUSSION**

### **SIMS investigations before the heat treatment**

In the samples which were characterised by SIMS method immediately after the deposition a well defined copper-carbon interface is visible (Fig 1). This is related to the very smooth carbon substrate ( $R_a \sim 1$  nm) which was used for the investigation [10]. In the case of copper coatings on untreated carbon substrates no nitrogen was detected at the interface (Fig.2), only a small peak of oxygen which is due to the oxygen in the residual gas (Fig 3). The carbon signal

appears sharp while the copper signal slowly fades out when coming to the interface. This may be attributed to the fact that the sputter rates for copper and carbon are very different and some intermixing may occur. While copper results in a higher sputter yield, carbon is very hard to remove from by the  $\text{Cs}^+$  ions. The sharp interface between the copper coating and the carbon substrate was already characterised in a former work by TEM measurements of the interface [8]. An interface zone in the range of some nanometers was found (~3-5 nm).

By increasing the time of the plasma pre-treatment (from 1 to 60 minutes) the peak height of nitrogen increases. As can be seen from Fig. 2, nitrogen is also found in the copper layer. This can be explained by the sample preparation process which uses nitrogen gas for the plasma pre-treatment of the carbon substrate, followed by a copper sputtering process in which Argon gas is used. Of course after the nitrogen plasma pre-treatment there is still nitrogen gas in the recipient which is successively incorporated into the copper layer during the growth of the copper film. In a similar way the amount of oxygen at the interface is increased with increasing nitrogen plasma pre-treatment time. The oxygen found in the copper-substrate interface is also related to impurities in the recipient. The nitrogen content found at the interface is increased with increasing plasma-pre-treatment time, especially during the first 5 minutes a strong increase is observed (Fig. 4).

AFM was used to determine the surface topography after the plasma pre-treatment as well as after the deposition of the copper coating. Immediately after the plasma pre-treatment the surface roughness was characterised by line scans as a function of the treatment time. Line scans showed that a slight increase of the roughness parameter after one minute is observed.

The characterisation of the copper coatings after the deposition showed no increase in surface roughness.

#### **SIMS investigations after the heat treatment**

After the heat treatment of the copper-carbon samples the nitrogen peak (Fig. 5) at the interface is broadened (mainly in direction to the copper coating). The shape of the signals for all plasma-treated samples is similar but the maximum peak height is lower compared to the samples prior to the heat treatment. From the integration of the nitrogen signals over the whole layer thickness it can be concluded that the total amount of nitrogen in the copper-carbon sample is the same.

AFM investigations of the copper layers after heat treatment (Figs 6a-d) show a smooth surface. After 60 minutes of heat treatment first areas of de-wetting were observed (Fig 6d). This explains also the higher carbon signal in this sample #410A because there are areas where the carbon substrate is visible and already sputtered by SIMS from the beginning of the measure-

ment (Fig 7). The roughness of the layers increases with increasing plasma treatment (Fig.4) time due to some copper clusters visible on the coating and starting of de-wetting. The grain size of the copper layer is clearly visible and found to be in the range of 2-3  $\mu\text{m}$  in the case of untreated and shortly plasma treated substrates while after longer treatment times the grains seem to be larger. Longer plasma pre-treatment does not result in well defined grain boundaries and leads either to copper cluster or to de-wetted areas.

## CONCLUSION

The results of this experimental work can be summarized in the following way:

- The pre-treatment of carbon substrates by a nitrogen plasma results in the as deposited stage in a higher adhesion strength of the coating. This can be explained by a chemical modification of the carbon surface together with a slight topographical modification (increased surface roughness)
- Nitrogen is found at the interface both in the as deposited and heat treated samples. The heat treatment leads to a nitrogen diffusion towards the copper free surface, but a temperature of 500°C for 5 minutes seems to be a too low to result in a reduced nitrogen amount in the copper layer. The detected nitrogen amount at the interface and in the copper layer increases with increasing plasma pre-treatment time strongly between zero and five minutes and reaches at longer treatments a level of saturation.
- Out of these results it is obvious that a nitrogen plasma pre-treatment influences the element distribution at the interface as well as the surface topography of the copper coating. By comparing the investigation of SIMS and AFM results before and after heat treatment, a short pre-treatment between one and five minutes is preferable with respect to the adhesion of the coating and the surface topography after heat treatment.

## ACKNOWLEDGEMENT

This work was supported by the Austrian Scientific "Fonds zur Förderung Wissenschaftlicher Forschung" (grants P14534-PHY, and P15116).

## TABLES

Table 1: Nitrogen Plasma Pre-Treatment and Copper Deposition Parameters

	Nitrogen Plasma Pre-Treatment		Copper Deposition
Pressure [Pa]	44	Ar Pressure [Pa]	0.4
RF Power [W]	50	Power [W]	300
Plasma Treatment Time [min]	60 (#410A)	Deposition rate [nm/min]	~1.7 nm/s
	30 (#411A)	Coating Thickness [nm]	500
	15 (#412A)		
	5 (#413A)		
	1 (#414A)		
0 (#415A)			

Table 2: Parameters for the SIMS measurements

Instrument	CAMCEA IMS 3f
Primary ions	Cs <sup>+</sup> @5.5keV
Primary intensity	50 nA
Rastered area	256 μm x 256 μm
Diameter Analyzed area	150 μm
Analyzed species	CsC <sup>+</sup> , CsN <sup>+</sup> , CsO <sup>+</sup> , CsCu <sup>+</sup>

# FIGURES

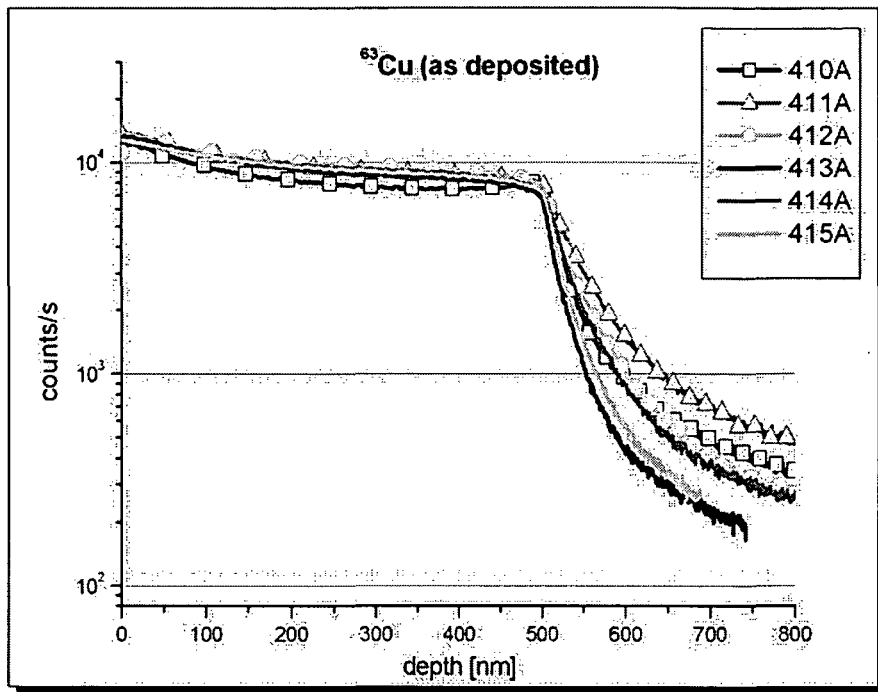


Fig 1: Copper Signal as a function of depth

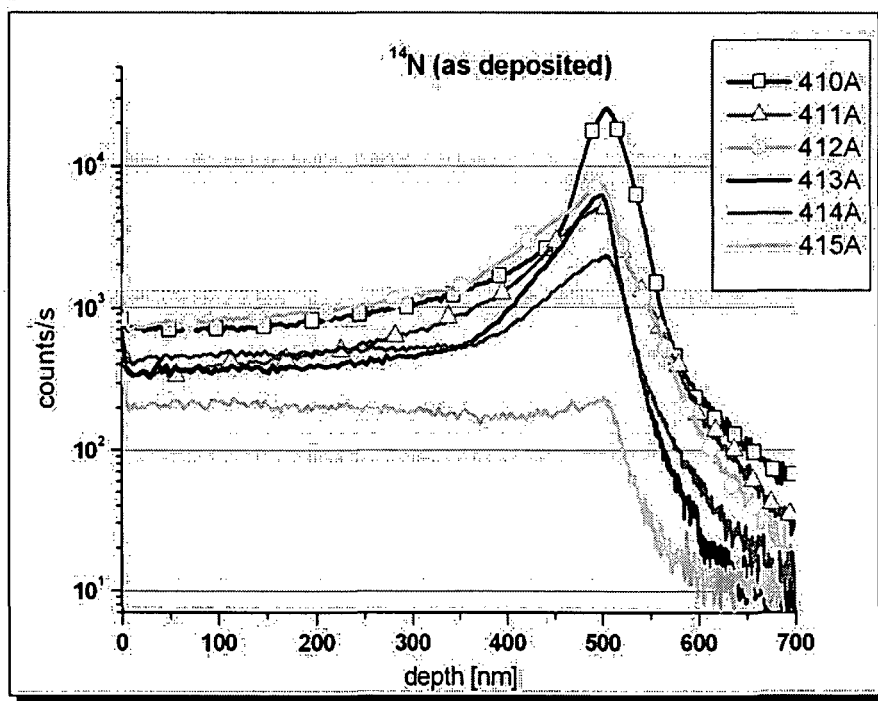


Fig 2: Nitrogen Signal as a function of depth

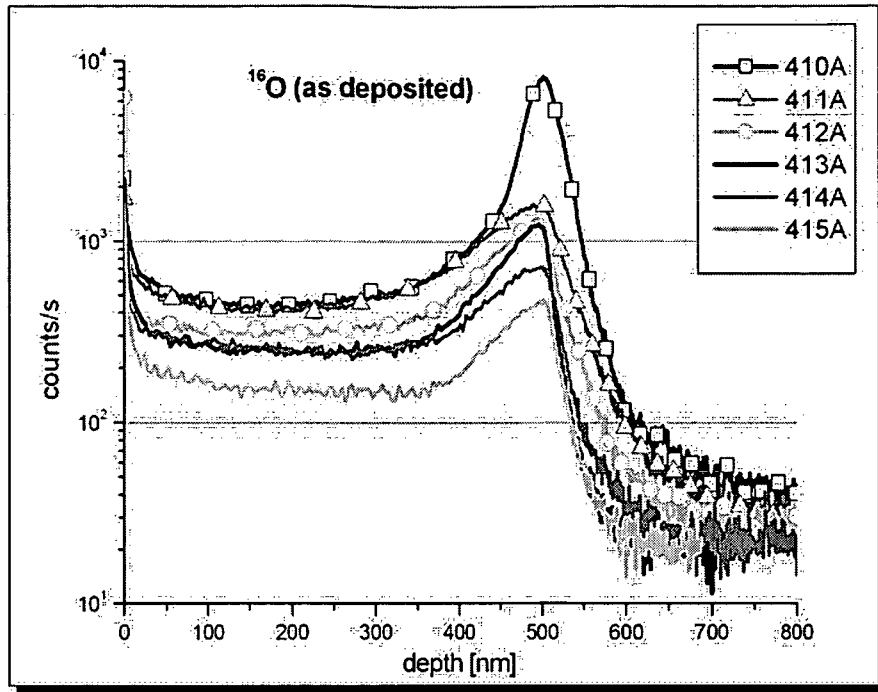


Fig 3: Oxygen signal of the as-deposited samples.

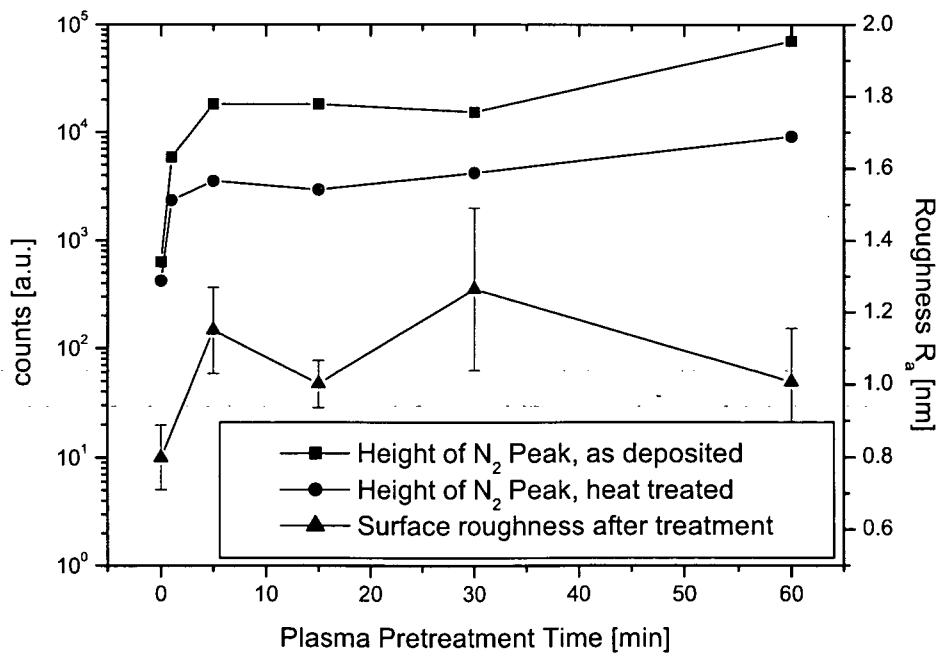


Fig. 4: Maximum values (electron multiplier counts from SIMS) of the N peaks at the C-Cu interface depending from the treatment time and surface roughness of the samples after plasma treatment

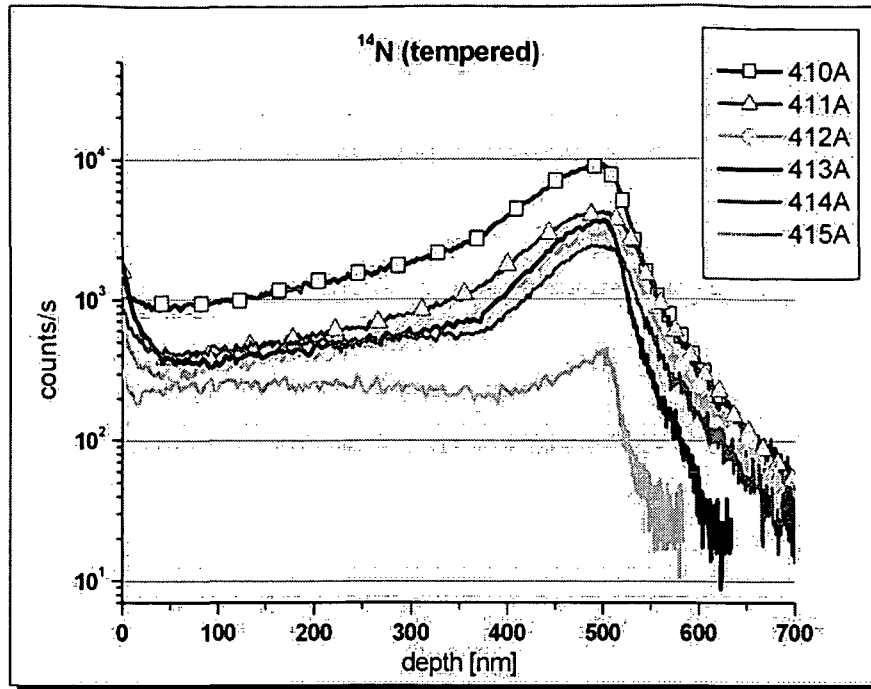
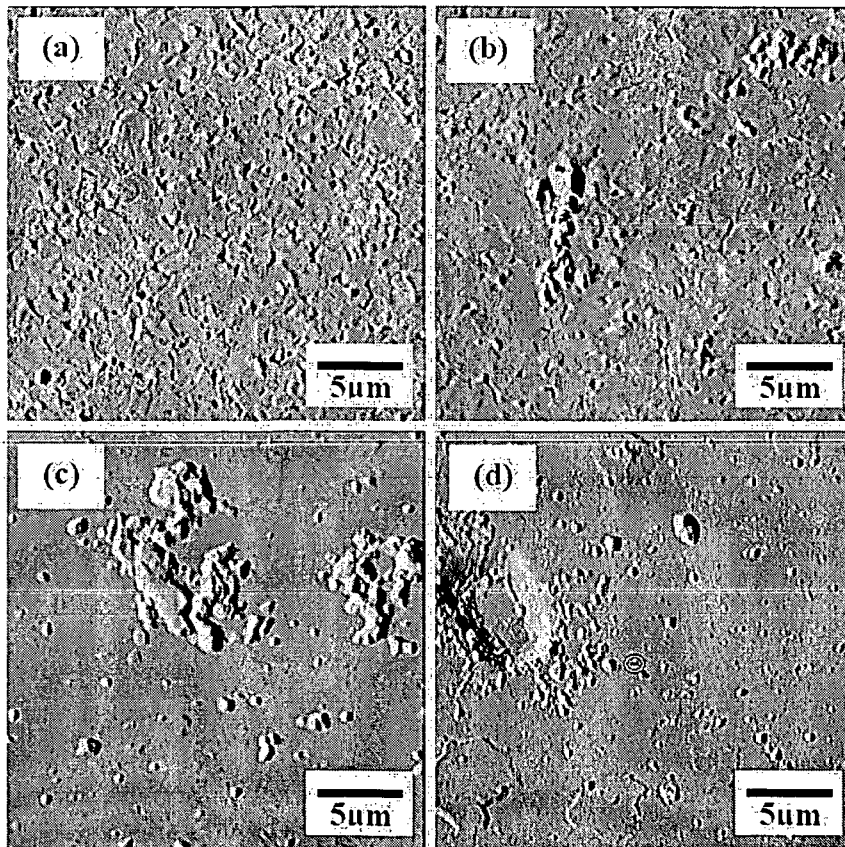


Fig 5: Nitrogen Signal as a function of depth (after heat treatment)



Figures 6 a-d: AFM image of a 500 nm thick copper layer on nitrogen plasma pre-treated carbon substrates (a) untreated (415A), (b) 1 minute (414A), (c) 15 minute (413A), (d) 60 minutes (410A)

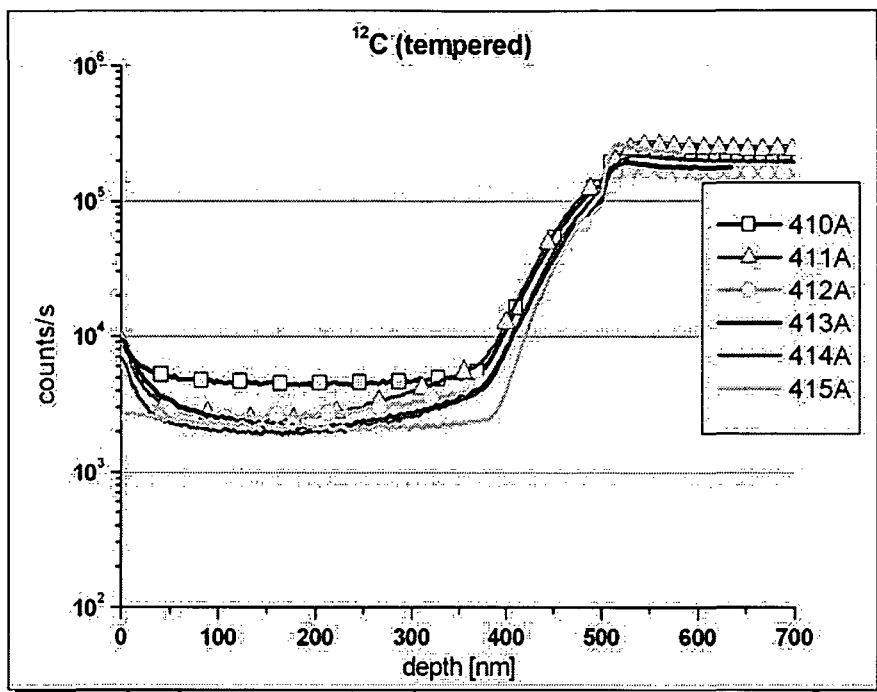


Fig 7: Carbon Signal as a function of depth (after heat treatment). The de-wetted area of sample 410A (N treatment 60min) cause the increase of the C-signal in the Cu coating (0 – 500 nm).

## REFERENCES

- [1] Devinent SM, Michal GM (1993) *Journal of Materials Engineering Performance* 2(3): 323-31.
- [2] Petitcorps YL, Poueylaud JM, Albingre L, Berdeu B, Lobstein PO, Silvain JF (1997) *Key Engineering Materials* 127-131:327-334
- [3] Wan YZ, Wang YL, Luo HL, Dong XH, Cheng GX (2000) *Mat.Sci. & Eng. A288* (1): 26-33
- [4] Oku T, Kurumada A, Sogabe T, Oku T, Hiraoka T, Kuroda K (1998) *Journal of Nuclear Materials* 257: 59-66
- [5] Moustafa SF, El-Badry SA, Sanad AM, Kieback B (2002) *Wear* 253 (7-8): 699-710
- [6] Leaflet HTW Hochtemperaturwerkstoffe GmbH (data-sheet available on [www.htw-germany.com](http://www.htw-germany.com), online August 2003)
- [7] Rosner M, Eisenmenger-Sittner C, Hutter H (2000) *Microchim. Acta* 133: 267-271
- [8] Eisenmenger-Sittner C, Neubauer E, Schrank C, Brenner J, Thomastik C *Thin Solid Films*: accepted for publication
- [9] Gao Y (1988), *J. Appl. Phys.* 64(7): 3760-3762
- [10] Neubauer E, Eisenmenger-Sittner C, Bangert H, Korb G (2003) *Vacuum* 71 (1-2): 293-298.

#### ***4.4 Conservation of Cultural Heritage***

##### **PUBLICATION II**

**SIMS and TM-AFM studies on weathered Cu, Zn, and brass (CuZn10, CuZn30) surfaces**

Journal of Trace and Microprobe Techniques (2003), 21(1), 49-62

##### **PUBLICATION III**

**Influence of increasing zinc contents in brass in the early stages of corrosion investigated by in-situ TM-AFM and SIMS**

Analytical and Bioanalytical Chemistry (2002), 374(2), 338-343

# SIMS AND TM-AFM STUDIES ON WEATHERED Cu , Zn AND BRASS- (CuZn10, CuZn30) SURFACES

Martin Rosner<sup>1</sup>, Christoph Kleber<sup>1,2</sup>, Manfred Schreiner<sup>2</sup>, Herbert Hutter<sup>1,\*</sup>

<sup>1</sup>Institute for Chemical Technologies and Analytics, Vienna University of Technology, Getreidemarkt 9, A-1060 Vienna, Austria

<sup>2</sup>Institute of Sciences and Technologies in Art, Academy of Fine Arts, Schillerplatz 3, A-1010 Vienna, Austria

\* for correspondence and reprint requests (h.hutter@tuwien.ac.at)

## Abstract

Polished samples of Cu, Zn and two brasses (CuZn10 and CuZn30) have been treated in synthetic air with 80% relative humidity (RH) and alternatively with 250 ppb SO<sub>2</sub> added to the moist air stream in a weathering box. Depth profiles of the corroded surfaces were made with dynamic-SIMS and the courses of the S- and O-signals were traced. The decay of the S- and the O-signal exhibited different behavior. While the O-signal decreased continuously through the corroded layer, the S-signal decreased much faster until it reached the background level at the half of the thickness of the altered layer. Surface features could be found with comparative TM-AFM- measurements that confirmed these SIMS results. The height of these features (measured with TM-AFM) matched with the determined thickness of the S enriched layer.

## Keywords

SIMS, TM-AFM, Weathering, Brass, Corrosion

## Abbreviations

SIMS, Secondary Ion Mass Spectrometry; TM - AFM, Tapping Mode Atomic Force Microscopy; RH – relative humidity

## INTRODUCTION

Brass alloys are used as material for industrial application (CuZn30) as well as for jewelry and for works of art (CuZn10) for a long time. With regard to the preservation

of cultural heritage and to suppress the corrosion of such works it is essential to get knowledge about the oxidation processes in the uppermost layers of brasses.

For this purpose two brasses Cu/Zn = 70/30 wt% (= CuZn30) and Cu/Zn = 90/10 wt% (= CuZn10) and the pure metals Cu and Zn have been investigated due to their oxidation behavior under humidified air (RH = 80%) and under humidified air with 250 ppb SO<sub>2</sub> added.

Secondary Ion Mass Spectrometry (SIMS) and Tapping Mode Atomic Force Microscopy (TM-AFM) are methods of choice for such investigation. The formation of surface features and their lateral information could be observed with in-situ TM-AFM where the head of the microprobe was used as a weathering chamber in order to adjust specific humidity and gas concentrations [1]. The SIMS depth profiling could determine the thickness of the O- and S- enriched layers ex-situ after the incrustation of the liquid corrosion products on the uppermost regions of the surface. The imaging mode of SIMS provides a lateral resolution of 1 μm. This scale is insufficient to image the corrosion products (diameter 200 – 400 nm) growing on these metal and alloy surfaces.

The SIMS-depth-scan signal is an average value across the analyzed surface area (150 x 150 μm<sup>2</sup>) and so it cannot be distinguished if it stems from higher or lower surface features. This disadvantage of SIMS is compensated by TM-AFM in this measurements, which provides topographical information.

## MATERIALS AND METHODS

### Samples and Sample Preparation

The used pure metals Cu and Zn (Johnson Matthey, France) and the brass alloy CuZn30 (Alfa AESAR, Austria) each had a thickness of 0.5 mm and trace impurities of max. 25 ppm. The CuZn10 was put for our disposal by Enzesfeld CARO Metallwerke AG, Austria, and had a composition of 90.42% Cu and 9.58% Zn.

The metal samples (∅ 10 – 15 mm) were abraded with SiC paper (Struers grit 1200 up to grit 4000) and polished with 1 μm and 0.25 μm diamond paste (Struers DP). Then the samples have been cleaned ultrasonically in absolute ethanol and were dried with a lint-free tissue to remove polishing particles.

For the corrosion process a setup as shown in Fig.1 was used. A flow of dry synthetic air (Messer Griesheim, Austria, purity 5.0, hydrocarbon-free) is divided into two separate flows. One stream was humidified in a bottle filled with distilled and

deionized water (generated with a Milli-Q<sup>®</sup> ultrapure water system from MILLIPORE) and then joined with the untreated airflow to an airflow with 80% relative humidity (RH). For the first series the four metal samples have been treated with the pure humidified air and for the second series after abrading and cleaning as described above 250 ppb SO<sub>2</sub> was added to the humidified airflow. As weathering chamber a top-hat-vessel with a base radius of 35 mm and a height of 70 mm fitted with gas in- and outlets was used. The weathering time was 60 h per series at an air stream of 40 l/h resulting in a dwell time of approximately 24 seconds. As the SIMS-investigations were carried out ex-situ, this time was chosen to ensure a sufficient thickness of the corrosion layers formed. Complementally, in-situ measurements using TM-AFM were carried out within 20 h of weathering with the same set-up as described in [2]. All four samples have been weathered simultaneously to provide the same flow conditions at each type of corrosion experiment (moist air and moist air with SO<sub>2</sub>).

Blank test with untreated metals have not been carried out in these investigations as is a well known fact and described in [2] that the pure Cu is naturally covered with Cu<sub>2</sub>O. All used metals and brasses have a purity of 99.999% with well defined inclusions. Furthermore a quantification of the depth profiles is not possible, because of missing well defined standard materials (expensive), and not necessary, because not the absolute concentrations of S and O, but the influence of the Zn concentration relatively to the pure metals has been investigated.

### SIMS Setup

The SIMS-depth profiles were carried out with a modified CAMECA IMS 3f with an O<sub>2</sub> and a cesium fine focus source [3]. Cs<sup>+</sup> ions with a primary ion energy of 14.5 keV and an ion intensity of 10 nA were used as primary ions. Only the ceside secondary ions (m/z > 133) e.g. Cs<sup>16</sup>O<sup>+</sup> (m/z = 149), Cs<sup>34</sup>S<sup>+</sup> (m/z = 165) with positive polarity were detected instead of <sup>16</sup>O<sup>-</sup> or <sup>34</sup>S<sup>-</sup> which usually are chosen for the analysis of electronegative elements. Furthermore the measurement of the ceside secondary ions shows enough sensitivity to detect the metal ions of the matrix elements. By the detection of these ceside ions it is expected that the unfavorable matrix effects (different ionization rates of each element depending on the matrix composition) will be reduced. A raster size of 250 x 250 μm<sup>2</sup> was chosen for an optimal depth resolution and a passable measuring time of 90 min to reach a depth of approx. 600 nm per profile. The analyzed area was 150 x 150 μm<sup>2</sup>.

## TM-AFM Setup

For the TM-AFM measurements a NanoSope III<sup>®</sup> MultiMode Instrument from Digital Instruments (DI<sup>®</sup>) was available. The AFM images have been recorded using the tapping mode (TM – AFM). The provided software allows the determination of the surface as well as of the surface features formed during the corrosion processes by two- and three-dimensional analysis. The software also allows the calculation of the rms –value (root-mean-square)  $R_q$ . Before, during and after weathering the  $R_q$  is used to compare the surface characteristics. The formula of  $R_q$  is:

$$R_q = \sqrt{\frac{\sum_{i=1}^n (Z_i - \bar{Z})^2}{n}}$$

$Z_i$ : height value of single data points in image

$\bar{Z}$ : mean value of all height values in the image

$n$ : number of analyzed data points

The images of the in-situ TM-AFM measurements had a size of  $5 \times 5 \mu\text{m}^2$ .

## RESULTS AND DISCUSSION

### SIMS Results

The interpretation of the SIMS depth profiles gained by dynamic SIMS exhibits major problems: during the bombardment of the uppermost layers the sputter equilibrium is not reached yet. The measured count rates of these first cycles may not be used for interpretation of the measurements. Therefore, the data of the first and second cycle have been rejected for the interpretation. The layer thickness was determined as the linear section (= exponential decay in logarithmic diagram) at the beginning of the depth profile. A trend line to the depth profile was applied in a defined range. This arbitrary chosen range was expanded starting from the third value forward to the sputter time when the regression value  $r^2$  dropped below 0.95 (=  $3\sigma$ ). This so determined value was taken as the relative layer depth.

### Weathering with humidified synthetic air (80% RH)

Figs. 2 - 5 show the depth profiles of the samples weathered with pure humidified air. Pure Cu shows the thinnest corrosion layer of 104 s, while with increasing of the Zn-content the layer thickness raised from 144 s for CuZn10 and for CuZn30. For Zn the

thickness of the oxidized layer increased to approximately 91 s. For the interpretation of these values the sputter rate (sputtered ions per hitting primary ion) has to be considered. The sputter-rates are listed in table 1 have been calculated with TRIM [4] (Transport of Ions in Matter) . For Cu and CuZn10 the sputter rate is approximately the same with 6 atoms/ion for Cu and 7 atoms/ion for CuZn10. For CuZn30 the sputter rate increases up to 8.5 atoms/ion and for Zn it is 12 atoms/primary ion, the double rate of Cu.

Corroded Zn showed a high background level of O, which complicated the exact determination of the layer thickness. The course of the Na signal helped to determine the thickness of the layer corroded at the weathering experiments. Although the water used to moisten the air stream was double deionized, SIMS measurements showed enough sensitivity to detect these traces of Na. This element could only stem from the moist air. Thus fact indicates the coverage of the Zn surface with corrosion products already after polishing while handling the sample in ambient air. The decrease of the Na signal at Cu, CuZn10 and CuZn30 is quite simultaneous to the decay of the O signals. At these samples the oxidized layer came only from the weathering process.

Table 2 shows the thickness of the O enriched layer in the first row for each pure metal and brass alloy in sputter time [s] and in estimated depth [nm], determined with DEKTAK II profilometer. Because of the surface roughness after the polishing procedure (diamond paste, 0.25 $\mu$ m) the depth in nm only could be considered with an high inaccuracy, although it is known that the growing oxide forms a homogeneous plain surface [2].

Weathering with humidified synthetic air (80% RH) and 250 ppb SO<sub>2</sub>

In Figs. 2 - 5 the depth profiles also of the samples exposed to synthetic humidified air with 250 ppb SO<sub>2</sub> are presented.

Each second row of table 2 lists the thickness (sputter time [s] and estimated thickness [nm]) of the layers containing O and S in the corroded surface. Compared to the experiments without SO<sub>2</sub> – addition, SO<sub>2</sub> causes a thickening of the oxide layer from the double to the fourfold thickness of corrosion with only synthetic humidified air. The decrease of the S-signal is much faster than the decay of the O-signal. The thickness of the oxide and sulfur - rich layer increases with the Zn-content in the brass. Only the corroded pure Zn differs significantly from the other specimen. The

layer containing sulfur seems not to be the thickest of all samples (364 s) at pure Zn as it could be expected corresponding to the trend. After consideration of the fact, that the calculated sputter rate (done with TRIM) is as double high as of pure Cu, the altered layer of pure Zn is the thickest of all weathered samples. Also the estimated depth of 50 nm for the sulfur-rich layer calculated from the measured depth (with profilometer) shows the same result. Unexpectedly the O containing layer at pure Zn is much thinner than at all the others. This fact certifies the assumption that Zn corrodes already during handling of these samples in the ambient air after grinding and polishing. Also Na (from deionized water) was only found down to a sputter time of 28 s.

### TM-AFM Measurements

#### Weathering with humidified synthetic air (80% RH)

All surface features had a quite uniform appearance. Their diameter reached from 50 nm (Cu) up to 115 nm (CuZn30) and they had a height from 4 nm to 12 nm.

#### Weathering with humidified synthetic air (80% RH) and 250 ppb SO<sub>2</sub>

At the images of these weathered surfaces two types of features were detected: lower and smaller features with a diameter from  $100 \pm 20$  nm to  $290 \pm 40$  nm and a height from  $15 \pm 3$  nm to  $27 \pm 3$  nm and larger and higher with a diameter from 200 nm for Cu up to 400 nm for Zn. The smaller features also appear at the weathering experiments without the addition of SO<sub>2</sub> to the moist air and were identified as oxides in a preceding work [1]. In consideration to the estimated depth of the sulfur-rich layers from the SIMS depth-profiles this leads to the conclusion that the larger features represent the sulfur – rich corrosion products. The dimensions of this S containing features are listed in table 3. Fig. 6 shows the untreated surface of Zn after polishing. In Fig. 7 both types of features can be seen. The larger features containing S developed preferentially at the large scratch on the left side. In Fig. 8 the weathered surface of CuZn30 with large S and smaller O containing features is depicted. All images show an area of  $5 \times 5 \mu\text{m}^2$  and were recorded after 19h (Zn) and 19h 26 min (CuZn30) of weathering.

## CONCLUSION

The height of the features containing sulfur determined with TM-AFM matches with the estimated depth from the SIMS depth profiles. As a consequence of the formation of a compact oxide layer the O-containing features are much smaller and thinner than the thickness of the layer containing oxygen determined with SIMS.

The corrosion behavior of brasses is strongly influenced by the Zn content. As Zn is compared to Cu, a base metal, increasing Zn contents cause thicker corroded layers. Addition of SO<sub>2</sub> to the reaction atmosphere causes a catalyzed corrosion of the samples. The thickness of the corroded layer increases compared to the corrosion without SO<sub>2</sub> from the double to the fourfold range. The higher SO<sub>2</sub> – contents on the top of the surface indicate a diffusion of Cu through the corrosion film towards the surface. The corrosion layer grows continuously on the top of the surface. O and S containing compounds do not infiltrate the fresh corrosion film and the bulk of the metals and of the brasses. The steady decrease of the O signal on pure Zn indicates a coverage of Zn already before the weathering experiments while handling the specimen in ambient air.

Acknowledgements. This work was financially supported by the Austrian Fund for Science and Research (FWF Project No. P 13160).

TABLES

**Table 1. Sputter rates of the investigated systems, calculated with TRIM**

	Cu	CuZn10	CuZn30	Zn
Sputter rate [atoms / primary ion]	6	7	8.5	12

**Table 2. SIMS depth profiling. Thickness of O- and S- enriched layers of corroded brasses and pure metals treated with synthetic air (80% RH) and alternatively with 250 ppb SO<sub>2</sub>, determined sputter time in [s] and estimated in [nm] (with Profilometer)**

	Cu		CuZn10		CuZn30		Zn	
		x		x		x		x
+250 ppb SO <sub>2</sub>		x		x		x		x
O- layer sputter time [s]	104	518	144	340	144	493	91	28
estimated depth [nm]	5	27	10	27	11	42	17	6
S- layer sputtertime [s]		280		289		391		364
estimated depth [nm]		14		17		26		50

**Table 3. Height and diameter of the large S containing features at the experiments with synthetic air (80% RH) with 250 ppb SO<sub>2</sub>, measured with TM-AFM**

	Cu	CuZn10	CuZn30	Zn
Height of S- features [nm])	15 ± 3	20 ± 5	30 ± 5	40 ± 10
Diameter [nm]	200	300-400	280-300	350-400

FIGURES

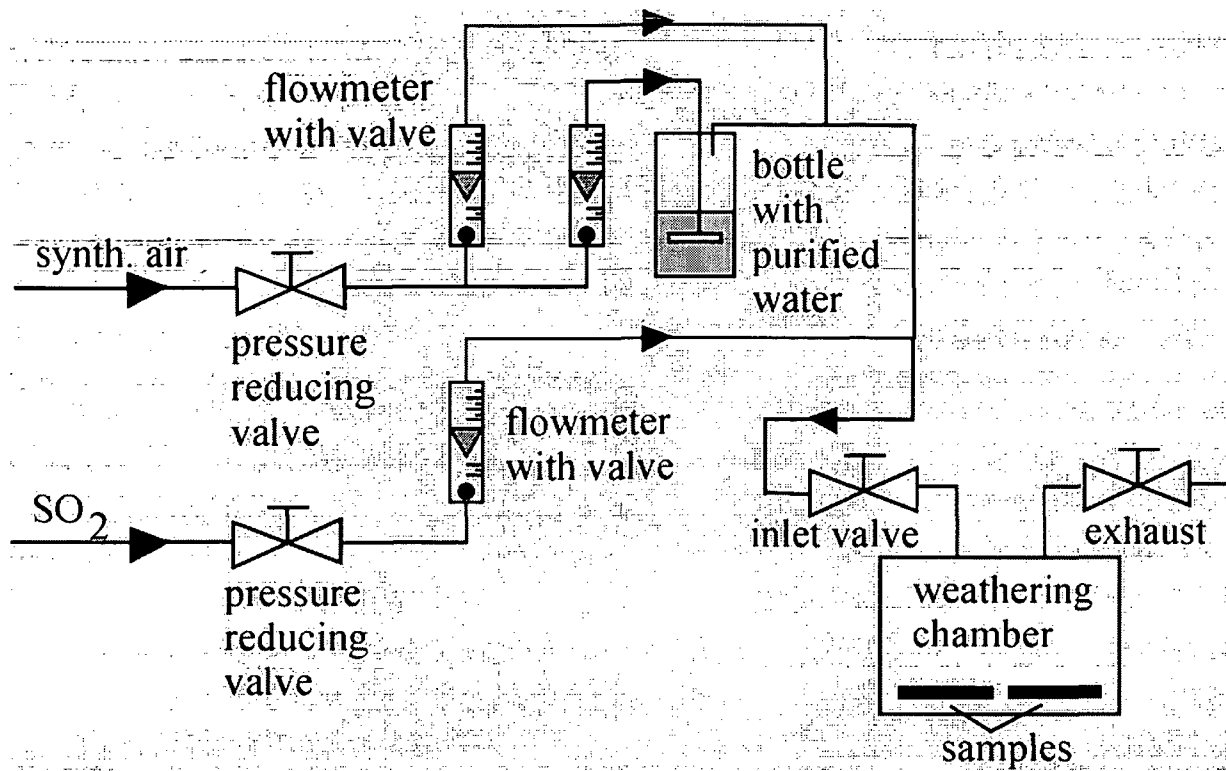


Figure 1. Setup for the corrosion of metal samples in a weathering chamber. Dry synthetic air is humidified with 2-step-distilled and deionized water up to 80% RH. For the second series 250 ppb SO<sub>2</sub> were added to the moist air stream.

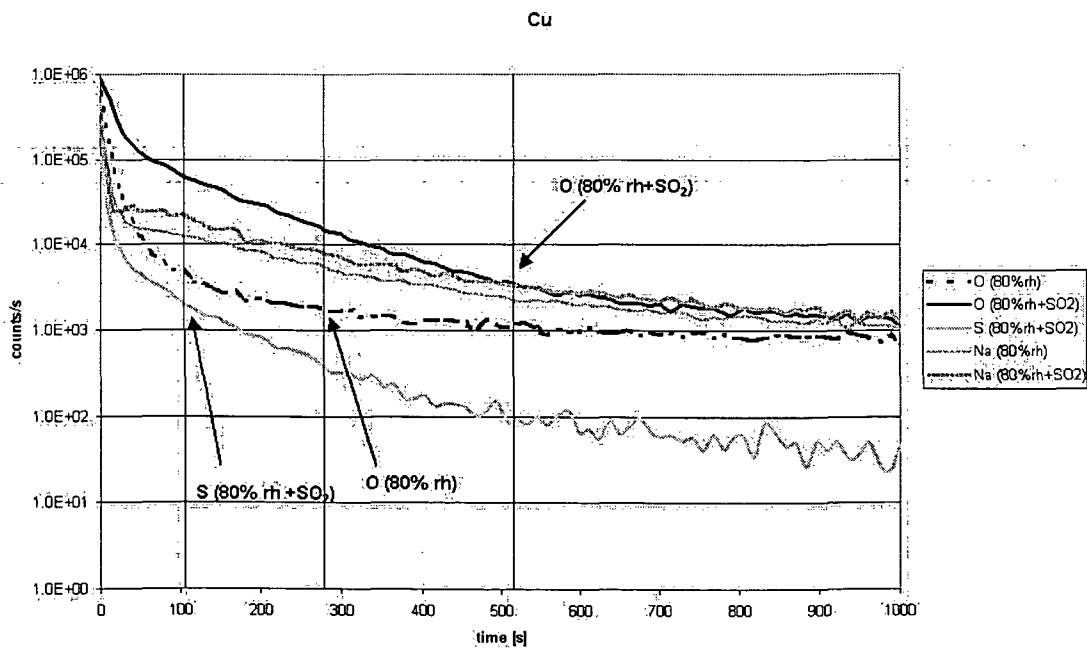


Figure 2

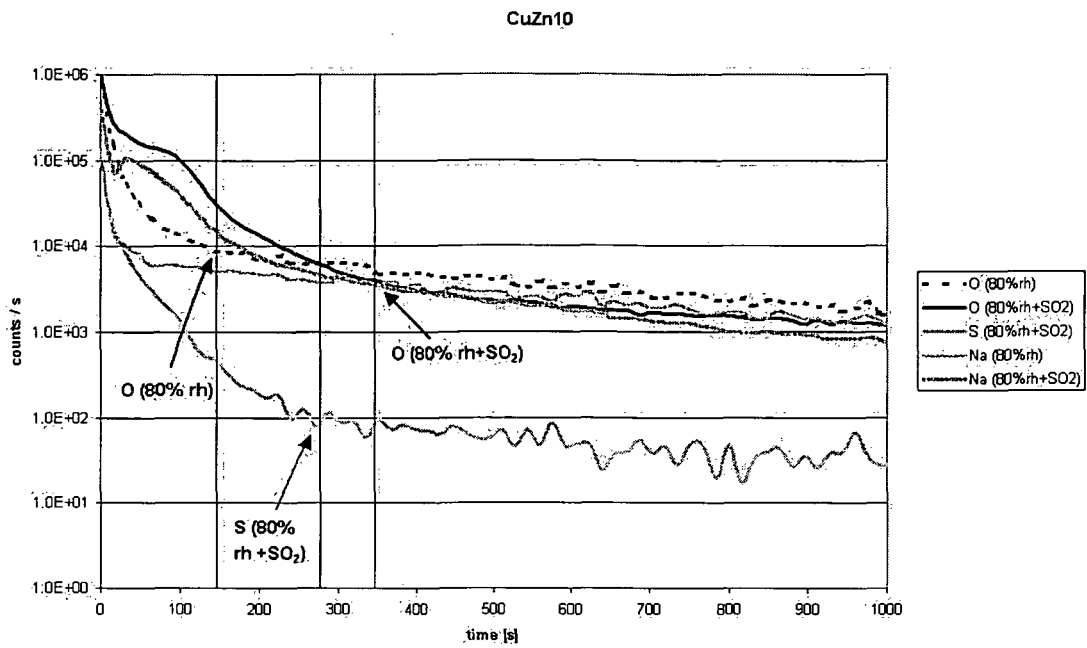


Figure 3

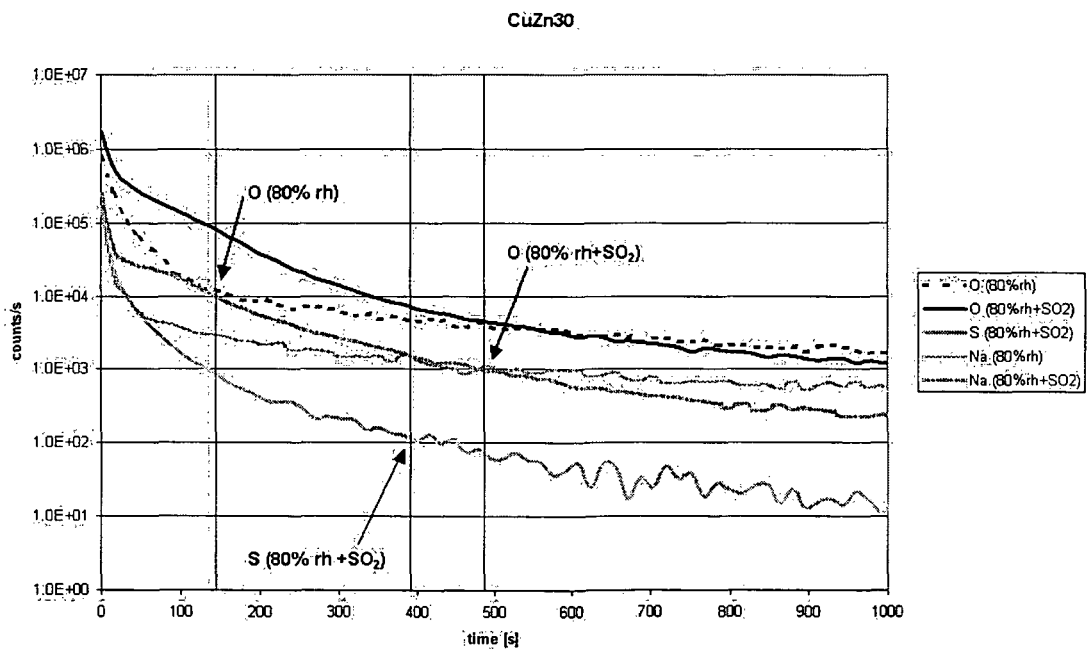


Figure 4

Zn

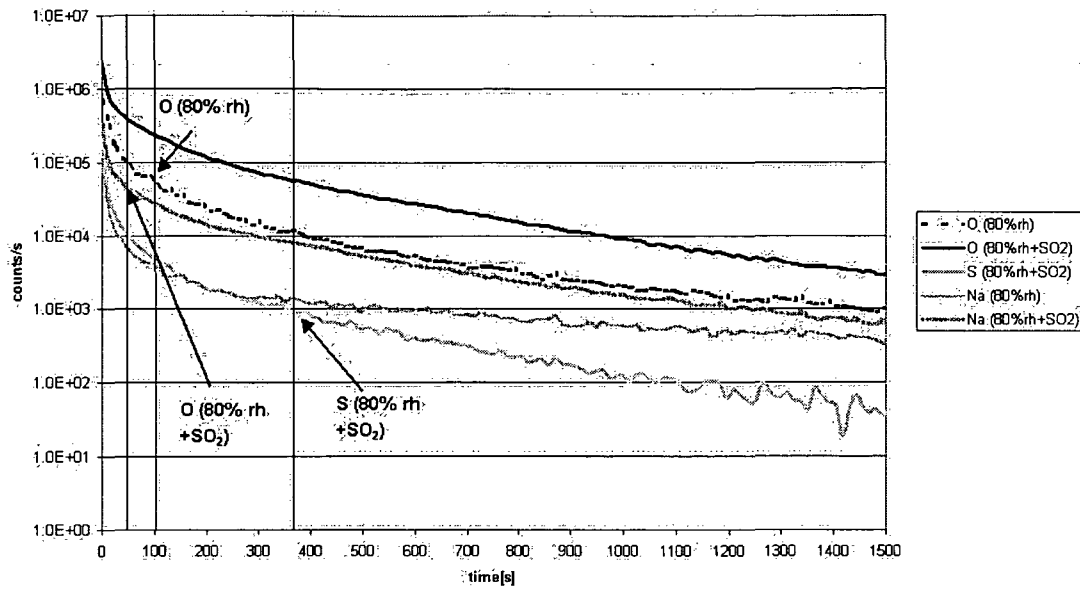


Figure 5

Figures 2-5. SIMS depth profiles of Cu (Fig.2), CuZn10 (Fig.3), CuZn30 (Fig. 4) and Zn (Fig. 5) weathered with moist air (80% RH) and alternatively with 250 ppb SO<sub>2</sub> added. The vertical lines indicate the thickness of the oxide-rich and sulfur-rich layers. SIMS – parameters: primary ions: Cs<sup>+</sup>; primary ion energy and intensity: 14,5 keV, 10 nA; sputtered surface: 250 x 250 μm<sup>2</sup>; analysed area: 150 x 150 μm<sup>2</sup>;

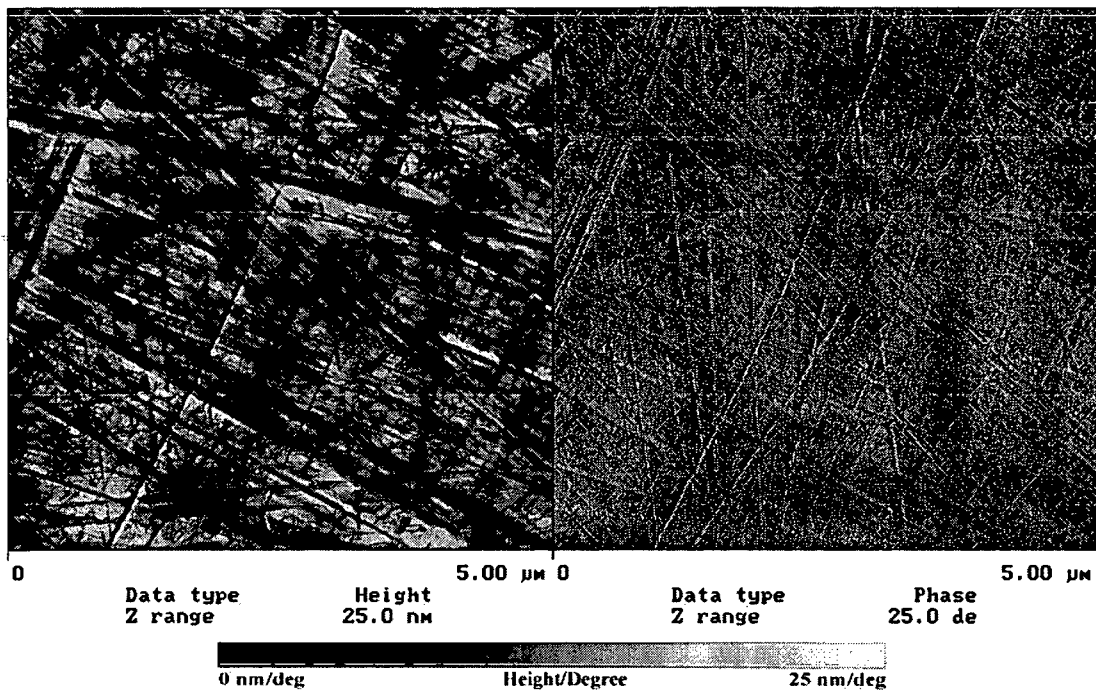


Figure 6. Topography and phase image of the surface of Zn after polishing and ultrasonic cleaning.

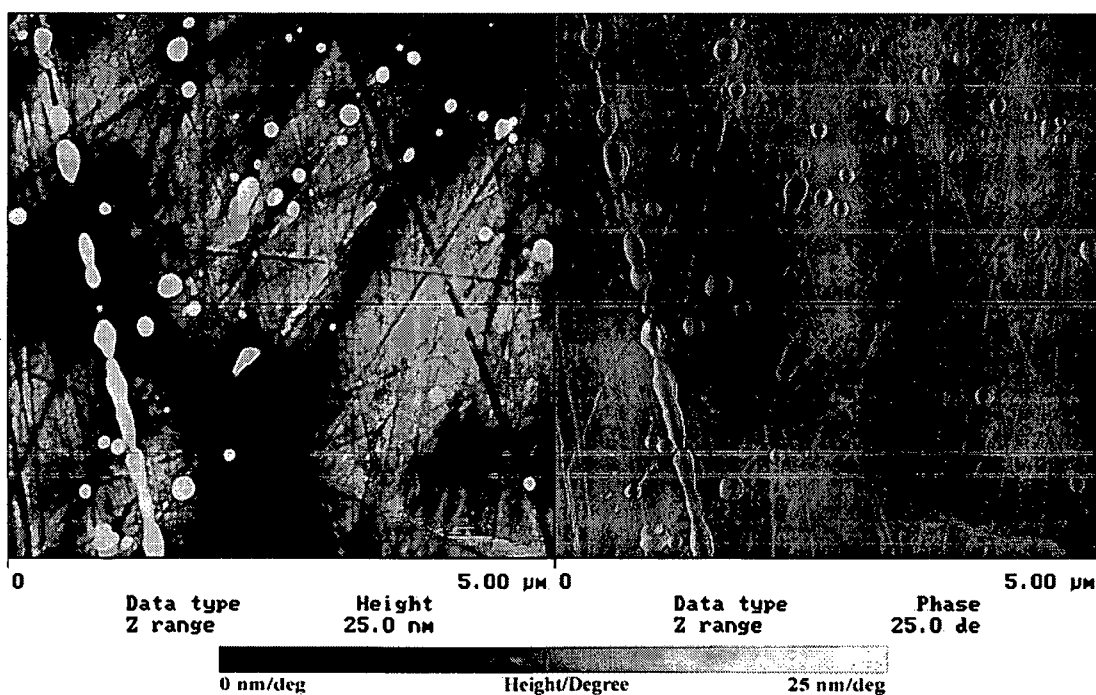


Figure 7. Topography and phase image of the surface of Zn after 19h of weathering. Large features containing sulfur and small features of oxides were formed during the corrosion process. The larger features containing S were formed preferentially along scratches.

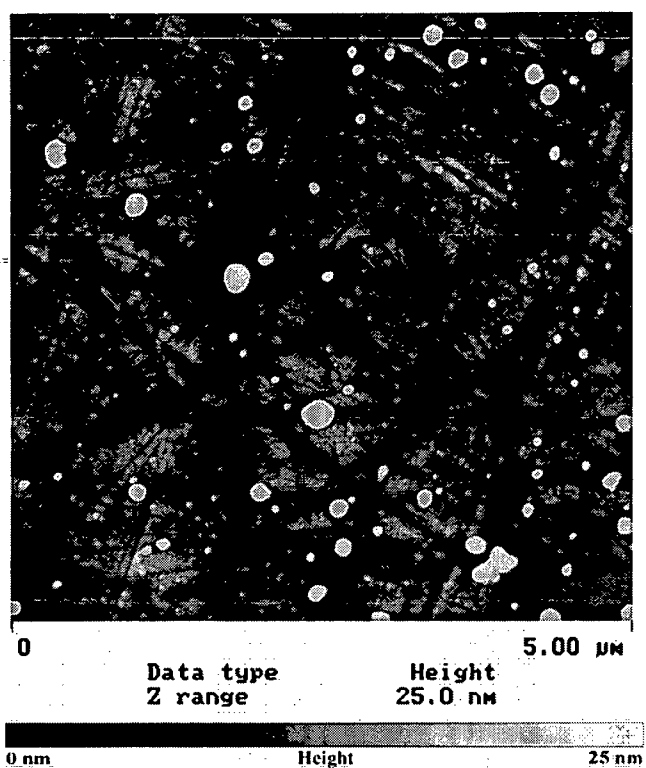


Figure 8. TM-AFM image of the surface of CuZn30 after 19h 26min weathering in humidified air with 250 ppb SO<sub>2</sub>. Smaller and larger features were grown during the corrosion process. The larger ones contain S and have diameters of 280 - 300 nm and a height of 30 nm.

## References

- [1] Wadsack, M., Schreiner, M., Aastrup, T., Leygraf, C. Combined in-situ investigations of atmospheric corrosion of copper with SFM and IRAS coupled with QCM. *Surf. Sci* **2000**, 454-456, 246-250
- [2] Kleber, Ch., Weissenrieder, J., Schreiner, M., Leygraf, C. Comparison of the early stages of corrosion of Copper and Iron investigated by in-situ TM-AFM *Appl. Surf. Sci.* **2002** 91251-9 in press
- [3] Hutter, H., Grasserbauer, M. Three dimensional ultratrace analysis of materials. *Mikrochim. Acta* **1992**, 107, 137-148
- [4] Ziegler, J. F. RBS/ERD simulation problems: stopping powers, nuclear reactions and detector resolution. *Nuclear Instruments & Methods in Physics Research, Section B: Beam Interactions with Materials and Atoms* **1998**, 136-138, 141-146

Christoph Kleber · Martin Rosner · Herbert Hutter  
Manfred Schreiner

## Influence of increasing zinc contents in brass in the early stages of corrosion investigated by in-situ TM-AFM and SIMS

Received: 22 January 2002 / Revised: 27 May 2002 / Accepted: 6 June 2002 / Published online: 21 August 2002  
© Springer-Verlag 2002

**Abstract** In-situ tapping mode atomic force microscopy (TM-AFM), a powerful, high-resolution imaging technique for determining the structure of surfaces and ex-situ secondary ion mass spectroscopy (SIMS), a multielement, high-depth-resolution method, were used to examine the influence of increasing zinc contents in brass in the early stages of corrosion. Four different samples (pure Cu, pure Zn, Cu/Zn=90/10 wt% and Cu/Zn=70/30 wt%) were studied in order to determine their chemical behaviour under various atmospheric conditions. The in-situ TM-AFM investigations were carried out in synthetic air with 60% relative humidity (RH) and 80% RH with 250 ppb SO<sub>2</sub>. The samples for the ex-situ SIMS experiments were weathered over a period of 60 h in 80% RH and 250 ppb SO<sub>2</sub>. The in-situ TM-AFM investigations have shown that an increasing Zn content in brass increases the corrosion rate.

**Keywords** Corrosion · In-situ measurements · AFM, SIMS · Corrosion kinetics · Weathering

### Introduction

Corrosion phenomena occurring on different metal surfaces such as copper and zinc has been studied for a long time using various analytical techniques such as infrared reflection spectroscopy (IRRAS), quartz crystal microbalance (QCM) and x-ray diffraction analysis (XRD). The investigations have proved the influence of humidity on pure metal surfaces referring to the early stages of corro-

sion [1, 2, 3, 4, 5, 6]. The studies have shown that the atmospheric corrosion behaviour of copper and zinc is quite complex. Despite clear evidence of the corrosion accelerating effect of SO<sub>2</sub> there is still a lack in detailed knowledge of the initial stages concerning the interaction of SO<sub>2</sub> with the metal surfaces in a submicrometer range. One of the studies [7] proposes that SO<sub>2</sub> is directly involved in the redox chemistry, thereby working as a cathodic depolarizer in the oxygen reduction reaction. A review to the theory of the interaction of water covering metal surfaces and the ambient atmosphere is given by the GILDES model [8].

TM-AFM has proven to be a very valuable tool for the analysis of thin films of oxides formed on metal surfaces, since the high lateral and depth resolution capability provides unique information on the structure, size and distribution of the features formed on the surface [9]. In addition, TM-AFM allows direct in-situ measurements during the corrosion process taking place under controlled conditions in a weathering chamber [10]. Moreover, the influence of an increasing humidity to the size and distribution of the features formed on the surfaces of the different samples can be investigated. In this study TM-AFM was applied to examine in-situ the influence of the Zn content in brass at various humidities and SO<sub>2</sub> contents in the atmosphere. SIMS measurements deliver the depth profile of the layers formed on the different sample surfaces under moist air with SO<sub>2</sub> and the thickness of these layers was used as an indication of the weathering rate.

### Experimental

#### Sample preparation and weathering conditions

Specimen of pure copper (Johnson Matthey, Paris/France, max. 25 ppm trace impurities), of pure zinc (Johnson Matthey, Paris/France, max. 25 ppm trace impurities), and of two brass alloys, Cu/Zn=70/30 wt% (Alfa Aesar, Vienna/Austria, max. 25 ppm trace impurities), Cu/Zn=90/10 wt% (Enzesfeld Caro Metallwerke AG, Enzesfeld/Austria) were mechanically abraded with SiC paper up to 2400 mesh, cleaned ultrasonically in ethanol absolute p.a., abraded afterwards with SiC of 4000 mesh and cleaned again in

C. Kleber (✉) · M. Rosner · H. Hutter · M. Schreiner  
Institute for Chemical Technologies and Analytics,  
Analytical Chemistry Division, Vienna University of Technology,  
Getreidemarkt 9/151, 1060 Vienna, Austria  
e-mail: chkleber@iac.tuwien.ac.at

C. Kleber · M. Schreiner  
Institute of Science and Technologies in Art,  
Academy of Fine Arts, Schillerplatz 3, 1010 Vienna, Austria

ethanol. Afterwards the samples were polished with 1- $\mu\text{m}$  polycrystalline diamond paste (Struers, DP paste P), cleaned in ethanol and then polished twice with 0.25- $\mu\text{m}$  polycrystalline diamond paste (Struers, DP paste P). After an additional ultrasonic cleaning in ethanol the samples were dried by blowing off with nitrogen (Messer Griesheim Austria, 5.0) and then transferred immediately to the AFM, where the weathering experiments could be carried out under controlled environmental conditions as already described in the literature [9, 10].

The samples for the SIMS investigations were exposed over a period of 60 h in 80% RH and 250 ppb  $\text{SO}_2$  under dynamic conditions in a desiccator with gas inlets and outlets. The flow rate of gas was 40 L/h similar to the conditions used in the TM-AFM.

#### In-situ TM-AFM measurements

The measurements were performed with a NanoScope III Multimode SPM from Digital Instruments (DI, Santa Barbara, CA, USA). The optical head of the AFM was rebuilt in order to use it as "weathering chamber" with gas in- and outlets. The in-situ measurements were carried out in the tapping mode using silicon cantilevers with integrated silicon tips (spring constant  $\sim 13\text{--}100$  N/m, resonance frequencies = 265–378 kHz). The used pyramidal tips have a base area of 4  $\mu\text{m} \times 4 \mu\text{m}$  and a height between 5 and 30 nm. The DI software used allows to generate two and three dimensional images, estimation of grain size, the possibility of height and distance measurements and the calculation of the bearing. This method provides the possibility to analyse the distribution surface height over a sample. By using the bearing analysis, it is possible to determine the height, where a specific amount of the surface is covered with an arbitrary chosen percentage (e.g. 50%) of corrosion features and vice versa (determination of the coverage in a arbitrary chosen height). This measurement provides additional information to standard roughness measurements such as the rms (root mean square)-roughness calculation ( $R_q$ ). The  $R_q$  is used to compare different surfaces of the investigated pure metals and alloys before, during, and after weathering. It is calculated by:

$$R_q = \sqrt{\frac{\sum_{i=1}^n (Z_i - \bar{Z})^2}{n}}$$

where  $Z_i$  is the height value of single data points in the image,  $\bar{Z}$  the mean value of all height values in the image and  $n$  the number of analysed data points within the image.

By the aim of the data received the calculation of the growth rate of the features – formed during weathering on the surface – can be calculated from time resolved measurements. Therefore, the diameter of one feature after a given time is divided by the weathering time.

In some cases the phase image is used instead of the conventional topographic image due to a better image quality for larger scans. The image contrast is given by the phase shift between the piezo oscillation driving the cantilever and the resulting oscillation of the cantilever. However, in the present study phase imaging was used due to the better image quality.

#### SIMS measurements

A modified CAMECA IMS 3f (France) with a Cs and an additional  $\text{O}_2$  fine-focus source was applied to obtain SIMS depth profiles of the samples. As primary ions  $\text{Cs}^+$  with an energy of 14.5 keV and an intensity of 10 nA were used.  $\text{MCs}^+$  detection was applied. By this procedure the adverse matrix effects can be reduced. The optimal parameters for a high depth resolution and an acceptable measuring time (90 min) were a raster size for the primary beam of 250  $\mu\text{m} \times 250 \mu\text{m}$  reaching a depth of 600 nm per profile, whereas the analysed area was 150  $\mu\text{m} \times 150 \mu\text{m}$ .

## Results and discussion

### Influence of increasing humidity related to the size and lateral distribution of the corrosion products formed

Figure 1 shows the freshly polished surfaces of the samples investigated (Cu, Zn, Cu/Zn=90/10, and Cu/Zn=70/30). Clearly visible in all images are the scratches caused from the polishing procedure. The specimen Cu/Zn=70/30 has the smoothest surface with an rms-roughness of 1.004 nm followed by the sample of pure Zn with an rms-roughness of 1.021 nm, the specimen Cu/Zn=90/10 with an rms-roughness of 2.087 nm, and the pure copper surface with an rms-roughness of 3,156 nm. In Fig. 1 it is also depicted that even a few minutes after sample preparation the surfaces show already features due to the contact of the sample with moist air during the transfer into the AFM. The head of the AFM was flushed with dry nitrogen before and during the acquisition of the first image. Using the bearing analysis enables the determination of the height, in which 50% (arbitrarily chosen) of the surface is covered by features. Thus it is possible to define the condition of the "starting surface" at the beginning of the experiment. The results of the bearing analysis are in accordance with the rms-roughness as a surface with a high amount of scratches and/or features yields to a high value of the calculated surface height (above or below a given height).

The sample Cu/Zn=70/30 has a surface coverage of the arbitrarily chosen 50% at 14.1 nm, the pure Zn sample at

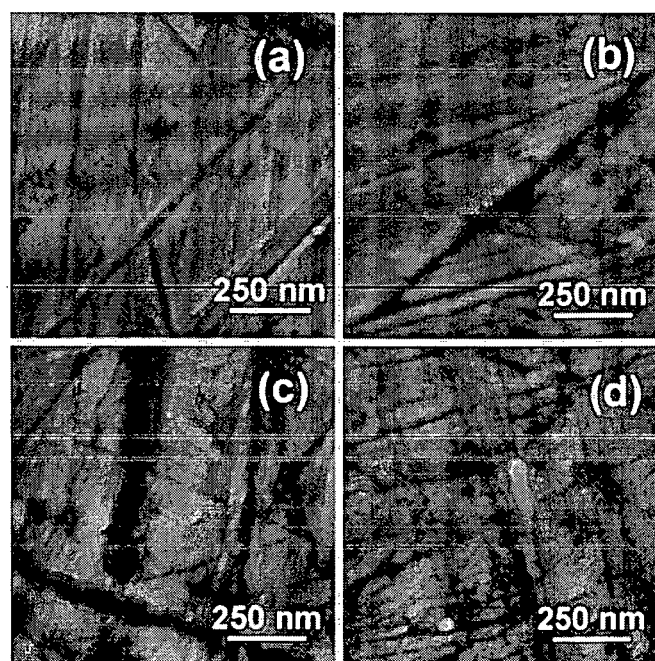


Fig. 1a–d TM-AFM images of the polished surfaces of the investigated samples. a Pure Cu, b pure Zn, c Cu/Zn=90/10 and d Cu/Zn=70/30. The scan size is 1  $\mu\text{m} \times 1 \mu\text{m}$  and the z-range is 25 nm from black to white

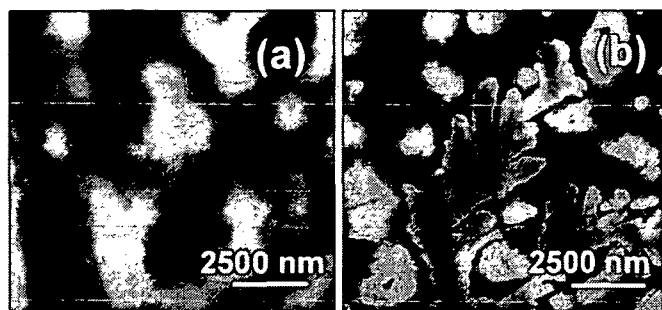


Fig. 2a,b Growth of a surface film on pure Zn in dry synthetic air as a tapping mode image and b phase image. The scan range is  $10\ \mu\text{m}\times 10\ \mu\text{m}$  and the z-range is 100 nm from black to white

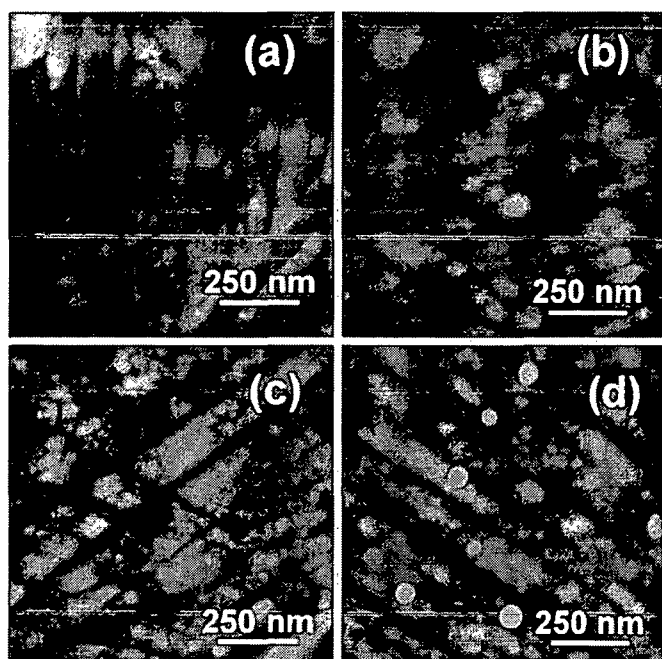


Fig. 3a-d In-situ TM-AFM images of the analysed surfaces. a Pure Cu, b pure Zn, c Cu/Zn=90/10 wt% and d Cu/Zn=70/30 wt%; after a weathering period of a 1307 min, b 1156 min, c 1290 min and d 1292 min in synthetic air containing 60% RH. The scan size is  $1\ \mu\text{m}\times 1\ \mu\text{m}$  and the z-range is 25 nm from black to white

25.8 nm, the specimen Cu/Zn=90/10 at 310.0 nm, and the pure Cu sample at 424.3 nm. These results show that the specimen Cu/Zn=70/30 has the most uniform surface followed by pure Zn, the specimen Cu/Zn=90/10 and pure Cu. Therefore, the conclusion can be drawn that the Zn specimen is covered by a film immediately after polishing. In Fig. 2 the formation of such features is demonstrated by the image of the topography (Fig. 2a) as well as the phase image (Fig. 2b), where the crystalline structure can be seen clearly. On the surfaces of the other three samples such corrosion phenomena could not be determined.

The exposure of the samples in synthetic air with 60% RH for 1300 minutes results in the formation of two types of corrosion phenomena shown in Fig. 3. On the surfaces

Table 1 rms-roughness and the dimensions of the features grown on the sample surfaces in synthetic air with 60% RH

Sample	Exposure time (60% RH) (min)	rms-roughness (nm)	Feature dimension	
			Diameter (nm)	Height (nm)
Pure Cu	1307	2.48	$50\pm 10$	$4\pm 3$
Pure Zn	1156	1.66	$100\pm 10$	$5\pm 2$
Cu/Zn=90/10wt%	1290	1.60	$70\pm 5$	$4\pm 2$
Cu/Zn=70/30wt%	1292	1.31	$80\pm 15$	$8\pm 5$

of pure Cu (Fig. 3a) and of the specimen Cu/Zn=90/10 (Fig. 3c) a homogenous film consisting of corrosion products was formed, whereas the surfaces of pure Zn (Fig. 3b) and Cu/Zn=70/30 (Fig. 3d) show additionally the formation of round features (with a diameter between 50 and 100 nm and heights of 4–8 nm (Table 1). The number of these features is higher for the specimen Cu/Zn=70/30 than on the surface of pure Zn. Pure Zn (Fig. 3b) as well as the specimen Cu/Zn=90/10 (Fig. 3c) are characterized by a homogenous distribution of same sized features, whereas on the pure Cu and Cu/Zn=70/30 surfaces the features are statistically distributed and have different diameters and heights. In Table 1 the diameters and heights of the features are summarized. Calculating the growth rate of the features by dividing their diameters by the weathering time (Table 1) leads to the conclusion that pure Zn has a weathering rate approximately twice of the corrosion of the other samples (pure Cu: 0.04 nm/minute; pure Zn: 0.09 nm/minute; Cu/Zn=90/10: 0.05 nm/minute; Cu/Zn=70/30: 0.06 nm/minute). These results are in good agreement with the rms-roughnesses (Table 1) as a high corrosion rate results in a smooth surface caused by a thick layer covering the scratches from polishing.

Weathering experiments in synthetic air with 80% RH for approximately 1300 min were carried out in order to study the influence of the humidity on the corrosion rate of the four samples. As can be seen in Fig. 4, the surfaces of pure Cu (Fig. 4a) and Zn (Fig. 4b) are comparable with Fig. 3a and 3b, respectively, whereas for the sample Cu/Zn=90/10 (Fig. 4c) and Cu/Zn=70/30 (Fig. 4d) a higher amount of the round features can be observed. Hence the corrosion rate of the sample Cu/Zn=70/30 has increased to 0.09 nm/min. The growth rate of the features formed on the sample Cu/Zn=90/10 is approximately 0.07 nm/min, which is 40% higher than in the experiment with 60% RH. Calculating the growth rate of the features on pure Cu and Zn yields to a weathering rate of 0.04 nm/min for Cu and 0.06 nm/min for Zn, which is similar to the corrosion rate under 60% RH. Table 2 summarizes the diameters and heights of the features formed as well as the rms-roughnesses.

SIMS measurements were performed in order to determine the thickness of the layers grown on the polished surfaces during weathering. Samples were exposed over a period of 60 h in a desiccator with gas inlets and outlets in synthetic air with 80% RH. The depth profiles obtained

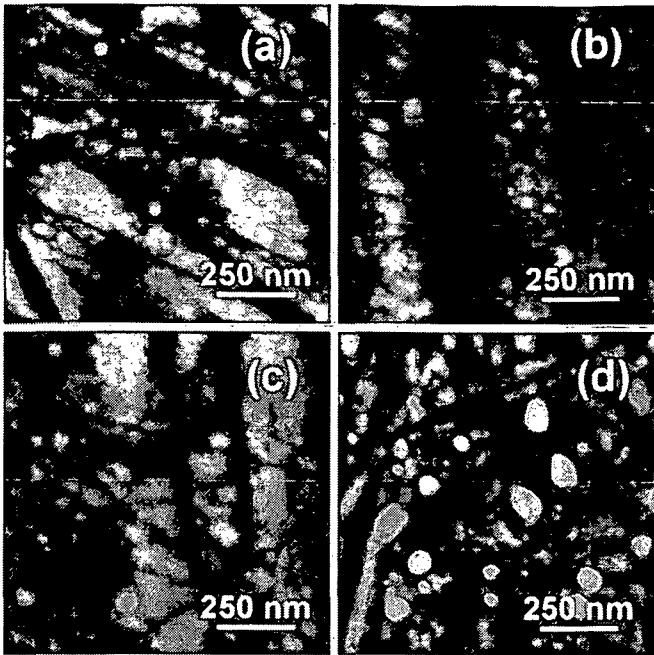


Fig. 4a-d In-situ TM-AFM images of the analysed surfaces. a Pure Cu, b pure Zn, c Cu/Zn=90/10 wt% and d Cu/Zn=70/30 wt%; after a weathering period of a 1380 min, b 1203 min, c 1359 min and d 1307 min in synthetic air containing 60% RH. The scan size is  $1 \mu\text{m} \times 1 \mu\text{m}$  and the z-range is 25 nm from black to white

Table 2 rms-roughnesses and the dimensions of the features grown on the sample surfaces in synthetic air with 80% RH

Sample	Exposure time (80% RH) (min)	rms-roughness (nm)	Feature dimension	
			Diameter (nm)	Height (nm)
Pure Cu	1380	2.47	$50 \pm 15$	$5 \pm 2$
Pure Zn	1203	1.33	$80 \pm 10$	$4 \pm 1$
Cu/Zn=90/10wt%	1359	1.91	$90 \pm 5$	$4 \pm 1$
Cu/Zn=70/30wt%	1307	2.34	$115 \pm 5$	$12 \pm 3$

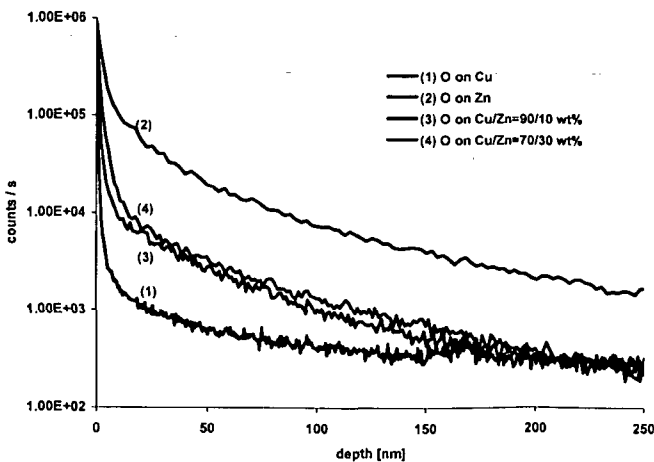


Fig. 5 Ex-situ SIMS depth profiles of oxygen ions detected from the investigated samples (weathered under 80% RH for 60 h)

for oxygen with  $\text{Cs}^+$  as primary ions are shown in Fig. 5. The layer thickness is given at a depth, where the count rate of the secondary ions has reached a value of 1/100 of the ion intensity at the beginning of the sputtering process.

For pure Cu a layer thickness of approximately  $35 \pm 5$  nm can be determined. The layer thicknesses for pure Zn is 90 nm, for the sample Cu/Zn=90/10 10 nm, and for Cu/Zn=70/30 20 nm. Thus it can be concluded that the layer formed on the sample surfaces grows four to five times faster on Zn than on Cu/Zn=70/30, nine times faster than Cu/Zn=90/10 and 18 times faster than on pure copper. These results are in good agreement with the rms-roughnesses, given in Table 2. A smoother surface characterized by a low rms-roughness has to be covered by a thick film, so that the scratches caused from polishing are covered by this film.

#### Influence of $\text{SO}_2$

It is known from literature [11] that  $\text{SO}_2$  in moist air shows a reaction sequence: by hydrolysis a bisulphite ion is formed yielding to metal-sulphito complexes, which finally may precipitate as corrosion products. Fig. 6 shows the surfaces of the samples investigated after a weathering period of approximately 1200 min in 80% RH and 250 ppb  $\text{SO}_2$ . The sample Cu/Zn=70/30 (Fig. 6d) is covered by the most and biggest features. This alloy shows roughly the same corrosion phenomena as pure Zn (Fig. 6b). On the

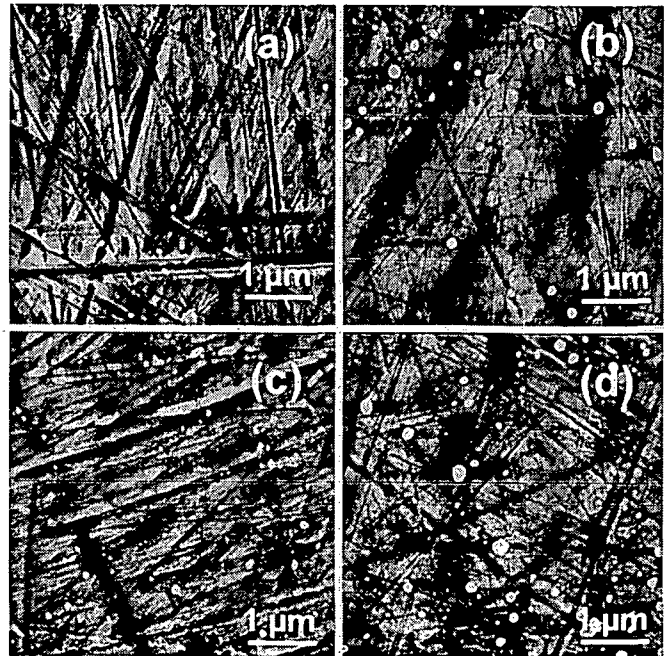


Fig. 6a-d In-situ TM-AFM images of the analysed surfaces. a Pure Cu, b pure Zn, c Cu/Zn=90/10 wt% and d Cu/Zn=70/30 wt%; after a weathering period of a 1192 min, b 1224 min, c 1310 min and d 1174 min in synthetic air containing 80% RH and 250 ppb  $\text{SO}_2$ . The scan size is  $5 \mu\text{m} \times 5 \mu\text{m}$  and the z-range is 25 nm from black to white

**Table 3** rms-roughnesses and the dimensions of the features grown on the sample surfaces in synthetic air with 80% RH and 250 ppb SO<sub>2</sub>

Sample	Exposure time (80% RH with 250 ppb SO <sub>2</sub> ) (min)	rms-roughness (nm)	Feature dimension	
			Diameter (nm)	Height (nm)
Pure Cu	1192	3.71	200±20	15±3
Pure Zn	1224	2.82	250±40	20±5
Cu/Zn=90/10wt%	1310	2.72	100±20	20±2
Cu/Zn=70/30wt%	1174	3.61	290±40	27±3

specimen Cu/Zn=70/30 and pure Cu SO<sub>2</sub> caused features starting mainly along the polishing scratches. This explains the similar value for the rms-roughness of the two samples. On pure Zn a statistically distributed formation of the round features all over the sample surface can be observed. For Cu/Zn=90/10 a surface with a great number of small features was obtained yielding to a low rms-roughness (Table 3).

The growth rate is the highest for Cu/Zn=70/30 (0.25 nm/min), whereas for pure Zn the corrosion rate of 0.19 nm/min, for pure Cu of 0.17 nm/min and finally for Cu/Zn=90/10 of 0.08 nm/min was determined. These results show that the big difference in the early stage corrosion of the two alloys (Cu/Zn=70/30 and Cu/Zn=90/10) is caused by their zinc content.

The layer thicknesses were determined by SIMS measurements already described. The samples were weathered in synthetic air with 80% RH and 250 ppb SO<sub>2</sub> for 60 hours. Fig. 7 shows the depth profiles of oxygen, where the layer thicknesses were determined as described above. For pure Cu a thickness of 21 nm, for pure Zn a thickness of 180 nm, for Cu/Zn=90/10 25 nm, and for Cu/Zn=70/30 30 nm was obtained. These results show that the layer grew eight times faster on pure Zn than on pure Cu and on the sample Cu/Zn=90/10 and six times faster than on Cu/Zn=70/30, which means that 250 ppb SO<sub>2</sub> in the moist air has increased the corrosion rate by a factor of approximately 2.5.

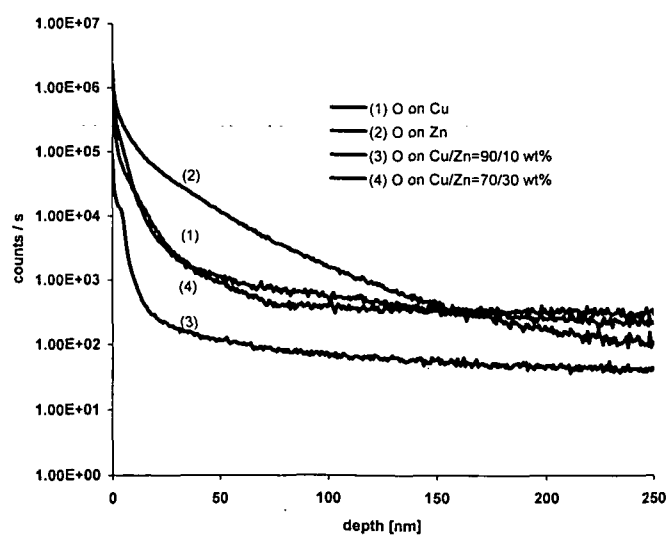


**Fig. 7** Ex-situ SIMS depth profiles of oxygen ions detected from the investigated samples (weathered in 80% RH with 250 ppb SO<sub>2</sub> for 60 h)

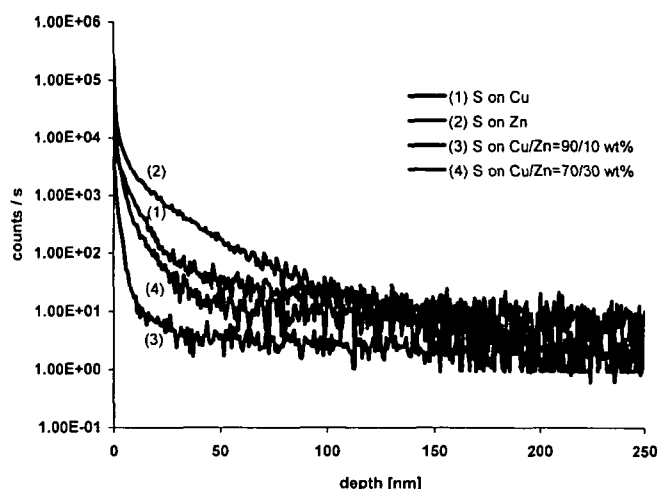


**Fig. 8** Ex-situ SIMS depth profiles of sulphur ions detected from the investigated samples (weathered in 80% RH with 250 ppb SO<sub>2</sub> for 60 h)

In order to determine, whether the SO<sub>2</sub>-caused features are assembled in the corrosion layer formed on the surface or on top of it, SIMS depth profiles for sulphur were acquired (Fig. 8). A comparison of the results with the depth profiles presented in Fig. 7 shows that the secondary ion intensity for sulphur decreases faster than for oxygen. At the definite depth (arbitrarily chosen) the intensity of sulphur is 100 times below the secondary ion intensity of oxygen. Therefore, it can be concluded that the SO<sub>2</sub>-caused features are settled on top of the corrosion layer and not integrated in the corrosion layer at all.

## Conclusions

In-situ TM-AFM and ex-situ SIMS measurements were used for studying the initial stages of corrosion of pure Cu, pure Zn, Cu/Zn=90/10 and Cu/Zn=70/30. Systematic investigations revealed that the moisture content of the surrounding atmosphere is a crucial factor for the growth rate of the features formed on the sample surfaces. Increasing the humidity yields to an accelerated weathering rate. An increased Zn content in the brass samples results also in a higher formation of corrosion products due to the different phases formed in the alloys. Also SO<sub>2</sub> in the moist air increases the corrosion. By the aim of the ex-situ SIMS measurements the cross-section distribution of these features could be estimated. Thereby it could be shown that independent from the Zn content of the brass

SO<sub>2</sub>-caused features only exist on the surface of the corrosion layer. This indicates a further reaction of the compounds (oxides) in the corrosion layer to secondary corrosion products (sulphates or sulphites).

---

### References

1. Rhodin T N (1950) *J Am Chem Soc* 72:930
2. Allen J A (1952) *Trans Faraday Soc* 43:273
3. Chawla S K, Rickett B I, Sankarraman N, Payer J H (1992) *Corr Sci* 33:1617
4. Perrson D, Leygraf C (1990) *J Electrochem Soc* 137:3163
5. Perrson D, Leygraf C (1993) *J Electrochem Soc* 140:1256
6. Wadsak M, Schreiner M, Aastrup T, Leygraf C (2000) *Surface Sci* 454–456:246
7. Chawla S K, J H Payer (1990) *J Electrochem Soc* 60:137
8. Graedel T E (1996) *Corr Sci* 38:2153
9. Schmitz I, Schreiner M, Friedbacher G, Grasserbauer M (1997) *Appl Surf Sci* 115:190
10. Kleber Ch, Weissenrieder J, Leygraf C, Schreiner M (2002) *Appl Surf Sci* 9125:1
11. Persson D (1999) Doctoral thesis, Department of Material Science and Engineering, Royal Institute of Technology Stockholm, Sweden

## ***4.5 Semiconductor Development***

PUBLICATION IV

**SIMS Measurements with high Depth Resolution of Arsenic in-drives in Silicon**  
submitted to: Analytical and Bioanalytical Chemistry

# SIMS measurements with high depth resolution of Arsenic in-drives in Silicon

M. Rosner<sup>1</sup>, D. Giubertoni<sup>2</sup>, M. Barozzi<sup>2</sup>, M. Bersani<sup>2</sup>, M. Anderle<sup>2</sup>, H. Hutter<sup>1,\*</sup>

<sup>1</sup>Institute for Chemical Technologies and Analytics, Vienna University of Technology, Getreidemarkt 9/E164, A-1060 Wien

<sup>2</sup>Istituto Trentino di Cultura, Fisica Chimica delle Superfici e Interfacce, Via Sommarive 18, I-38050 Povo (Trento)

\*corresponding author

email: h.hutter@tuwien.ac.at

phone: +43-1-58801/15120

fax: +43-1-58801/15199

## Abstract

The analysis of the depth distribution for dopants in state-of-the-art semiconductors with junction depths below 50 nm under the Si substrate surface is limited by the depth resolution of the SIMS method. Also the use of SIMS instruments of the newest generation is not sufficient to characterize such ultra shallow implants in in-diffusions. This work shows the improvement of the depth resolution of SIMS by forward convolution of a diffusion model function with the response function of the SIMS instrument determined by measuring a sample with a buried (monoatomic)  $\delta$ -layer. The assumed diffusion model was fitted until the best matching of the convoluted depth profile with the measured profile was reached. With this method the diffusion of implanted As over an interface between polycrystalline to monocrystalline Si was studied.

Keywords: high depth resolution, forward convolution, SIMS, drive-in diffusion

## Introduction

Semiconductor industry is still a fast expanding branch with a large potential of innovation. It is obvious that research for improvement and the development of new production technologies and possible applications is a major field of interest and therefore semiconductor industry has to deal with enormous costs for the improvement of their products. New devices for computers have to be smaller and faster and contain a higher number of transistors than the precedent generation. In order to have this performance the characteristics of ultra shallow junctions described in the National roadmap for semiconductors [1] bring also new challenges to analysis techniques. To design devices preparatory work at test benches to get data for process simulations and for the scheduling of production lines has to be done. In this stage of development analytical techniques are used to assure the results and to refine production and simulation parameters. However, the correct interpretation of analytical data is an essential step for the development of new devices.

Secondary Ion Mass Spectrometry is nowadays playing a powerful role in analysis of trace elements in semiconductors, high performance materials and coatings. The main advantages are high sensitivity and a large dynamic range measuring depth profiles, the capability of direct surface imaging and detecting of 3D-species distribution. SIMS can detect all elements (including hydrogen) within a typical detection limit range from 1 ppm to 1 ppb, and is also able to distinguish various isotopes of one element with high mass resolution.

Depth profile analysis is the most important application of SIMS. For the study of diffusion processes in semiconductor materials SIMS is an essential technique. However, the technological development requires an exact determination of very sharp interfaces and ultrathin films on the scale of one or several atomic layers, despite the fact that this is still beyond the power of most SIMS instruments. As device thickness shrink into that scale improved depth profiling methods will be needed.

The depth resolution can be estimated by several methods, for example by means of the decay length [2]; this is the distance  $x$  until the signal  $I$  decreases by a factor of  $e$  (equation 1).

$$\lambda = \frac{x_2 - x_1}{\ln \frac{I_2}{I_1}} \quad (1)$$

Besides instrumental and sample related factors, depth resolution of SIMS depends on the nature of ion-solid interactions. Most important processes are atomic mixing, recoil implantation, and radiation and defect induced diffusion. Among these effects atomic mixing plays a dominant role; it should be minimized in order to get high depth resolution. This can be achieved by using low primary ion energy, grazing incidence and molecular species in the primary beam. In addition, low-energy ion beams [3] suffer usually from worse focusing of the primary beam and low current densities. In the case of drive-in diffusion the active zone is in higher depths, so it is necessary to use high sputter speeds to limit the measurement time. The instrument used for this study eliminates some of these problems, as bad focusing of the primary beam or low current densities. The Cameca IMS Wf (SC Ultra) has a totally new designed primary column and a new extraction lens system to obtain high extraction potential to the secondary column at ion impact energies down to 250eV both for  $O_2^+$  and  $Cs^+$  primary beams and therefore better yield for positive and negative secondary ions [4].

The design and development of modern bipolar transistor architectures like Heterojunction-Bipolar-Transistors process- and device-simulation plays a major role for submicron process technologies. The TCAD approach does not only cut the development costs, but also provides deeper insight into the overall device functionality. This information can be used to optimise device behaviour with respect to speed and analog performance, before any expensive experimental tests have to be carried out in fabrication. However the predictive power of such an approach depends strongly on the quality of simulation model calibration, like diffusion model constants and various other parameters.

For the case of poly-crystalline silicon Emitter bipolar transistors the out-diffusion of Arsenic from the polycrystalline Si to the monocrystalline substrate determines the base-width of the transistor in first-order (together with the base-profile width and dopant concentration). Since the direct measurement of the out-diffusion profile is very difficult, due to above shown factors, a combined inverse modelling approach was chosen to obtain the real out-diffusion distance of arsenic from the polysilicon-single crystal silicon interface.

A measured SIMS profile can be described as a convolution of the original undistorted profile with the SIMS response function. This response function is determined by measuring a Ge- $\delta$ -layer [5]. A forward convolution method was applied by performing point to point convolution of an assumed, undistorted model diffusion with the SIMS response function. The model diffusion was fitted until the best match with the measured As in-drive depth profile was received.

## Experimental

### *Ge – delta ( $\delta$ -)layer samples*

To determine the SIMS response function  $\delta$ -layer samples are used. As our investigated system was As in Si the measurement of As  $\delta$ -layers in Si would have been appropriate to perform the following data analysis. Because it is hardly possible to produce capped MBE  $\delta$ -layers of As (because of the vapor pressure) Ge was used instead of As. Ge has a comparable atomic weight to As (Ge: 72,61 amu, As: 74,92 amu) and the difference of the chemical behavior is negligible for these studies. dyn-TRIM calculation have shown that the sputter behavior is of As and Ge can be assumed as nearly the same.

On two 4" cz-grown Si(100) p-type wafer 1 atomic germanium ML (resp. 10 ML) and a silicon capping layer of 50 nm were grown with molecular beam epitaxy (MBE). The deposition rates were 0.05nm/s for Si and 0.01 nm/s for Ge. The targets have been held at room temperature during the

deposition. The 50 nm capping layer is essential to gain a sputter equilibrium until the  $\delta$ -layer is reached during the depth profiling. The obtained SIMS depth profile of these  $\delta$ -layers is used as response function of the SIMS-instrument [6].

#### *As - implant*

On two 4" cz-grown Si(100) p-type wafers (samples As#1, As#2) 200 nm of amorphous Si have been deposited by CVD. Then arsenic with an energy of 80 keV and a dose of  $1 \cdot 10^{16}$  at/cm<sup>2</sup> was implanted into the CVD-Si-layer in each of the samples. Each sample has been treated with an RTP diffusion step (sample As#1: 960°C@10s, sample As#2: 1000°C@10s). The RTP treatment led to rapid recrystallization of the amorphous CVD Si-layer and fast diffusion of the implanted As through this polymorphous Si. The native SiO<sub>2</sub> layer between the prime wafer and the deposited Si is assumed not to be continuous, so that some spots remain where the implanted As can diffuse through. Because of this reason it was not possible to etch off the capping polycrystalline Si to save measuring time. The stopping of the etching process could not be determined exactly and the risk of unwanted artifacts caused by the etching process was too high.

#### *SIMS Set-up*

The SIMS –measurements have been carried out in a Cameca SC Ultra, which corresponds to a slightly modified IMS Wf (Cameca, Courbevoie, F). The SC Ultra is equipped with a new floating primary column and a new screened extraction system, which allow the reduction of the impact energy down to 250 eV, both under conditions of high acceleration voltage in the ion sources and high ions transmission in the secondary column [7]. Measurements at such low energies are useful for thin layer samples or ultra shallow implants. For these studies a primary ion impact energy of 1 keV was chosen to gain an acceptable measuring time in the range of 2h/profile for the As in-drive samples. The Ge- $\delta$ -layer additionally have been measured with 500eV primary intensity to show the depth resolution capabilities of the instrument. At lower energies the time demand to sputter layers

of more than 200 nm of thickness is too extensive. The used primary ions were  $\text{Cs}^+$ , the analyzed secondary ion species were both  $\text{AsSi}^-$  to get a good detection limit and  $\text{CsAs}^+$  to get profiles with reduced matrix effects.

A summary of the conditions for the SIMS measurements is shown in table 1.

The IMS Wf was equipped with an in-line crater measurement unit [8] based on the principle of interference of two laser beams (the first in the sputtered crater, the second on the unsputtered surface as reference), nevertheless the crater depths have been also determined by a KLA Tencor P15 Profilometer. The difference of the depth scales was in the range of 5%. One major problem of the laser interference method is the depth calibration if a transparent to laser wavelength material is present (e.g.  $\text{SiO}_2$ ); this effect shifted the depth scale at the profiling of the Ge- $\delta$ -layers to lower values due to thin native oxide in the surface region of the samples.

## Results and Discussion

### *Ge – $\delta$ - layers*

For the determination of the SIMS response function and to find the optimum measuring conditions for the As in-drive samples at first the Ge  $\delta$ - layers have been analyzed. The response function is determined by implantation of primary ions, atomic mixing of substrate atoms and surface roughening during the sputter process. The decay length was used as a degree for the depth resolution at certain measuring parameters. The decay length indicates the length until the signal shows a decay of e. Table 1 shows the determined values for both  $\delta$ -layer samples at different impact energies of the primary ions and for different evaluated secondary ions. It can be seen that the values of the decay lengths of the 1ML and the 10ML  $\delta$ -layers differ slightly in a range of 5% - 8% for the same energy. This leads to the conclusion that broadening of the SIMS profile arises from SIMS artifacts and not from the thickness of the layer. The slope of 1ML Ge shows a shifted

gaussian peak, while at the 10 ML sample a plateau region of approx. 3.5 to 4 nm can be recognized. This corresponds to 7 - 8 monolayers of Ge. Also the integrated value of the curve areas give an approach for 7 monolayers Ge. The depths of the buried  $\delta$ -layers is 46 nm for the 1ML sample and 47nm for the 10ML sample.

Only the profile of the 1ML Ge can be used to describe the SIMS response function. The profile of the 10ML sample cannot be used for this purpose because of its plateau shape.

#### *As in-drives*

The SIMS depth profiles of the As in-drive samples are shown in Figs 2a and 2b. The quantification was done by determination of the Relative Sensitivity Factor (RSF) of an implant standard. In the diagrams the origins of the x-axis are set at the interface between poly- and monocrystalline Si, where the matrix signal of Si showed the most significant change. From -200nm to -10 nm one can recognize the rest of the shape of the original implantation; the x-axis is compressed in this region, to enlarge the interesting depth region around the interface. To represent the ratios of the decay length to each graph the slope of the Ge- $\delta$ -layer is added. Note that the intensities of Ge are normalized to the maximum of the As concentration and they don't show a real Ge concentration. A summary of the decay lengths can be found in table 3. As can be seen in the profiles the calculated values of the Ge- $\delta$ -layer on sample As#1 (RTP: 960°C) don't show any significant difference. At sample As#2 (RTP: 1000°C) the decay lengths are higher compared to the  $\delta$ -layer. This hints to the assumption that at 1000°C diffusion through the interface occurs, while at the 960°C sample the As decay in the prime wafer shows a SIMS artifact mostly induced by atomic mixing and surface roughening.

The apparent increase of the As concentration at the interface can be explained with the matrix-effect of SIMS. A change of the sample matrix causes a change in the secondary ion yield. In SiO<sub>2</sub>, an enhancement of the As signal occurs [9]. With the use of MCs<sup>+</sup> as secondary ions this matrix effect can be reduced [10] and the signal change induced by changed matrix is lower. At the profiles

of  $\text{CsAs}^+$  the maximum concentration is two times lower than at the profiles of the  $\text{AsSi}^-$  secondary ions.

The  $\text{CsAs}^+$  profiles show an upslope of the As-concentration 5 nm before the interface. This phenomenon cannot be explained only by means of a matrix effect and hints to a real enrichment of As in this region, because the matrix effects should be reduced by ceside measurements. At the  $\text{AsSi}^-$  measurements this upslope cannot be observed.

### *Convolution*

An inverse modeling of the distorted SIMS profiles was made by convolving an assumed undistorted diffusion profile (=model profile) with the SIMS response function. For this procedure the profile of the Ge- $\delta$ -layer was normalized and then convolved with the model profile point by point. The resulting convolution was fitted to the measured As profile trying to vary parameters until the best match of both graphs was reached. Additionally the background level of each measurement was added to each data point of the convolution. The background levels have been an a range between  $1 \cdot 10^{17}$  and  $1 \cdot 10^{18}$  at/cm<sup>3</sup>. The diagrams with the model diffusion, the convoluted profiles and the measured As profiles for the sample As#2 (RTP: 1000°C) are shown in Figs. 3a and 3b. To take into account the matrix effects at the change from Si to  $\text{SiO}_2$  at the interface the signal excitation in the decay slope a kink at the value of the constant As concentration ( $2 \cdot 10^{20}$  at/cm<sup>3</sup>) before the interface was set. The slope after this kink can be supposed as the real in-diffusion. The determined decay lengths are 3.0nm ( $\text{AsSi}^-$ ) and 2.9nm ( $\text{CsAs}^+$ ), the difference between these values is below 5%. The native  $\text{SiO}_2$  layers causing the As signal excitation have an average thickness between 2 to 3 nm at both samples, this corresponds to 4 and 5 oxide layers. As a real increase of the As concentration in the range from 5 to 7 nm before the interface it was assumed from the distorted depth profiles of sample As#2 with detection of  $\text{CsAs}^+$  this increase must also be set for the model profile to match the convolved curve with the measurement.

As a cross check the same convolution procedure was done with the measurements of sample As#1 (RTP: 960°C). The results are shown in Figs 4a and 4b. For the region around the interface the increase of the As at the AsSi<sup>-</sup> measurements was assumed as matrix effect due to the SiO<sub>2</sub> interface. For the CsAs measurement the increase in the last 5nm remains present also in the undistorted model diffusion profile. The calculated decay length after the interface are 0.1nm (AsSi<sup>-</sup>) and 0.3nm (CsAs<sup>+</sup>) and much lower than on atomic layer of Si (lattice constant of Si:0.54nm).

### Conclusions

Low energy SIMS in combination with forward convolution modeling allows the reconstruction of an ultra shallow drive-in diffusion over a dynamic range of 3 decades (percent range to 100 ppm range) within an interval of 15 nm in depth. With this method an enhancement of the original SIMS depth resolution is possible. Further these investigations lead to the result that diffusion through a SiO<sub>2</sub> interface occurs only at temperatures higher than 1000°C. The knowledge of this fact is important to develop a new generation of semiconductors with extremely low junction depths. Also the thickness of the native SiO<sub>2</sub> layer could be estimated.

**Acknowledgments:** The authors thank Dr. Minixhofer (Austriamicrosystems) to provide the arsenic-in-drive samples and Dr. Schaeffler (Univ. of Linz, A) for the production of the Ge- $\delta$ -layer samples.

This work was financially supported by the Austrian Science Fund (FWF) and the Province Government of Lower Austria (Niederösterreichische Landesakademie).

## Tables

**Table 1.** Experimental conditions for SIMS measurements

Instrument	Cameca IMS Wf (Cameca, Courbevoie, F)
Primary Ions	Cs <sup>+</sup> @ 10 nA
Incidence Angle	neg. secondary: ~45°; pos. secondary: ~ 67° to sample surface
Primary Energy	500 eV and 1keV, "floating column"
Sputtered / Analyzed Area	200 x 200 μm <sup>2</sup> / 88 x 88 μm <sup>2</sup>

**Table 2.** decay lengths of δ-layer samples in nm

analyzed species	primary intensity	polarity / incidence angle	λ (1ML)	λ (10 ML)
GeSi	1 keV	neg / 45°	1.7	1.8
CsGe	1 keV	pos / 67°	1.7	1.7
Ge	1 keV	neg / 45°	1.9	1.9
Ge	500 eV	neg / 45°	1.3	1.6
GeSi	500 eV	neg / 45°	1.3	1.4

**Table 3.** decay lengths (in nm) of As in-drive samples compared with Ge δ-layer

analyzed species	primary intensity	polarity	λ (1ML Ge)	λ (As#1)	λ (As#2)
GeSi/AsSi	1 keV	neg	1.7	1.6	2.8
CsGe/CsAs	1 keV	pos	1.7	1.6	2.4

Figures

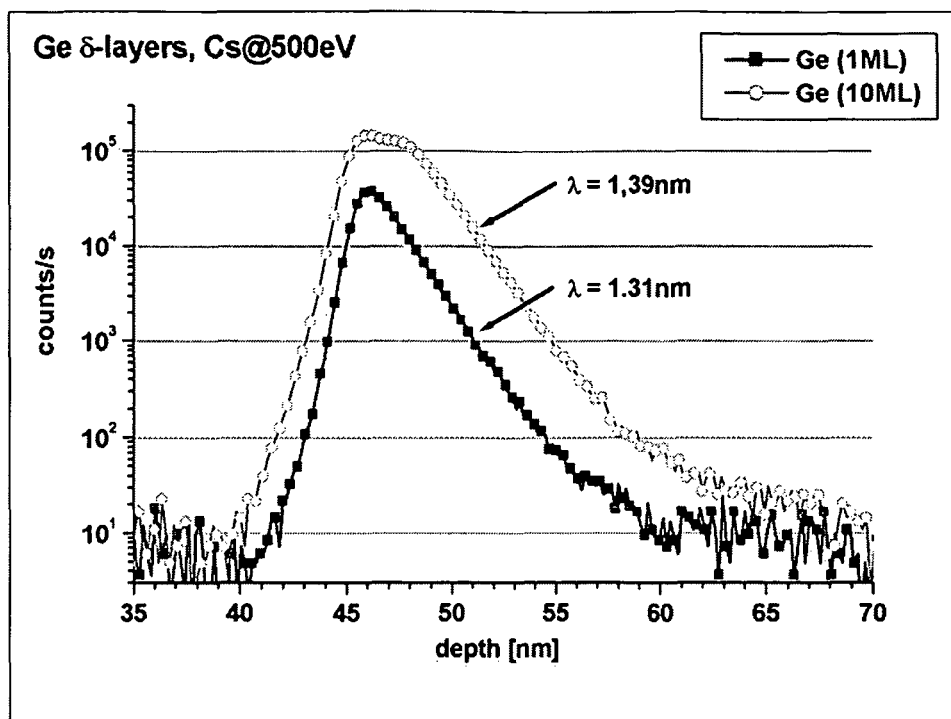


Figure 1 SIMS depth profile of the Ge-d-layer samples. The 1 monolayer (ML) sample shows a sharp maximum, while at the 10 ML sample already a plateau can be observed.

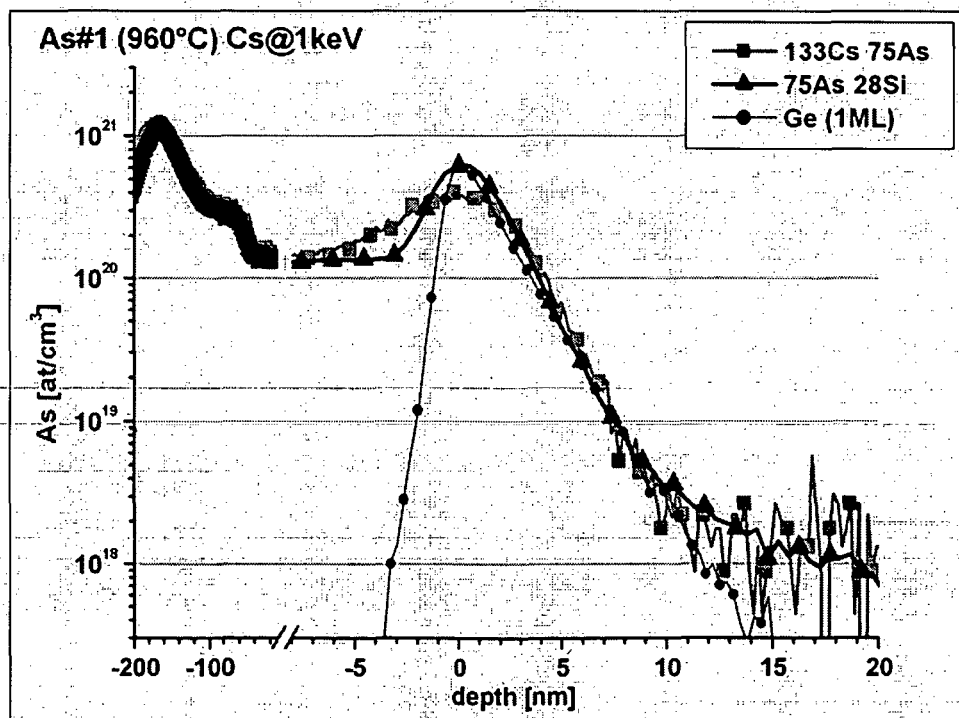


Figure 2a SIMS depth profiles of sample As#1(RTP at 960°C) and the Ge monolayer sample. The interface between the mono-Si and the poly-Si was set as origin. At the first 150 nm the slope of the As implantation can be recognized. The As profile was measured in the negative ( $\text{AsSi}^-$ ) and in the positive ( $\text{CsAs}^+$ ) mode, both with  $\text{Cs}^+$  primary ions at 1keV.

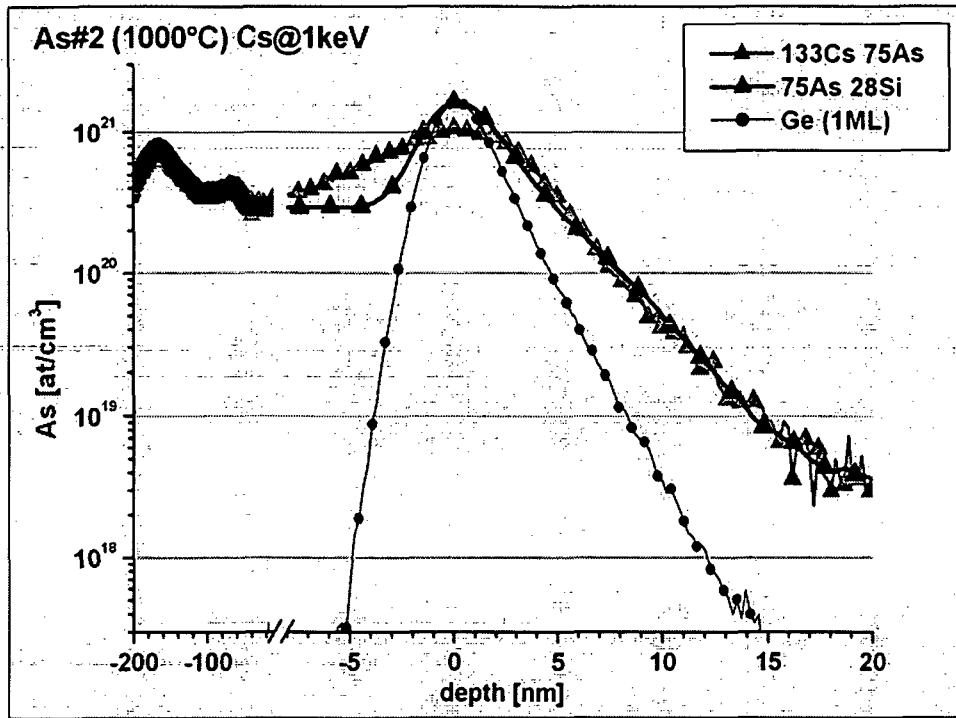


Figure 2b. SIMS depth profiles of sample As#1(RTP at 960°C) and the Ge monolayer sample. Explanation: see Fig. 2a

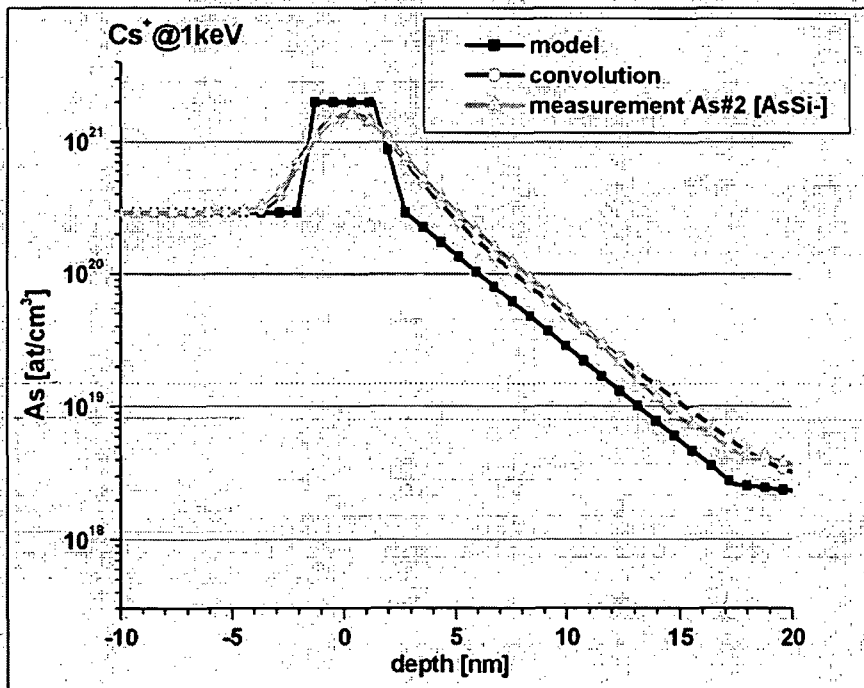


Figure 3a. Reconstructed in-diffusion profile (=model) of As in sample As#2 (RTP 1000°C). The model was convolved point by point with the normalized profile of the Ge- $\delta$ -layer (=SIMS response function) until the best fit with the measurement of the As drive in was reached.

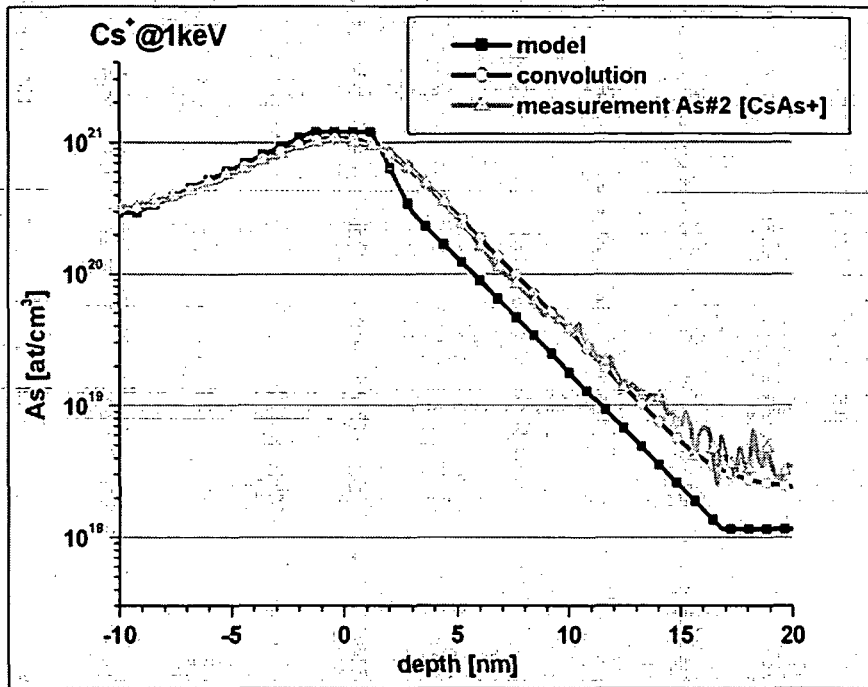


Figure 3b. Explanation: see Fig 3a. Due to a reduced matrix effect at the measurement of  $\text{CsM}^+$  secondary ions the matrix effect of the  $\text{SiO}_2$  at the interface is reduced by a factor of 3.

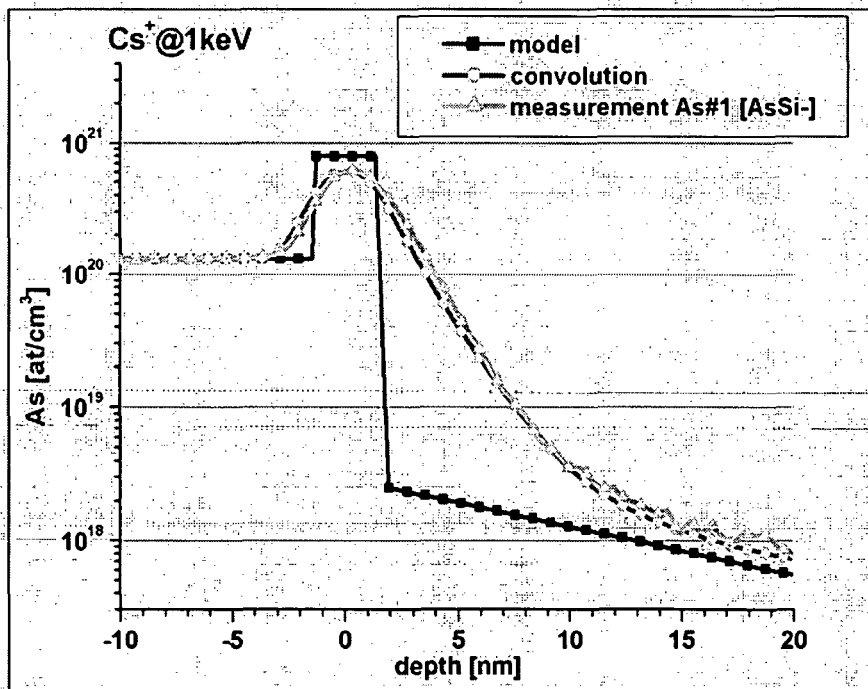


Figure 4a. Cross check of the convolution method with sample As#1 (RTP 960°C). Only with the assumption of no in-diffusion a match with the measured profile can be obtained.

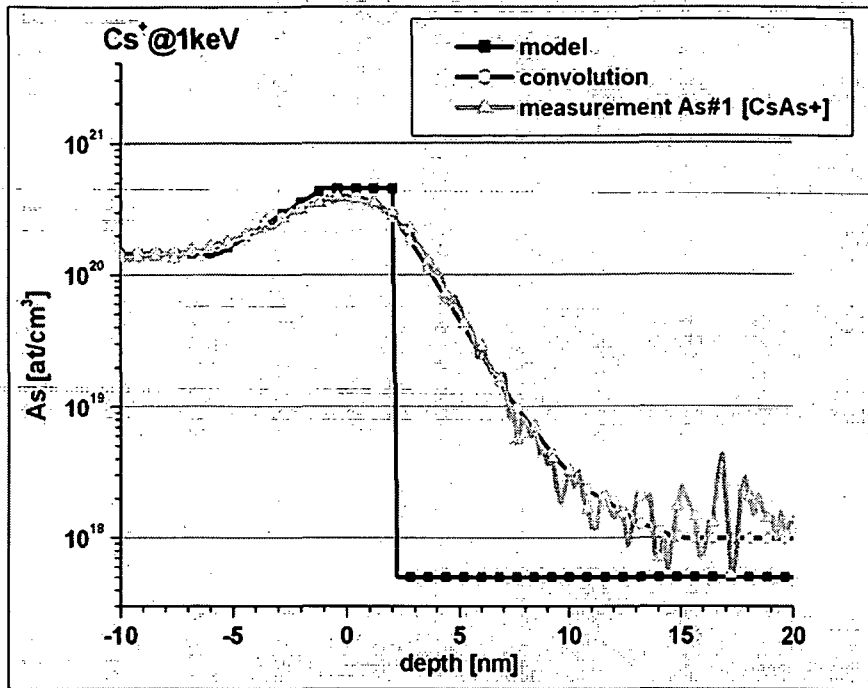


Figure 4b. Explanation: see Fig 4a.

---

## References

- 1 **The International Technology Roadmap for Semiconductor**, Semiconductor Industry Association, San Jose, CA (2001)
- 2 Wilson, R. G., Stevie, F. A., Magee, C. W. **Ion Beam Mixing and Depth Resolution in Secondary Ion Mass Spectrometry: A practical Handbook for Depth Profiling and Bulk Impurity Analysis**, John Wiley & Sons 1989, p2.1-2
- 3 Wittmack, K **Towards the ultimate limits of depth resolution in sputter profiling: beam-induced chemical changes and the importance of sample quality**. Surf. Interface Anal (1994), 21(6-7), 323-335
- 4 De Chambost E., Boyer B., Rasser B., Schuhmacher M., **Ultra low energy Cs bombardement on a magnetic sector SIMS instrument**. Secondary Ion Mass Spectrometry SIMS XII, edited by A. Benninghoven, P. Bertrand, H-N. Migeon and H.W. Werner, SIMS XII Conference Proceedings, Chichester: John Wiley & Sons (2000), 533-536
- 5 Montandon, C.; Bourenkov, A.; Frey, L.; Pichler, P.; Biersack, J. P. **Distortion of SIMS profiles due to ion beam mixing: shallow arsenic implants in silicon**. Radiation Effects and Defects in Solids (1998), 145(3), 213-223
- 6 Dowsett, M. G., Barlow, R. D., Allen, P. N. **Secondary-ion mass spectrometry analysis of ultrathin impurity layers in semiconductors and their use in quantification, instrumental assessment, and fundamental measurements**. J. Vac. Sci B (1994), 12(1), 186-198
- 7 Schuhmacher, M.; Rasser, B.; Desse, F. **New developments for shallow depth profiling with the Cameca IMS 6f**. J. Vac. Sci. B: (2000), 18(1), 529-532
- 8 De Chambost, E.; Monsallut, P.; Rasser, B.; Schuhmacher, M. **Depth scale calibration of SIMS depth profiles by means of an online crater depth measurement technique**. Appl Surf Sci (2003), 203-204, 391-395
- 9 Wilson, R. G., Stevie, F. A., Magee, C. W. **Matrix Effects** in Ref. 2, p. 2.3-1
- 10 Gao, Y. **A new secondary ion mass spectrometry technique for III-V semiconductor compounds using the molecular ions CsM<sup>+</sup>**. J. Appl. Phys. (1988), 64(7), 3760-2

## ***4.6 Development of Electrochemical Sensors***

PUBLICATION V

**SIMS Investigations of Oxidized Surfaces on Vanadium-Titanium-Alloys**  
submitted to *Analytical and Bioanalytical Chemistry*

# SIMS INVESTIGATIONS OF OXIDIZED SURFACES ON VANADIUM-TITANIUM-ALLOYS

Martin Rosner<sup>1</sup>, Torsten Bachmann<sup>2</sup>, H. Hutter<sup>1</sup>

<sup>1</sup> Institut für Chemische Technologien und Analytik der TU Wien, Getreidemarkt 9 / 164  
A-1060 Wien, Austria, [www.cta.tuwien.ac.at](http://www.cta.tuwien.ac.at)

<sup>2</sup> Kurt-Schwabe-Institut für Mess- und Sensortechnik e.V. Meinsberg, Fabrikstraße 69,  
D-04720 Ziegra-Knobelsdorf, Germany, [info@ksi-meinsberg.de](mailto:info@ksi-meinsberg.de)

## ABSTRACT

Alloys of high purity vanadium and titanium can be used as potentiometric sensors. These sensors are produced by anodic oxidation of these alloys in H<sub>2</sub>SO<sub>4</sub>. The structure of the passivation layer influences the electrochemical properties of the material. As Secondary Ion Mass Spectrometry (SIMS) allows the detections of all elements in concentrations down to the ppm range and its imaging capabilities can be combined with its depth profiling possibilities it is the method of choice to perform studies of these material. These so achieved 3D images give an insight into the investigated material as the analyzed volumes can be pictured as 3-dimensional cubes. The results of 3D-SIMS show clearly the oxide layers formed on the surface and the influence of the preparation method. Because of the anodic oxidation in sulfuric acid a interrelationship, between the spatial distribution of oxides and sulfur was detected.

**Keywords:** Vanadium-titanium alloy, anodic oxidation, 3D – SIMS

## INTRODUCTION

Thin oxide layers on high purity transition metals (group 4 ... 6 of PTE) are suited as selective redox electrodes in aqueous solutions. For example analytical determinations of hydrogen peroxide in acid etching baths have been performed potentiometrically in a concentration range of  $3 \cdot 10^{-3}$  to 1 M by Bachmann et al. [1]. The sensor system consists of a compact alloyed vanadium core with a functional passive oxide layer on the surface, formed by controlled potentiostatic anodic passivation in sulfuric acid. Investigation with regard to the structure and semiconductor properties of the sensitive layer has been carried out in former times with XPS, AES and photocurrent measurements [2]. The oxide covering layer has been identified as TiO<sub>2</sub> and V<sub>2</sub>O<sub>5</sub>.

SIMS is the method of choice for the analysis of alloy components as well as of impurities. All elements (even H) with concentrations down to the ppm range can be detected. In the imaging mode SIMS allows a lateral resolution of approx. 1  $\mu\text{m}$ . By the combination of imaging and depth profiling 2-dimensional images can be recorded as a function of sputter time. Piling up these images (usually 64 frames) and processing them with 3D software [3] allows to generate 3-dimensional images from the alloyed elements as well as from the impurities. These 3D cubes represent a volume of 150 x 150  $\mu\text{m}$  in lateral and 10 $\mu\text{m}$  in depth. The investigations of these anodically oxidized layers of Ti/V alloys were focused on the behavior of the sulfur and oxygen depending on the alloy composition.

## EXPERIMENTAL

### *Sample Preparation*

Cylindrical slices of vanadium and titanium of high purity (99.9%) and 3 alloys (V-10Ti, V-20Ti, V-40Ti) with a diameter of 10mm and a thickness of 1mm were embedded in an insulating polymer with copper wires as electronic leads mounted inside. The slices have been grinded with different SiC grinding paper (maximum granulation 4000), rinsed thoroughly with distilled water, cleaned in an ultrasonic bath with ethanol for 10 min and then washed with acetone.

After this procedure the samples have been oxidized anodically in a 50% sulfuric acid at 298K at a polarization potential of +1.75V relative to a saturated silver chloride electrode for 900s.

### *SIMS Setup*

SIMS investigations were performed with a strongly modified [4] Cameca IMS 3f (Cameca, Courbevoie, France). The unit is equipped with an additional primary magnet for the use of a fine focus cesium primary ion source. The measurements have been performed with both  $\text{Cs}^+$ - and  $\text{O}_2^+$ - primary ions. With  $\text{Cs}^+$  the electronegative elements (O, S, ...) while with  $\text{O}_2^+$  the electropositive elements (Ti, V, Na,...) can be characterized.

Due to its stigmatic set-up the IMS 3f works in the same way as an optical microscope, meaning that each point on the double channel plate detector represents one point on the sample surface. The 2D images are recorded with a CCD camera for further processing with a PC.

For 3D imaging 64 2-dimensional images (diameter: 150  $\mu\text{m}$ ) of each desired mass are recorded during the sputtering process down to a depth of 10  $\mu\text{m}$ . These 64 images are piled to

one 3D cube with an in-house developed program based on the vtk (visualization tool kit) – library [3]. The resolution of the IMS 3f is 1  $\mu\text{m}$  laterally and approx. 10 nm in depth (in 3D mode).

## RESULTS AND DISCUSSION

To characterize the formation of O- and S- enriched features (from the oxidation with  $\text{H}_2\text{SO}_4$ ) the sample was sputtered with  $\text{Cs}^+$  primary ions. Under  $\text{Cs}^+$  bombardment primarily electro-negative elements as O $^-$  or S $^-$  are ionized to be analyzed. Figs. 1a-d show the 3-dimensional distributions of oxygen within the samples. The analyzed volumes are 150 x 150  $\mu\text{m}$  in lateral and 10  $\mu\text{m}$  in depth for each cube. As the lateral resolution in imaging SIMS is in the range of 1  $\mu\text{m}$  the detected oxygen-rich features can be assumed to have a diameter of 5 to 10  $\mu\text{m}$ . From these series of increasing Ti content one can recognize straightforward, that higher Ti contents influence the formation and the structure of the oxide coating. The oxidation of pure vanadium (Fig. 1a) does not form any coating layer, only oxygen-rich features are developing. For V-40Ti (Fig. 1c) the oxide layer is nearly closed with a few remaining holes, while at pure Ti (Fig. 1d) a continuous oxide layer is formed.

The measurement of sulfur with SIMS exhibits the major problem, that the m/z ratio of  $^{16}\text{O}_2$  and for the major isotope of sulfur ( $^{32}\text{S}$ ) is equal. Therefore the minor isotope  $^{34}\text{S}$  was analyzed to avoid mass interference. As can be seen in Figs. 2a-d there is a direct coherence between the oxygen-rich features and the incorporation of sulfur (from  $\text{H}_2\text{SO}_4$ ) in the passivation layer. For each sample the distribution of sulfur is congruent to the oxygen distribution (compare Figs. 1a-d). While the oxygen-rich columns show a quite uniform  $^{16}\text{O}$  concentration within their range,  $^{34}\text{S}$  decreases continuously and is not uniformly distributed.

To get information on the structure of titanium, measurements with  $\text{O}_2^+$  primary ions and detection of the positive secondary ions have been done. For pure Ti (Fig. 3a) no appreciable inclusions and no surface coating could be detected. The sputtering of samples with  $\text{O}_2^+$  causes the so-called chemical enhancement effect, meaning that the signal is very sensitive to the chemical nature of the surface. Because the Ti in the  $\text{TiO}_2$  has an higher ion yield due to this effect, the  $^{48}\text{Ti}$  signal for these features is higher compared to the surrounding unoxidized Ti. So the image of  $^{48}\text{Ti}$  in sample V-10Ti (Fig. 3b) shows the same shape as for  $^{16}\text{O}$  (compare Figs 1a-d).

To clarify the origin of the detected “columns” of oxygen, EPMA analysis of the nearly unoxidized vanadium (no covering layer) has been performed. Fig 4a shows a SEM shot of

the surface (magnification: 2000x). The dark regions correspond to the oxygen-rich features. Further EDS analysis was done to identify the elemental composition near these features (Figure 4b). The brighter regions in the EDS images show clearly an enrichment of oxygen.

Figure 5 shows an example (alloy V-50Ti [5]) for a depth profile performed with Auger electron spectroscopy (AES) by sputtering with  $\text{Ar}^+$  ions. It can be seen that more than 40% (at/at) of oxygen is on the surface. This content decreases with the depth. Oxygen is not anymore detectable below a depth of 250nm. In the same scale the contents of vanadium and titanium increase. Their amount is about 50% in depth in each case. The depth profile shows a good agreement with the structure of the features detected in 3D-SIMS.

The formation of a closed oxygen coating on V-40Ti and on pure vanadium, respectively the absence of a typical passivation layer on pure vanadium explains the change in the electrochemical behavior of the samples [5] and in their spectral response obtained in photocurrent measurements [2].

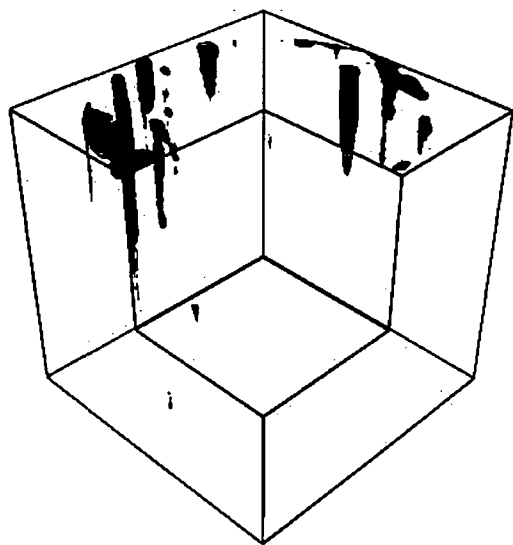
## CONCLUSION

As it is demonstrated with 3D-SIMS an increasing the Ti content influences the formation and the degree of coverage with  $\text{TiO}_2$ . In correlation to former studies on the electrochemical properties the behavior of the passive layers on the alloys is different at Ti contents more than 40% (w/w). This effect can be explained with the formation of a continuous oxide layer which is promoted by the presence of Ti. In contrast for pure vanadium a passivating layer is totally absent. Because of the anodic oxidation in sulfuric acid, an interrelationship between the spatial distribution of oxides and sulfur was detected.

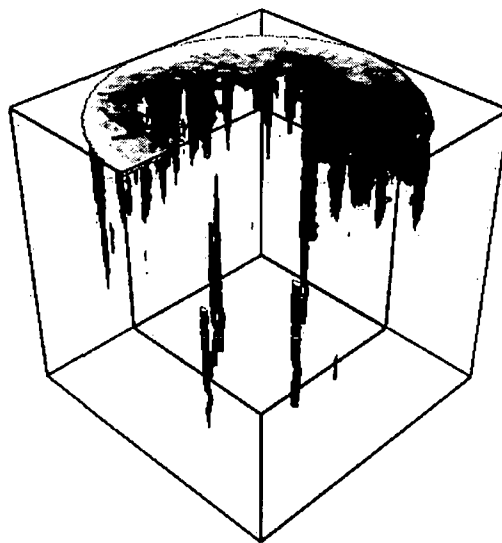
## ACKNOWLEDGEMENTS

This work was financially supported by the Austrian Fund for Science and Research (FWF Project No. P 13160) and by the foundation "Stiftung Industrieforschung Köln" (Research practical training T3/2000).

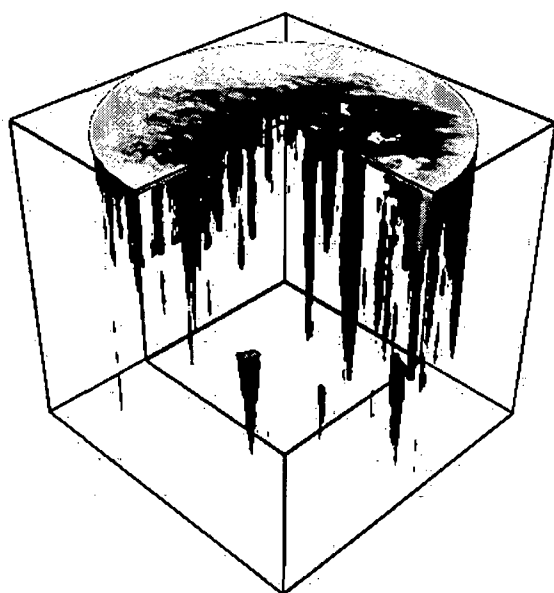
## FIGURES



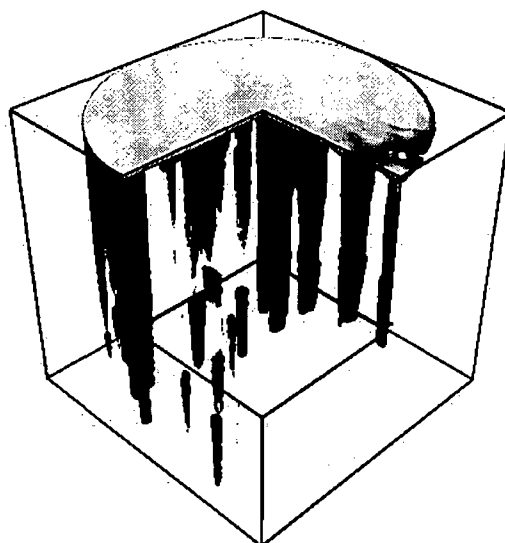
a



b

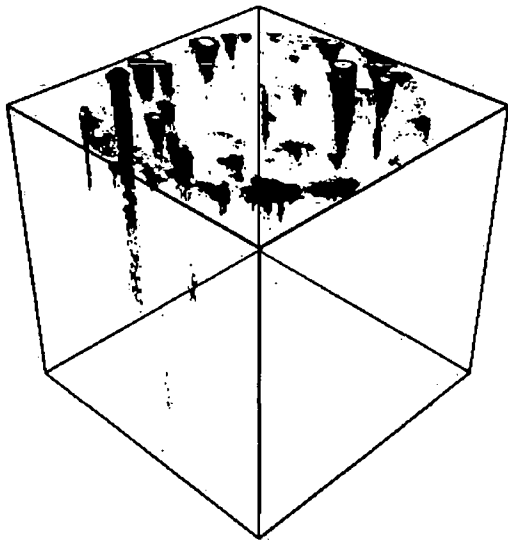


c

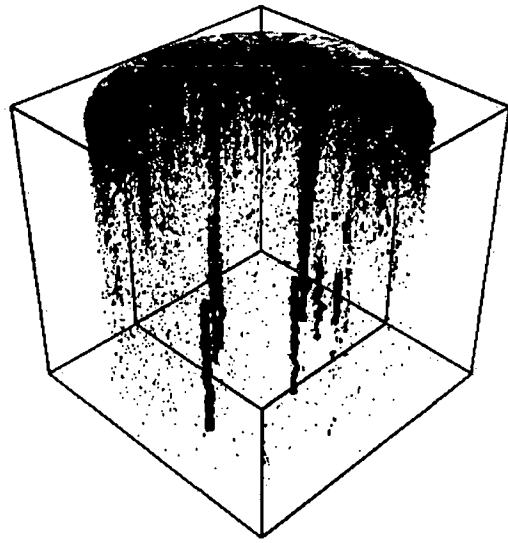


d

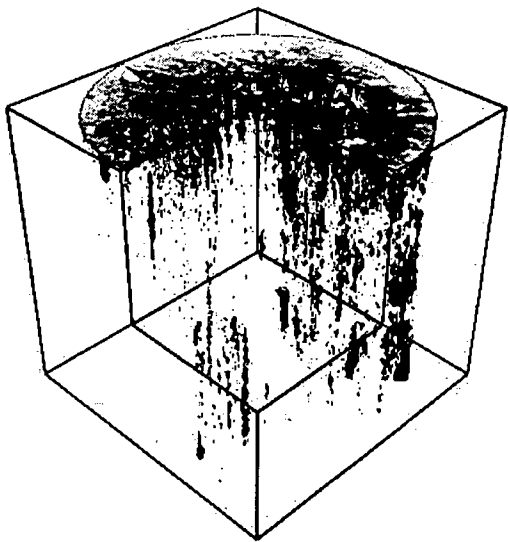
Figs 1a - d. <sup>16</sup>O distribution (isosurface cubes) of V (a), V-10Ti (b), V-40Ti (c) and Ti (d). Dimensions:  $x/y = 150 \times 150 \mu\text{m}^2$ ;  $z = 10 \mu\text{m}$ . The images show the dependency of the Ti content for the formation of a continuous surface coating. While Fig. 1d is totally covered with  $\text{TiO}_2$ , 1b and 1c show only partial coverage.



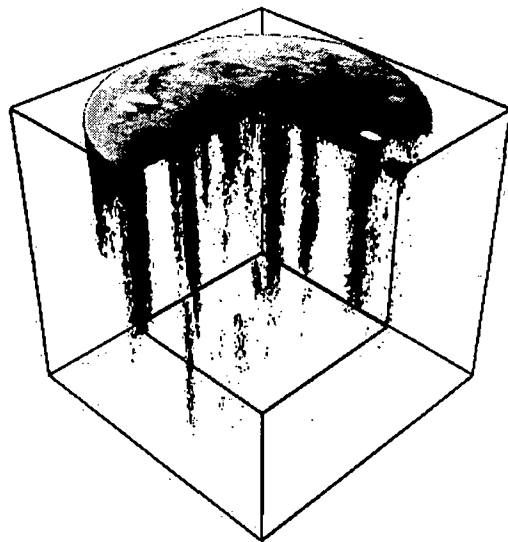
a



b

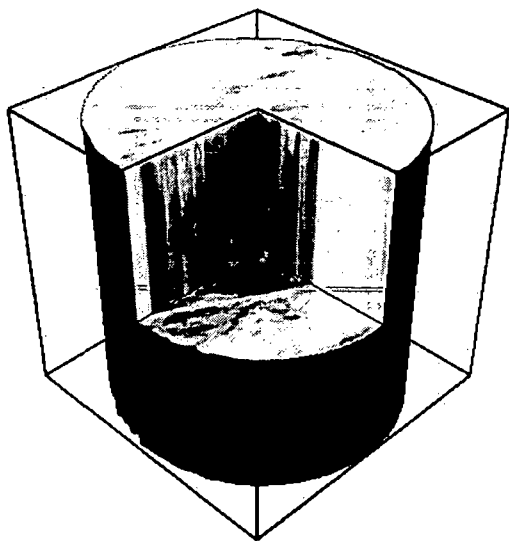


c

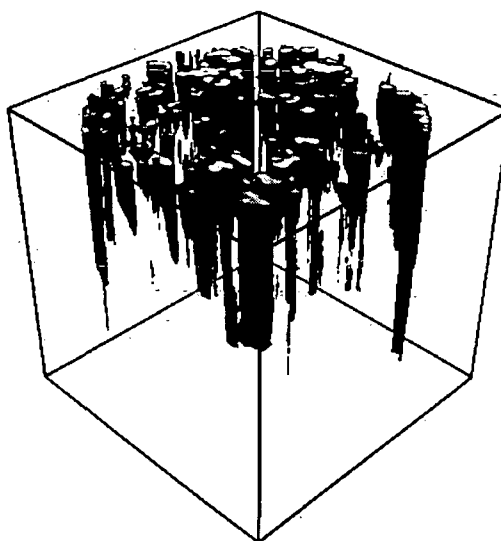


d

Figs 2a -d.  $^{34}\text{S}$  distribution of V, V-10Ti, V-40Ti and Ti. The relation between the incorporation of oxygen caused by the anodic oxidation and sulfur from the  $\text{H}_2\text{SO}_4$  is evident.



a



b

Figs 3 a and b.  $^{48}\text{Ti}$  distribution - isosurface view. Ti(a), V-10Ti (b).



a



b

Figs 4a and b. SEM-shot (a) and distribution analysis of V (dark) resp. O (bright) with EDS (b) of oxidized pure Vanadium. The oxygen-rich features detected with 3D-SIMS can be clearly identified.

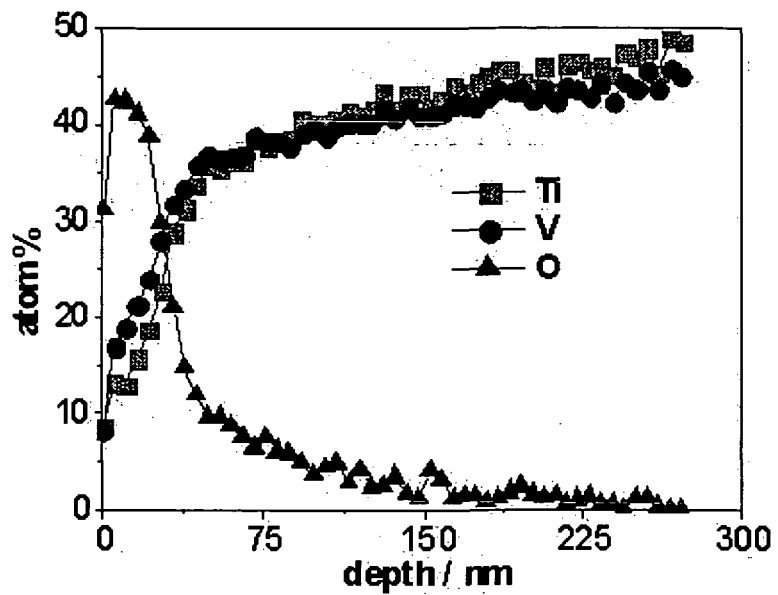


Figure 5. AES depth profile obtained on V-50Ti. The oxygen concentration on the surface is 40% (at/at) and decreases with the depth.

## REFERENCES

---

- 1 T. Bachmann, W. Vonau, P. John: Hydrogen peroxide concentration in acid etching baths. *G.I.T. Laboratory Journal* **7** (2003) 149-150
- 2 T. Bachmann, W. Vonau, P. John: Study of the structure of passivated vanadium-titanium alloys and their semiconductor properties. *Anal Bioanal Chem* **374** (2002) 715-719
- 3 H. Hutter, K. Nowikow, K. Gammer: Visualization of 3D-SIMS measurements. *Appl Surf Sci* **179** (2001) 161-166
- 4 H. Hutter, M. Grasserbauer: Development and Application of a New Imaging System for SIMS. *SIMS VIII-Proceedings of the Amsterdam Conference*, Wiley 1992, p. 533
- 5 T. Bachmann, U. Guth, W. Vonau: Physical and Electrochemical Properties of Vanium Alloy Oxide Layers Prepared by Anodic Passivation. *Ionics* **7** (2001) 172-177

#### ***4.7 Powder Metallurgy and Steel***

##### **PUBLICATION VI**

##### **2D- and 3D Investigations on hot-pressed steel powder HS 6-5-3-8**

**Analytical and Bioanalytical Chemistry (2002), 374(4), 597-601**

##### **PUBLICATION VII**

##### **AES and SIMS analysis of non-metallic inclusions in a low-carbon chromium steel**

**Analytical and Bioanalytical Chemistry (2003), 376(2), 255-259**

# 2D- and 3D SIMS investigations on hot-pressed steel powder HS 6-5-3-8

M. ROSNER (\*), G. PÖCKL, H. DANNINGER, AND H. HUTTER

*M. Rosner, H. Hutter, H. Danninger*

*Institute for Chemical Technologies and Analytics, TU Vienna, Getreidemarkt 9, A – 1060 Vienna*

*G. Pöckl*

*Material Center Leoben, A - 8700 Leoben*

**Abstract** Processing of steel with powder metallurgical methods such as sintering or hot-pressing have proven to be a powerful tool for the production of industrial parts and for components in automotive industry. Series of steel-powders (HS 6-5-3-8) produced by gas atomization has been hot-pressed in a graphite tube at temperatures from 820 °C to 1050 °C. The samples have been characterized with a Secondary Electron Microscope (SEM) due to their porosity and then investigated with 2D- and 3D- SIMS. The spatial distribution of the non-metallic impurities and the covering oxide layer of the single particles has been traced dependent to the pressing temperature.

Powders pressed at temperatures higher than 880°C exhibited different precipitation behavior of the impurities and an excessive loss of the covering oxide layer of the single powder particles.

---

(\*) corresponding author, email: [mrosner@iac.tuwien.ac.at](mailto:mrosner@iac.tuwien.ac.at)

Keywords: 3D-SIMS, powder metallurgy, hot pressing, deoxidation

## **Introduction**

Powder metallurgical methods in processing of steel such as hot-pressing and sintering have proven to be a powerful tool for the production of industrial parts. The quality of the resulting steel is determined by the distribution of the alloy components, impurities, and of the emerging oxides and carbides in the pressed samples. Further it is needful to improve the production process with regard to the use of raw material and the consumption of energy.

SIMS allows the generation of distribution images in the 3D-mode. Because of its ability to determine all elements an wide concentration ranges 3D-SIMS is the method of choice to investigate the influence of the distribution of trace elements as well as of main components and offers new aspects in the solution of problems in material science. These investigations of pressed powders focused on the behavior of the impurities and the oxides depending on the sintering temperature.

## **Experimental**

### **Powder Production and Characterization**

The steel powder HS 6-5-3-8 was produced by gas atomization from the liquid metal alloy. The chemical analysis of the steel powder yielded the results shown in table 1.

The sieve analysis of the particles gave an average size of 70  $\mu\text{m}$  with only a few particles greater than 500 $\mu\text{m}$ . The density analysis (after Archimedes) exhibited a significant density increase according to the sintering temperatures. The densities varied from 6.9  $\text{g}/\text{cm}^3$  for the sample pressed at 820°C to 7.7  $\text{g}/\text{cm}^3$  for the 1050°C sample (dense steel HS 6-5-3-8: 8,1  $\text{g}/\text{cm}^3$ ).

## Hot pressing

A graphite tube with a diameter of 20 mm was filled with the steel powder. At the bottom and at the top the sample space was margined with punches of graphite. Both punches were moved against each other with a hydraulic press. The usage of graphite limited the pressure to approx. 400 bar. The movement of the punches could be traced with measurement strips. The pressing procedure was stopped when no more movement could be determined. The distances and the holding times were dependant on the pressing temperatures and are shown in table 2. The uncertainty of the temperature measurement was about 20°C due to the scales of the electric equipment.

## SIMS investigations

SIMS investigations were performed with a strongly modified *Cameca IMS 3f* (Cameca, Courbevoie, France). The unit is equipped with an additional primary magnet for the use of a fine focus cesium primary ion source. The measurement conditions are shown in table 3. The measurements have been performed with both  $\text{Cs}^+$ - and  $\text{O}_2^+$ - primary ions. With  $\text{Cs}^+$  the electronegative elements (O, C, S, Cl,...) while with  $\text{O}_2^+$  the electropositive elements (K, Ca, Na,...) have been characterized.

The IMS 3f works in the same way as an optical microscope in the stigmatic mode, meaning that each point on the double channel plate and the phosphor screen represents one point on the sample surface. The 2D images on the phosphor screen are recorded with a CCD camera for further processing with a PC [1].

For 3D imaging 64 2D images of each desired mass are recorded during the sputtering process down to a typical depth of 10  $\mu\text{m}$  in the investigated pressed

steel powders. These 64 images are piled to one 3D cube with an in-house developed program based on the *vtk (visualization tool kit)* – library [2].

The resolution of the IMS 3f is 1 $\mu$ m laterally and approx. 50 nm in depth (in 3D mode).

## **Results and Discussion**

### **SEM measurements**

SEM measurements (Philips XL30) have been carried out to identify the alignment and the geometry of the resulting pores of the pressed powders. At 880°C (Fig1a) aggregates of pores and only a few of contact points can be detected, while at 940°C (Fig 1b) the number of the contact points increases appreciable until virtually no pores can be found at a temperature of 1050°C (Fig 1c).

### **SIMS measurements**

As the SEM measurements showed a high porosity of the samples pressed at low temperatures ( $\leq 880^\circ\text{C}$ ) the SIMS measuring positions have to be chosen at points without any hole on the surface. One problem in SIMS analysis is the matrix dependency of the ionization rates. Such matrix effects lead to different signal intensities for one detected ion type within an inhomogeneous sample surface, e.g. steel samples with precipitations as investigated in this work.

### **$\text{O}_2^+$ primary ions**

Especially metal ions and electropositive elements can be detected when using  $\text{O}_2^+$  primary ions. The 2D images show a significant difference in the distribution of K, Ca, Al and Si which are typical impurities in the analyzed steel. At 820°C

(Fig 2a-2d) these elements could be found uniformly distributed in the space between the single sintered powder particles. Only Al and Si slightly exhibit starting precipitation at the boundaries. The images of the sample pressed at 950°C (Fig 3a - 3d) show increased precipitation of all elements at the particle boundaries.

### ***Cs<sup>+</sup> primary ions***

The use of these primary ions is favorable to detect electronegative elements as Cl, S, N, O as well as carbides and oxides. The 3D-distributions of S, Cl and AlO depend on the pressing temperature and are displayed in Figs. 4 - 6 in the isosurface mode. In the isosurface mode points with the same intensity are displayed as one surface. The cubes plot a volume of 150µm x 150 µm in lateral and 10 µm in height (= sputtered depth). In agreement with the measurements with O<sub>2</sub><sup>+</sup> primary ions the impurities are uniformly distributed in the space between the powder particles at a temperature of 820°C. At 880°C and 1050°C the impurities appear as precipitations at the particle boundaries. The loss of the covering oxide layer must take place in the small temperature interval from 820°C to 880°C. This effect can be observed by tracing the behavior of the aluminum oxide precipitations during the raise of the pressing temperatures.

### **Conclusions**

SIMS and REM investigations of hot pressed steel powders showed the dependency of the precipitation processes of the impurities from the pressing (= sintering) temperature. The change of precipitation behavior appears at a temperature already below 880°C, while at 820°C all impurities are uniformly distributed in the area between the sintered powder particles. This effects can be

explained with the excessive loss of oxygen from the covering oxide layer of the powder particles and the increased mobility of the impurities at higher temperatures. In [3] pressed steels have been investigated with reference to their deoxidation properties. These investigations have been performed with thermal gravimetric methods as Differential Thermal Gravity (DTG) and Differential Thermal Analysis (DTA) in combination with mass spectrometry and showed significant loss of mass at temperatures between 600°C and 950°C depending on the alloy compositions. For a comparable Cr-Mn-Mo-V alloyed hot-pressed powder most of the mass loss occurs at temperatures above 850°C. So the results of these 2D/3D – SIMS measurements agree with the DTG/DTA results.

**Acknowledgements:** The authors thank the Material Center Leoben (MCL) and the Austrian Science Fund (FWF) for the financial grant of these works.

**References:**

- [1] H. Hutter, M. Grasserbauer (1992), Development and Application of a New Imaging System for SIMS. SIMS VIII-Proceedings of the Amsterdam Conference. Wiley 1992, p. 533.
- [2] Hutter, H.; Nowikow, K.; Gammer, K., Visualization of 3D-SIMS measurements. Appl. Surf. Sci. (2001), 179(1-4), 161-166
- [3] H. Danninger, C. Gierl, G. Leitner, K. Jaenicke-Roessler, S. Unami (2000) Deoxidation process during sintering of chromium alloyed PM steels. Sintering Science and Technology, Edited by R. M. Germann, G. L. Messing and R. G. Cornwall. Pennsylvania State University 2000.

**Table 1:** element composition of the HS 6-5-3-8 steel powder in % (m/m)

C	Cr	W	Mo	V	Co	Si	Mn	Al, O, S, N, Ti
1,3	4	6	5	3	8	0,-0,4	0,2-0,4	each < 0,1

**Table 2:** Distances of the measurement strips and holding times during the pressing process.

temperature [°C]	distance [mm]	holding time [h]
820	6,9	7
880	7,5	3
940	7,7	5
1050	8,4	7

**Table 3.** SIMS measurement parameters

primary ions	Cs <sup>+</sup> , O <sub>2</sub> <sup>+</sup>
beam intensity	100 nA (Cs <sup>+</sup> ), 1μA (O <sub>2</sub> <sup>+</sup> )
beam energy	14.5 keV(Cs <sup>+</sup> ), 4.5 keV (O <sub>2</sub> <sup>+</sup> )
sputter area (raster)	300 x 300 μm <sup>2</sup>
image diameter	150 μm

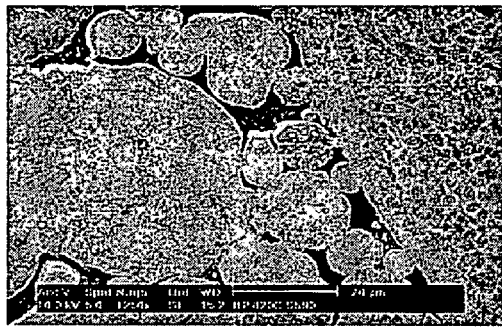


Fig 1a

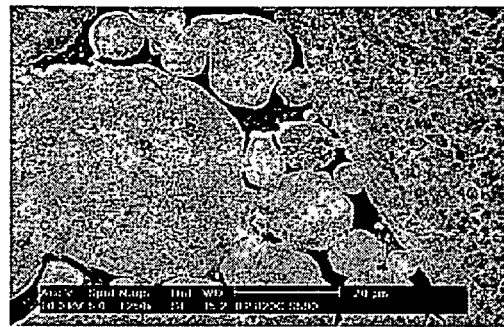


Fig 1b

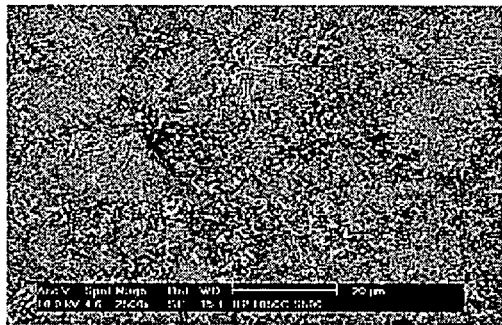
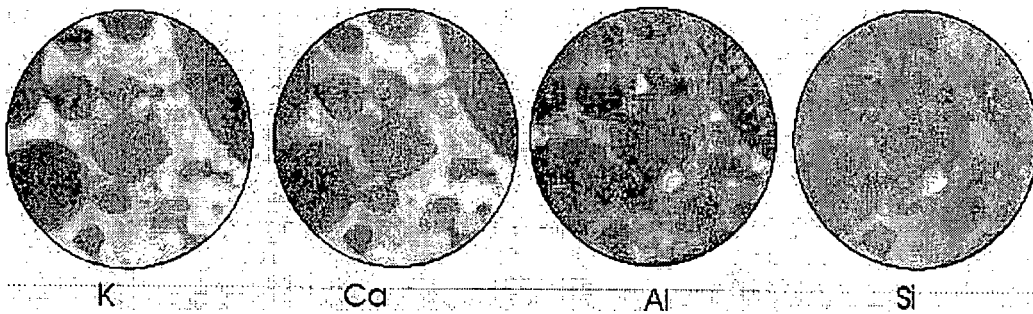
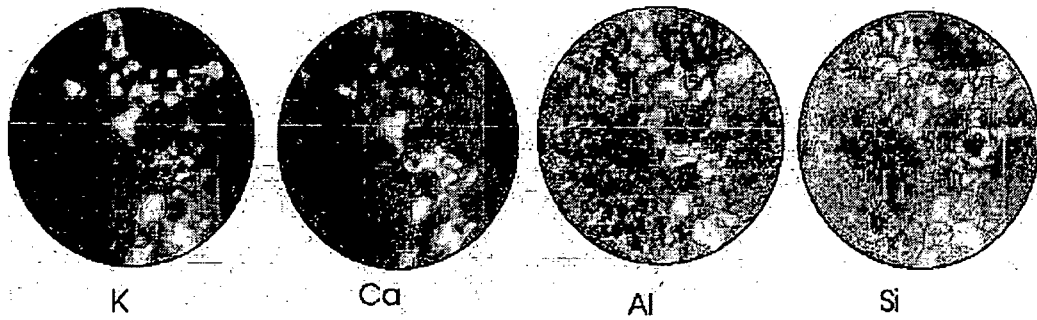


Fig 1c

Figure 1. SEM images of hot pressed steel powder HS 6-5-3-8. a) pressed at 820°C, b) at 940°C and c) at 1050°C. scale bar: 20μm, acceleration voltage: 100kV



Figures 2a-2d. SIMS images of steel HS 6-5-3-8 pressed at 820°C. Primary ions:  $O_2^+$ ; intensity: 1μA; primary voltage: 4.5 keV; diameter of images: 150μm



Figures 3a-3d. SIMS images of steel HS 6-5-3-8 pressed at 950°C. Primary ions:  $O_2^+$ ; intensity:  $1\mu A$ ; primary voltage: 4.5 keV; diameter of images:  $150\mu m$

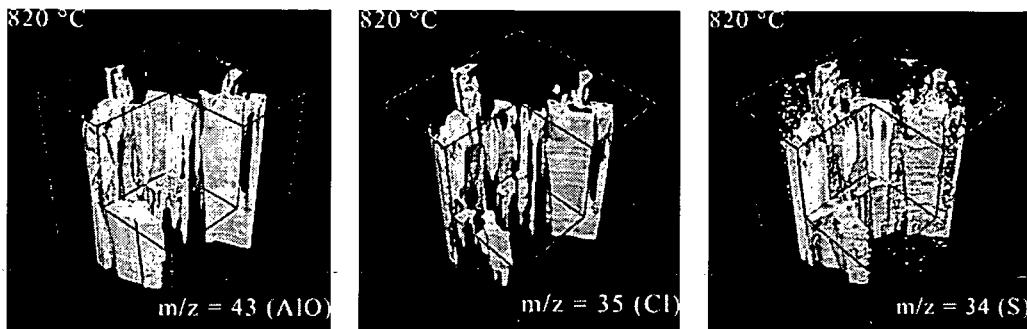


Fig 4a

Fig 4b

Fig 4c

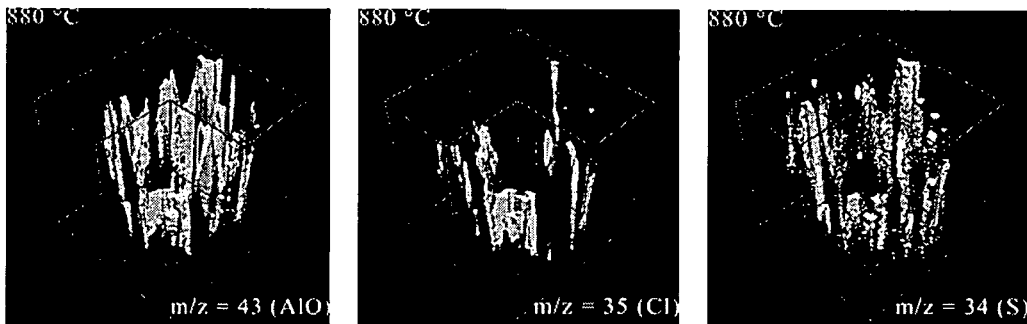


Fig 5a

Fig 5b

Fig 5c

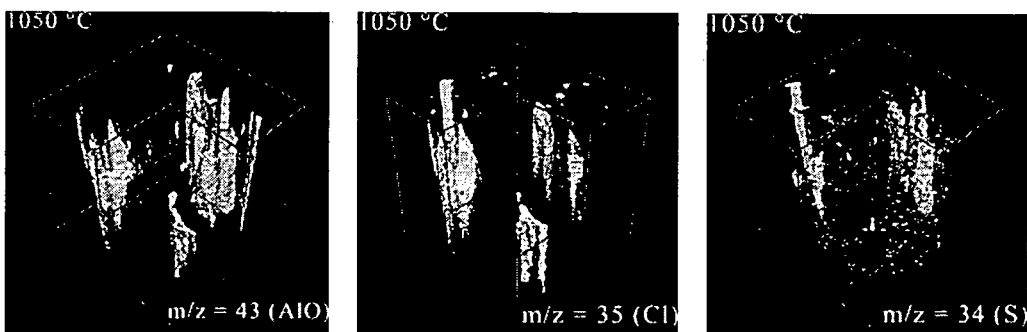


Fig 6a

Fig 6b

Fig 6c

Figures 4-6. 3D - isosurface views of AIO, Cl and S generated with the *Visualizer* -tool. Lateral image size:  $150 \times 150 \mu m$ , height:  $10\mu m$ . Figs 4a-c show the steel powder pressed at 820°C, Figs. 5a-c pressed at 880°C, and Figs 6a-c the steel powder pressed at 1050°C.

Katharina Gammer · M. Rosner · G. Poeckl · H. Hutter

## AES and SIMS analysis of non-metallic inclusions in a low-carbon Chromium-steel

Received: 24 September 2002 / Revised: 7 January 2003 / Accepted: 23 January 2003 / Published online: 24 April 2003  
© Springer-Verlag 2003

**Abstract** In the final step of secondary metallurgical steel processing, calcium is added. Besides Mg, Ca is the most powerful deoxidiser and desulfurisation agent. It reacts with dissolved oxygen and sulfur and reduces oxides and sulfides thereby forming non-metallic inclusions. Within this paper we present the analysis of such inclusions in a low-carbon chromium-steel. Depending on the time of quenching of the steel sample, different structures were revealed by REM, Auger and SIMS: If the steel was quenched immediately after Ca-addition, non-metallic inclusions that appeared to have “cavities” could be detected with SEM. SIMS investigations of these particles showed ring-shaped structures and revealed that the ring is made up of Al, Ca, Mg, O and S. No secondary ions however could be retrieved from the core inside the ring, thus leaving the nature of the “cavities” unclear. If the steel sample was quenched 3 min after Ca addition, inclusions did not have a ring-shaped structure but a compact one.

**Keywords** Non-metallic inclusions · Low-carbon chromium-steel · Ring-shaped structures · SIMS · AES · SEM

### Introduction

Oxygen and trace elements such as sulfur, nitrogen, phosphorus, chlorine, sodium and potassium in steels mostly remain from the production process. Generally they have negative effects on the properties of the steel as they cause increased brittleness, lower corrosion resistance and toughness.

Therefore, in a post-processing step the amount of oxygen and sulfur has to be reduced. The most important de-

oxidisers are Al and Si, which are added in different ways and form  $\text{Al}_2\text{O}_3$  and  $\text{SiO}_2$ . The deoxidisation products can crystallize homogeneously or heterogeneously (which means that impurities act as initial nuclei) [1]. In both cases over-saturation of the melt with Al and O is necessary. At the beginning, oxide growth relies on diffusion of reaction partners to the surface of the non-metallurgical inclusions, later on the collision of smaller particles to form larger ones [2]. Because of the low density of  $\text{Al}_2\text{O}_3$  the particles ascend in the melt. Thereby they collide and coagulate forming larger particles that are separated at the surface.

Finally the amount of oxygen is further decreased by the addition of Ca [3], which is the most potent deoxidisation and desulfurisation agent besides Mg. In general it is added to the melt in the form of a wound wire. At high temperatures (1500 °C) Ca is present in the form of a gas. It only liquidises under high load. Therefore the wire only dissolves at the bottom of the vessel forming bubbles that emerge through the melt. Thereby Ca–Al oxides are formed with a low melting point which are thus present in the liquid state. They can absorb a lot of sulfur giving rise to CaS. The Ca–Al oxides are separated at the surface which consequently leads to a further reduction of oxygen in the melt.

The type of non-metallic inclusion found in steel depends very much on the amount of Ca added. At higher Ca contents more calcium aluminate inclusions with an  $\text{Al}_2\text{O}_3$ –CaO core and a scale of CaS and MnS are found whereas the number of particles made up of MnS and of  $\text{Al}_2\text{O}_3$  decreases. At Ca concentrations above 30 ppm MnS is fully replaced by CaS in highly desulfured melts

Generally four types of non-metallic inclusion were described by Presern et al. [4]. The most typical one is made up of a CaO– $\text{Al}_2\text{O}_3$  core and a thin CaS shell. At 1500 °C the melt contains Ca–Al oxide particles with dissolved S. It is believed that these particles absorb more S from the surrounding melt at their surface and CaS crystallizes. Thus the particle is separated into two phases – an outer solid phase rich in sulfur and an inner phase made up of CaO– $\text{Al}_2\text{O}_3$  which is still liquid at the high temperatures that prevail during secondary steel treatment.

K. Gammer (✉) · M. Rosner · G. Poeckl · H. Hutter  
Institute for Chemical Technologies and Analytics,  
151 TU Wien, Getreidemarkt 9, 1060 Wien, Austria  
e-mail: kgammer@pop.tuwien.ac.at

In the course of our investigations on the formation of non-metallic inclusions, particles were detected that apparently had a ring-shaped structure in the SEM image. Although ring-shaped inclusions had already been detected for different inclusions in steel [5] with a different chemical composition remaining from other processing steps, this phenomenon was new in the context of Ca addition. Thus it was decided to perform further investigations using AES (in combination with SEM) and SIMS.

SEM and AES have a high lateral resolution and, additionally, AES enables elemental information to be obtained. However, AES has an unfavourable detection limit and it can only deliver information from the near-surface region. Therefore sample preparation might falsify results. SIMS was chosen because of its high detection power (all elements can be detected within the ppm range, even hydrogen) which allows verification of the presence of minor components too. Moreover SIMS can remove the surface layers and can thus rule out possible defects stemming from polishing the steel specimen as it might be argued that the "cavities" inside the inclusions that were uncovered by SEM are caused by the sample preparation.

## Experimental

The steel samples were prepared the following way. Samples of the low-carbon Cr-Steel (0.05% C, 13% Cr, 0.4% Si, 0.25% Mn) were melted in a five-kilogram induction furnace. After the whole sample was melted, the slag was removed and the temperature was adjusted to about 1580 °C – approximately 60 degrees above the melting temperature. Then the melt was pre-oxidised with aluminium. After five minutes calcium was added to the melt and one sample was taken and cast immediately afterwards. The other one was taken three minutes later.

The SIMS equipment used throughout this investigation was a modified Cameca IMS 3 f. The original beam deflection unit was replaced by a digital scan generator communicating with the controlling workstation via a specially designed parallel interface unit. The instrument was equipped with a double channel plate capable of single ion detection.

For 3D distribution analysis, images were recorded in the stigmatic imaging mode (ion microscope mode) by a CCD-camera which records the signal of the channel-plate illuminated by the secondary ions. For homogeneous illumination the  $O_2^+$  primary ion beam was scanned over a sample area of  $350\ \mu\text{m} \times 350\ \mu\text{m}$ , while the analysed area was set to  $150\ \mu\text{m} \times 150\ \mu\text{m}$ . In order to achieve a better signal/noise ratio, 256 frames were added up. Mass spectra, depth profiles and 3D images were recorded with  $Cs^+$  (primary ion current: 140 nA, ion energy: 14.5 keV) and  $O_2^+$  (primary ion current: 1.5  $\mu\text{A}$ , ion energy: 5.5 keV) primary ions.

In the scanning mode, a small spot primary ion beam with a low intensity is scanned over the sample area step by step with a certain time per pixel. The secondary ions are counted by the electron multiplier and presented as a 2D image. This operation mode enables lateral resolution of 0.2  $\mu\text{m}$  to 0.5  $\mu\text{m}$ . For these investigations, a sample area of  $16 \times 16\ \mu\text{m}$  with  $64 \times 64$  pixels was chosen. The scanning time per pixel was varied between 64 ms for masses with high intensity (Fe, Cr, Mn) and 262 ms for masses with lower intensity (such as Na, K, Mg and Ca). Thus the acquisition time for one image was between 1 and 18 min. Both samples were analysed with  $Cs^+$  and  $O_2^+$  primary ions, the primary ion current was about  $10^{-12}$  A. As the beam diameter was optimized manually the primary ion intensity varied slightly.

Auger measurements were performed with a high resolution Auger Electron Spectrometer from VG Microlab 310 F.

## Results and Discussion

In the course of investigations on the non-metallic inclusions in steel, some samples were quenched down shortly after the addition of Ca. Thereby some spherical structures with a kind of "cavity" in the middle were found with SEM, which were further analysed with AES.

A SEM image of an inclusion in sample A – the one which had been quenched immediately after Ca addition – was recorded with the AES facility (Fig. 1). The topology shows kind of a "cavity" inside the particle. Using AES, line scans were drawn over this particle to retrieve changes in the chemical composition within the particle, to explain the nature of the area that resembles a hole (Fig. 2). As can be seen from Fig. 2, the main component of the particle is Ca, whereas inside the "cavity" only O and Fe could be found. However, this diagram must be read carefully since the quantification algorithm used adds up atomic concentrations to 100% and thus does not consider increased or decreased total atomic density. Because of the Secondary Ion AES image (Fig. 1), which rather supports the idea of a "hole", it thus seems possible that these Fe and O signals just stem from surface contamination on the bottom of the "hole" (Auger Electrons are only retrieved from the near-surface region). Therefore, in order to rule out any surface-specific effects it was decided to perform SIMS measurements. Moreover, with the help of AES only the concentration of major elements can be measured because of the rather unfavourable detection limit of AES.

First of all, SIMS 3D images were recorded. Such 3D images are gained by piling up SIMS microscope images sequentially, while the primary beam sputters the sample [6]. Thereby inclusions made up of Ca, Mg, Al, O and S were found, however no spherical structures could be revealed. Fig. 3 shows some elemental 3D distribution images of inclusions in sample A. Due to the fact that SIMS



Fig. 1 SEM image of an inclusion found in sample A, which had been taken immediately after calcium addition. A dark core which resembles a hole can be seen in the left upper quadrant. The image was taken by the Auger system

Fig. 2 An AES scan line drawn over the inclusion depicted in Fig. 1 is shown. The line scan was made along L1

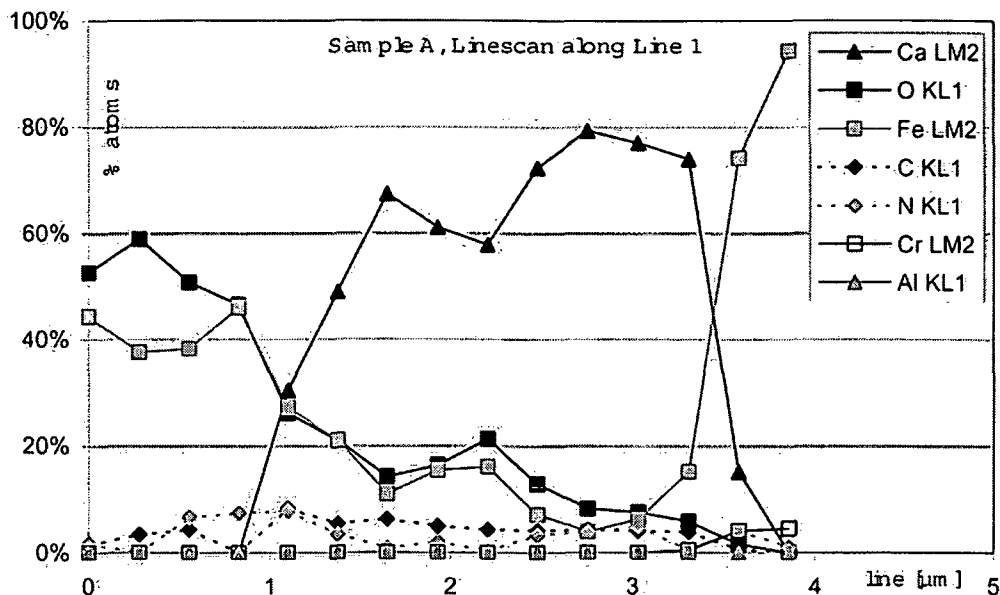
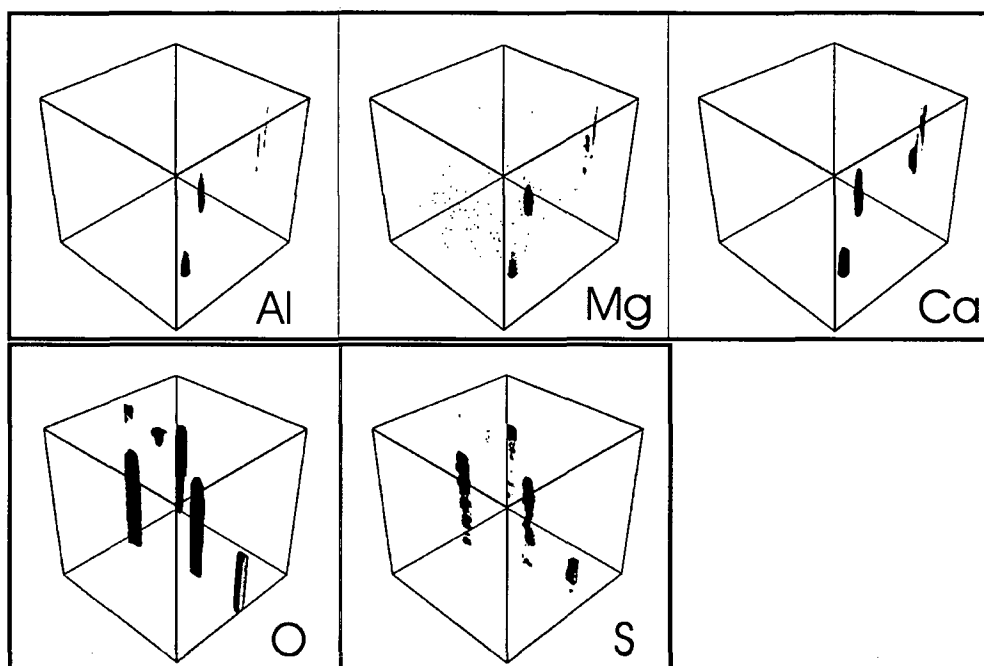


Fig. 3 3D images of sample A showing inclusions. Dark colour represents areas of high concentration of the respective element. The volume elements shown are  $150 \times 150 \times 15 \mu\text{m}$  in size. The Ca, Al and Mg distribution was recorded using  $\text{O}_2^+$  primary ions whereas for the O and S distribution analysis  $\text{Cs}^+$  primary ions were used. Since SIMS 3D measurements require destruction of the sample, the  $\text{O}_2^+$  and  $\text{Cs}^+$  measurements had to be performed at different locations. No spherical structure of the inclusions can be derived from these 3D images. This may be due to the low lateral resolution of 3D imaging



3D measurements requires sputtering and therefore destruction of material, the upper half of Fig. 3 ( $\text{O}_2^+$  as primary ions) shows different inclusions from those in the lower half ( $\text{Cs}^+$  as primary ions). The inclusions in samples A and B looked very similar and elemental 3D distribution images of inclusions in B are therefore not presented. The inclusions found were estimated to be about  $2\text{--}7 \mu\text{m}$  in diameter. Considering the lateral resolution of 3D imaging, which is about  $2 \mu\text{m}$ , it was assumed that the resolution might have been insufficient to resolve the "holes" and that Raster Scanning SIMS with a lateral resolution in the range of  $0.5 \mu\text{m}$  might yield better results. However, Raster Scanning once again retrieves an image of the surface similar to AES and results might be falsified by sam-

ple pre-treatment like polishing. Therefore we had to sputter down some micrometres to remove the upper surface layers, using a strong primary ion beam, before recording Raster Scanning images.

In fact, Raster scanning SIMS revealed inclusions with a ring-shaped structure (in approximately 3 out of 10 inclusions) in sample A. Using  $\text{O}_2^+$  primary ions we could prove the presence of Ca, Mg, Al in the ring (Fig. 4) whereas from the core no secondary ions signal could be yielded. In order to rule out the possibility that other elements than the ones recorded were present we made mass spectra of the inclusion only, but no further elements were detected. Using  $\text{Cs}^+$  primary ions, O and S were proven to be the corresponding anions in the ring. In the core however,

**Fig. 4** Raster-scanning greyscale images of a ring-shaped inclusion found in sample A. Bright colour represents areas with a high concentration of the respective element. Mg, Al, Ca, and Cr images were recorded using  $O_2^+$  primary ions. The C, O, S and CaO images were taken using  $Cs^+$  ions. The sample area presented is  $16 \times 16 \mu m$  with  $64 \times 64$  pixels. As can be seen the ring is made up of Mg, Al, Ca, O, and S. The concentration of the matrix elements (represented by Cr) is very low in the range of the inclusion. In the core no elements were detected

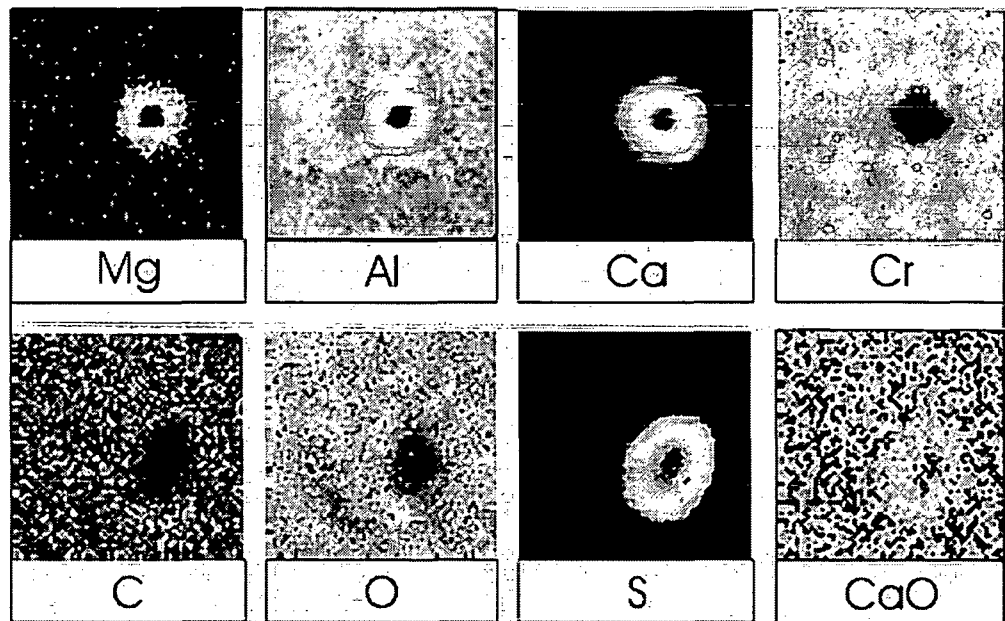
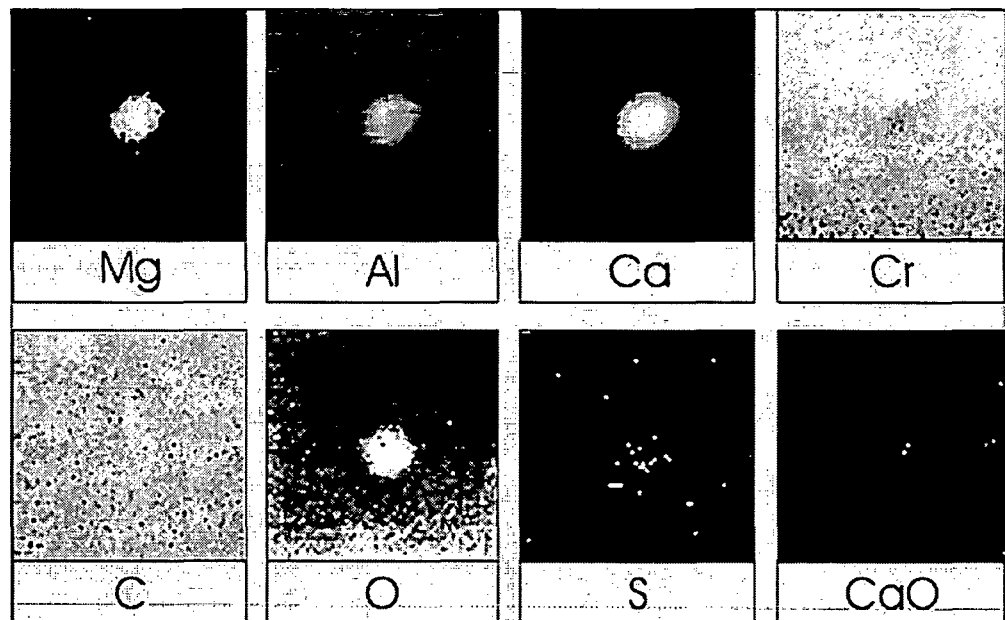


**Fig. 5** Raster-scanning greyscale image of an inclusion in sample B. Measurement conditions, sample area and visualization are the same as for Fig. 4. The inclusion is also made up of Mg, Al, Ca, O and S, but no spherical structure could be detected



only a slight signal for oxygen could be retrieved which might stem from residual gas. Thus there are still doubts about the nature of the core.

In the other specimen, B, only compact inclusions were found. These are also made up of Ca, Mg and Al as cations and O and S as anions (Fig. 5).

Finally SIMS line scans of the inclusions were made, once again using  $O_2^+$  primary ions, but no further information was gained. Fig. 6 shows the  $O_2^+$  line scan drawn over the inclusion, which is shown in Fig. 4. There is also a rapid decrease in the Ca, Mg and Al signal in the middle of the inclusion, just like in Fig. 4.

Despite our investigations, the nature of the core in the spherical inclusions remains rather unclear and further re-

search will be necessary. One guess is that during the floating of the Ca bubbles in the melt, Ca reacts with oxygen at the surface ("shell") of the bubble forming CaO and gaseous Ca is trapped inside. During the solidification of the steel, Ca condenses and later nothing can be found during the measurement. If the melt is allowed to react longer as for sample B, probably no gaseous Ca is left within the bubble possibly because Ca is fully reacted to CaO or diffuses out of the bubble. However, this is just one theory that can give an explanation for the phenomena encountered. It still needs further proof.

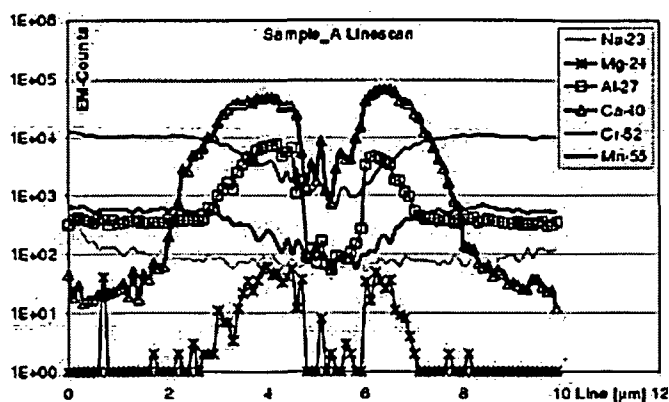


Fig. 6 Line scan using  $O_2^+$  primary ions over the ring-shaped inclusion that was found in steel sample A. It also shows that the ring is made up of Ca, Al, and Mg. Apparently the outer shell of the ring seems to contain Ca rather than Al, which is located further inside. In the middle of the inclusion the Ca, Al and Mg signal suddenly decreases by 2 magnitudes and no other signal can be found which rises in compensation

### Conclusions

The non-metallic inclusions formed during the final deoxidation of steel were investigated: Two different samples taken after Ca addition were investigated by SEM, AES and SIMS. The samples taken shortly after Ca addition show inclusions of size 4 to 7  $\mu\text{m}$ . Whereas most of the

oxide particles are spherical, about one third of them has a ring-shaped structure according to SIMS. These particles show large contents of Al, Ca, Mg, O and S.

No information about the chemical composition of the core of the ring-shaped particles could be gained and only some speculations about its nature and its origin could be made. The most probable theory says that during floating of the Ca bubbles in the melt, Ca reacts with the desolated oxygen at the shell and gaseous Ca is trapped in the core. During solidification of the steel Ca condenses and later nothing can be found during the measurement

The second sample which was taken a few minutes later does not contain those hollow inclusions since the melt is allowed to react longer. All particles are spherical with a size of 3 to 5  $\mu\text{m}$  and have a high content of Al, Ca, O and some S.

### References

1. Förster E, Richter H (1968) Arch Eisenhüttenwesen 39:595–604
2. Lindborg U, Torsell K (1968) Trans Metall Soc AIME 242:94–102
3. Förster E, Klapdar W, Richter H, Rommerswinkel HW, Sprezler E, Wendorff J (1974) Stahl Eisen 94:474–485
4. Presern V, Kmetec D, Voluny O, Hastie JW (1991) Radex Rundschau 1/2:433–443
5. Brunner C, Hutter H, Piplits K, Gritsch M, Pöckl G, Grasserbauer M (1998) Fresenius J Anal Chem 361:667–671
6. Hutter H, Grasserbauer M (1992) Microchem. Acta 107:137

## 5 REFERENCES

---

- 1 M. P. Seah, D. Briggs in: Practical Surface Analysis Vol. 2, ed. By D. Briggs and M. P. Seah, Wiley (1992), p13
- 2 R.G. Wilson, F.A. Stevie, Ch.W. Magee in: Secondary Ion Mass Spectrometry – A practical Handbook for Depth Profiling and Bulk Impurity Analysis, John Wiley & Sons (1989), p. I-1
- 3 H. Hutter in Surface and Thin Film Analysis edited by H. Bubert and H. Jenett, Wiley-VCH, Weinheim (2002), p 106
- 4 [www.srim.org](http://www.srim.org)
- 5 J. F. Ziegler, J. P. Biersack, U. Littmark, The Stopping and Ranges of Ions in Matter, Vol. 1: The Stopping and Range of Ions in Solids. (1985), p 321ff
- 6 [www.cea.com/tutorial.htm](http://www.cea.com/tutorial.htm)
- 7 M. Grasserbauer in: Angewandte Oberflächenanalyse, Springer-Verlag, Heidelberg (1986), p. 8
- 8 H. W. Werner, A. E. Morgan, Charging of insulators by ion bombardment and its minimization for secondary ion mass spectrometry (SIMS) measurements, J. Appl. Phys. 47 (1976) 1232-1234
- 9 R. Stuck and J. P. Ponpon, Sputter induced roughening during profiling of metal films deposited onto silicon, Secondary Ion Mass Spectrometry VI, ed. by A. Benninghoven A. M. Huber, and H. W. Werner, Wiley, New York (1988), p 507-512
- 10 P. A. W. van der Heide, M. S. Lim, S. S. Perry, J. Kulik, An AFM and TEM study of ripple topography growth during SIMS ultra shallow depth profiling of Si. Secondary Ion Mass Spectrometry XII, eds.: A. Benninghoven et al., Elsevier (2000), p 485-488
- 11 see Ref [2], p 1.5-1
- 12 G. D. Robertson Jr, P. K. Vasudev, R. G. Wilson, V. R. Deline, Appl. Surf. Sci 14(1) (1983) 128-33
- 13 W. Vandervorst, F. R. Shepherd Secondary ion mass spectrometry profiling of shallow, implanted layers using quadrupole and magnetic sector instruments., J. Vac. Sci. Technol. A 5(3) (1987) 313-320
- 14 [www.ncsu.edu/aif/SIMS/papers/SIMS%20Theory.pdf](http://www.ncsu.edu/aif/SIMS/papers/SIMS%20Theory.pdf)

- 
- 15 K. E. Mayerhofer in: SIMS investigations of Al-Sn Sputter Bearings, Diploma Thesis, TU Wien (2003), p.13
- 16 see Ref [1], p. 32 ff
- 17 M. von Ardenne, Z. Phys. 109 (1938) 338
- 18 A. Benninghoven, F. G. Rüdener, H. W. Werner, Secondary Ion Mass Spectrometry Wiley & Sons (1987), p.469
- 19 see Ref. [18], p. 478
- 20 see Ref [1], p. 61
- 21 see Ref [2], p 4.1-1
- 22 M. Gritsch in: Application of SIMS for the Characterization of Commercial High Performance Materials, doctoral thesis, TU Vienna 2000, p. 21
- 23 H. Hutter, M. Grasserbauer, Three dimensional ultratrace analysis of materials, Microchim. Acta 107 (1992) 137-148
- 24 K. Gammer, K. Nowikow, H. Hutter, Visualization of 3D SIMS measurements, Appl. Surf. Sci. 179/(1-4) (2001) 161-166
- 25 Y. Gao, A new secondary ion mass spectrometry technique for III-V semiconductor compounds using the molecular ions  $CsM^+$ . J. Appl. Phys. 64(7) (1988) 3760-3762
- 26 M. Schuhmacher:oral presentation at „SIMS solutions for next-generation microelectronics”, October 2002 in Trento (I), [http://fcs.itc.it/approach\\_Schuhmacher.pdf](http://fcs.itc.it/approach_Schuhmacher.pdf)
- 27 E. de Chambost, B. Boyer, B. Rasser, M. Schuhmacher, Ultra low energy Cs bombardment on a magnetic sector SIMS instrument, Secondary Ion Mass Spectrometry XII, eds.: A. Benninghoven et al., Elsevier (2000), p. 533
- 28 E. de Chambost, P. Monsallut, B. Rasser, M. Schuhmacher, Depth scale calibration of SIMS depth profiles by means of an online crater depth measurement technique, Appl. Surf. Sci. 203-204 (2003) 391-395
- 29 [http://www.cameca.fr/html/crater\\_measurement.html](http://www.cameca.fr/html/crater_measurement.html)
- 30 J.G.M. van Berkum. Improving SIMS Depth Profiling by Sample Rotation. Secondary Ion Mass Spectrometry XII, eds.: A. Benninghoven et al., Elsevier (2000,) p 55
- 31 A. Benninghoven, Chemical Analysis of Inorganic and Organic Surfaces and Thin Films by Static Time-of-Flight Secondary Ion Mass Spectrometry (TOF-SIMS) Angew. Chem. Int. Engl. 33 (1994) 1023-1043

- 
- 32 H. F. Arlinghaus in: Surface and Thin Film Analysis edited by H. Bubert and H. Jenett, Wiley-VCH, Weinheim 2002, p 88
- 33 D. Fraser Reich in TOF-SIMS: Surface Analysis by Mass Spectrometry, ed. by J.C. Vickerman and D. Briggs, IMPublications, p 113
- 34 E. Niehuis, T. Grehl, Dual Beam Depth Profiling, Secondary Ion Mass Spectrometry XII, eds.: A Benninghoven et al, Elsevier (2000), p 49
- 35 G. Gillen, M. Walker, P. Thompson, J. Bennett, Use of an SF<sub>5</sub><sup>+</sup> polyatomic primary ion beam for ultrashallow depth profiling on an ion microscope secondary ion mass spectroscopy instrument J. Vac. Sci. Technol. B 18(1) (2000) 503
- 36 G. Gillen, S. Roberson, A. Fahey, M. Walker, J Bennett R. T. Lareau, Characterization and Metrology for ULSI Technology: 2000 International Conference, edited by D. G. Seiler et al., American Institute of Physics (2001) p. 687
- 37 D. Stapel, A. Benninghoven, Application of atomic and molecular primary ions for TOF-SIMS analysis of additive containing polymer surfaces Appl. Surf. Sci. 174(3-4) (2001) 261-270
- 38 The Static SIMS library, version 2, Ed. by J.C. Vickermann, D. Briggs and A. Henderson. Surface Spectra. Manchester, UK (1999)
- 39 G. Friedbacher in Surface and Thin Film Analysis edited by H. Bubert and H. Jenett, Wiley-VCH, Weinheim 2002, p 277f
- 40 <http://jan.ucc.nau.edu/%7Ewittke/Microprobe/ProbeIntro-EMP.html>
- 41 <http://www.phl.com/genf.asp?ID=281>
- 42 H. Bubert and J.C. Rivière in: Surface and Thin Film Analysis edited by H. Bubert and H. Jenett, Wiley-VCH, Weinheim (2002) p 32ff
- 43 M. G. Dowsett, R. D. Barlow, P. N. Allen, Secondary-ion mass spectrometry analysis of ultrathin impurity layers in semiconductors and their use in quantification, instrumental assessment, and fundamental measurements. J. Vac. Sci B 12(1) (1994) 186-198
- 44 S. Knaus, A. Nennadal, B. Froschauer. Surface and Bulk Modification of Polyolefines by Functional Aryl Nitrenes as Highly Reactive Intermediates. Macromol. Symp. 176 (2001) 223-232

# CURRICULUM VITAE

## PERSÖNLICHE DATEN

---

Name: **DI Martin ROSNER**  
Geburtsdatum und -ort: 2. März 1973 in Steyr, OÖ  
Familienstand: ledig  
Staatsbürgerschaft: Österreich  
Adresse: A-1070 Wien, Neustiftgasse 56/24

## STUDIUM

---

- 12/00 – 11/03** TU Wien, Dissertation am Institut für Chemische Technologien und Analytik, „Application of Secondary Ion Mass Spectrometry (SIMS) in the Development of new materials“, Betreuer: Prof. Herbert Hutter
- 09/02 – 02/03** Aufenthalt am *Istituto Trentino di Cultura* in Trient (I) im Rahmen der Dissertation (SIMS-Messungen an Halbleitern und Polymeren)
- 10/91 – 01/00** TU Wien, Studium der Technischen Chemie, Studienzweig Analytische und Physikalische Chemie; Diplomarbeit: „Characterization of Tribological Coatings (Al-Sn and Cu-Pb) with SIMS“ am Institut für Analytische Chemie bei Prof. H. Hutter; Abschluss als Diplomingenieur: 01/2000

## SCHULAUSSILDUNG

---

- 09/83 – 06/91** Stiftsgymnasium der Benediktiner in Seitenstetten, humanistischer Zweig  
Maturaabschluss: 06/1991

## BISHERIGE BERUFSTÄTIGKEIT

---

- seit 12/00** TU Wien, Inst. f. Chemische Technologien und Analytik: wissenschaftlicher Mitarbeiter der AG Physikalische Analytik
- 01/00 – 02/00** TANN-Papier GmbH, Traun: Abteilung F&E (GC – und HPLC – Analytik)
- 08/97 – 09/97** Austria Buntmetall GmbH, Amstetten: Abteilung Qualitätswesen (Werk-  
**u. 07/98 – 08/98** stoffprüfung und Metallographie)

## PRÄSENZDIENST

---

- 03/00 – 10/00** Präsenzdienst abgeleistet beim Pionierbataillon 3 in Melk (NÖ)

## STUDIENBEGLEITENDE TÄTIGKEITEN

---

- 01/93 – 06/98** Zentralausschuss der Österreichischen Hochschülerschaften: Mitarbeiter der Studien- und Maturantenberatung
- 07/01 – 06/03** Hochschülerschaft an der TU Wien: Studienrichtungsvertreter und Mitglied der Studienkommission Doktorat Technische Naturwissenschaften

Wien, am 27. Oktober 2003